Theory and Experiment on the Transport of Surfactant from Micellar Solutions to a Clean Air/water Interface: Experimental Evidence of Direct Micelle Adsorption Route

by

Fenfen Huang

A Dissertation Submitted to the Graduate Faculty in Engineering in Partial Fulfillment of the Requirement for the Degree of Doctor of Philosophy

THE CITY UNIVERSITY OF NEW YORK

2009

This manuscript has been read and accepted for the Graduate Faculty in Engineering in satisfaction of the dissertation requirement for the degree of Doctor of Philosophy

Date	Prof. Charles Maldarelli (Mentor) Chair of Examining Committee
Date	Prof. Gabriel Tardos Executive Officer
	Prof. Alexander Couzis
	Prof. Ilona Kretzschmar
	Prof. Raymond S. Tu
	Prof. Ponisseril Somasundaran
	Supervisory Committee

THE CITY UNIVERSITY OF NEW YORK

ABSTRACT

Theory and Experiment on the Transport of Surfactant from Micellar Solutions to a Clean Air/water Interface: Experimental Evidence of Direct Micelle Adsorption Route

by

Fenfen Huang

Advisor: Professor Charles Maldarelli

The Benjamin Levich Institute for Physico-Chemical Hydrodynamics

Chemical Engineering Department of the City College of New York of CUNY

This dissertation studies the transport of surface active (surfactant) molecules, dissolved in an aqueous phase, to an initially clean air/water interface, and the reduction in surface tension which accompanies this adsorption. The study focuses on the transport in the case in which the bulk concentrations of surfactant are above a critical value for which aggregates of surfactant molecules (micelles) form in the bulk phase (the critical micelle concentration or CMC). The study will examine micellar solutions which form approximately spherical aggregates, using a polyethoxylated surfactant as a model.

This thesis proposes a second route for transport of surfactant to a clean air/water interface from a micellar solution: The direct adsorption of the micelle onto the surface. A model for the kinetics of micelle attachment to the surface is developed, and the equilibrium distribution of monomer and micelle on the surface as a function of the bulk

concentration is computed from this kinetic expression. A theory is developed to describe the dynamic adsorption when a clean interface is created in a micellar solution which includes the direct adsorption route. The simulations demonstrate that the direct route circumvents the limiting monomer kinetic barrier and allows ultrafast tension reductions. Dynamic tension experiments for micellar solutions are undertaken and compared to the theory to determine the kinetic constants for direct micelle adsorption. The simulations show excellent agreement with the measured tension reductions over a range of micellar concentrations.

The thesis also reports experiments that provide verification of the direct adsorption of micelles onto a clean air/water interface. These experiments tag the micelles in the bulk solution with a hydrophobic dye, Nile Red, which partitions into the micelles. By comparing the rate at which the dye accumulates on the surface - first for micellar solutions in which the dye is in the micelle, and secondly, for sub-micellar solutions, in which the dye is present as a free molecule in solution - the direct micelle adsorption route is validated. The rate at which the dye accumulates on the surface is measured either from the dynamic tensions themselves or by fluorescence measurements in which donor fluorophores of a phospholipids dye on the surface, through fluorescence resonance energy transfer (FRET), non-radiatively transmit energy to Nile Red adsorbing on the surface. Both techniques demonstrate that in the case of sub-micellar solutions the Nile Red adsorbs slowly to the surface with a delayed induction period, while in the case of micellar solutions the Nile Red incorporated in the micelles is quickly brought to the surface in overwhelming amounts that then desorb back into the bulk at equilibrium. This difference is shown to validate the hypothesis of direct micelle adsorption.

ACKNOWLEDGEMENTS

This dissertation could not have been done without Prof. Charles Maldarelli who not only served as my advisor but also provided constant support and encouraged me throughout the pursuit of this project. I appreciate his dedication to his students, teaching, and research. His stimulating suggestions and encouragement helped me in all the time of research and writing of this thesis. He has been invaluable in improving everything from my presentation skills to my general personality. I would like to express my gratitude to the executive officer of dissertation defense, Prof. Gabriel Tardos, and supervisory committee members, Prof. Alex Couzis, Prof. Ilona Kretzschmar, Prof. Raymond S. Tu and Prof. Ponisseril Somasundaran. I thank them for their time and effort in reviewing this work. I am grateful to Rongzeng Xu and Andrew Eng for providing mechanical and technical support during my study at City College. I would like to thank my many friends and colleagues at City College with whom I have had the pleasure of working over the years. These include Zongqin Zeng, Yu Sun, Qingqin Cui, Bin He, Xiujuan Cao, Bin Ren, Nikhil Kalyankar, Makonnen Payne, Jon Halverson, Shyam Vaidya, Rhoit Inagle and Nikhil Bhole. All of them made my stay at City College an unforgettable one.

Especially, I would like to give my heartfelt thanks to my parents for their love and support, for their firm faith in me, for teaching me the importance of higher education, and for always encouraging me to work harder and better. I would also like to thank my husband Jianhai Bao for his love, continues support, encouragement and patience. My son Victor H. Bao, who was the motivation of my academic life and who will continue to inspire me to move forward for the rest of my life, thank you!

Contents

List of Tables

Tables

List of Figures

Figures

Chapter 1

Introduction

A surfactant is an amphiphilic molecule consisting of a nonpolar hydrophobic group (the tail which interacts with other molecules through dispersion forces) and a polar or hydrophilic group (its "head", which is capable of hydrogen bonding to water). The hydrophobic group usually consists of a chain of methylene ($-CH_2-$) groups, while the polar group commonly consists of carboxylic (-COOH), hydroxyl (-OH), amine ($-NH_2$) or ethylene oxide ($-OCH_2CH_2-$) groups The polar and nonpolar groups are spatially disjoint from each other in the molecule. The structure of a "simple" surfactant molecule is shown in Figure 1.1. As a result of their amphiphilic nature, surfactants are typically sparingly soluble in both organic solvents and water, but strongly adsorb on interfaces that separate an aqueous phase from either a gas phase or a hydrophobic oil phase to form a monolayer. Once adsorbed at an interface, a surfactant reduces the surface or interfacial tension. The term "Surfactant" comes from " surface acting agent," referring to its ability to reduce the surface tension by adsorbing onto an interface.

When surfactant is dissolved in an aqueous phase, at low enough bulk concentrations, the surfactant molecule can be dissolved as single molecules in the aqueous phase. As the bulk concentration increases, surfactant molecules can aggregate in the bulk to form structures which minimize the free energy. The surfactant molecules in these structures are arranged so that the polar groups of the molecule remain in contact with the water molecules, and the hydrophobic chains are segregated in regions shielded by the polar groups. Several geometries are possible depending on the relative size of the chain and

the polar groups, the temperature and concentration. Examples include: (i) spherical micelles in which polar groups are arranged as a spherical corona and the hydrophobic groups extended into a spherical interior (Figure 1.2), (ii) cylindrical aggregates in which the polar groups are arranged on the surface of a cylinder with the chains extending interior to the cylinder and (iii) bilayers in which the polar groups are arranged in opposing planes with the chains extending between the plains. When surfactants assemble in hydrophobic oil, the aggregate is referred to as a reverse micelle and analogous structures exist, with the heads arranged in core regions with dissolved water, and the tails maintaining favorable contact with the oil phase. At a given temperature, the concentration at which aggregates form is termed the critical micelle concentration of CMC.

In the absence of aggregation, the transport of surfactant from a bulk solution onto an initially clean interface involves the kinetic adsorption of surfactant from the sublayer underneath the surface onto the surface, followed by the diffusion of surfactant molecules from the bulk to the surface to compensate for the sublayer adsorption. The adsorption dynamically reduces the surface tension from the clean value γ_0 until an equilibrium monolayer with a tension γ_e is obtained. This process is theoretically very well understood, and models for the transport have been validated by measurements of the dynamic reduction in tension as surfactant adsorbs to a clean surface. These experiments, upon comparison with theory, have allowed the measurement of the kinetic rate constants and independent measurements of the diffusion coefficient. Comprehensive reviews on the applications and the theory related to the dynamic adsorption of surfactants from sub-micellar solutions to an interface can be found in references[1-5].

For solutions below the CMC, the rate of the dynamic surface tension reduction is proportional to the bulk concentration of the surfactant as both diffusion and kinetic adsorption increase with the concentration of surfactant. As the surfactant concentration increases beyond the CMC, aggregates form in the bulk, and it is observed experimentally that the rate of tension relaxation for adsorption to a clean interface continues to shorten with concentration, and in fact ultra-fast reductions in tensions can be achieved. Many interfacial technologies require the rapid reduction in the tension of an initially clean interface, and surfactants are used for this purpose. The use of surfactants to rapidly reduce the tension is particularly important in aqueous systems and include the development of therapeutic lung surfactants to treat the respiratory distress syndrome[2, 6], ink-jet printing [7], air-assist atomization [8], pesticide sprays [3], film coatings [9, 10], and the generation of foams [11, 12] and emulsions [1]. In many of these applications, micellar solutions are commonly used to obtain as rapid a reduction in tension as possible. Since ultra fast tension reductions are required, very large micelle concentrations are used and values in excess of 10 times the CMC are usual.

Theoretical studies of the transport of surfactant from micellar solutions to an initially clean surface have been the subject of several publications. These publications have attempted to explain the continued reduction in dynamic tension as the bulk concentration increases above the CMC. The process is far from being understood. The current models assume that the acceleration in the transport rate is the result of the disassembly of the micelles which results as the micelle/monomer equilibrium is perturbed by the adsorption of monomer to the surface. The extra monomer resulting from the aggregate disassembly diffuses to the surface and adsorbs onto the surface. Thus, in this formulation, micelles

act as reservoirs for the diffusion and adsorption of monomer. Most of the research using this framework has focused on the formulation of the kinetics of the disassembly process.

The models developed to date are not in complete accordance with experiments. In particular, comparison of the model predictions to dynamic tension experiments indicate that even if the aggregates disassociate infinitely fast, the monomer released by the disassociation cannot diffuse and adsorb to the interface rapidly enough to explain the increasingly rapid reduction in tension with concentration. Recent molecular dynamics simulations of surfactant organization at the air/water interface suggest another route that can explain the acceleration in the adsorption rate. These simulations have shown that, for concentrations above the CMC, hemimicellar structures can exist at the air/water interface. In these structures the chains of the surfactant lie along the surface to form a hemi-micellar base. MD simulations have also shown such structures to develop at the aqueous/hydrophobic solid interface, where they, along with other aggregate structures, have also been observed experimentally using atomic force microscopy methods. The existence of the hemimicelle structure at the air/water interface suggests that an alternate route for adsorption of surfactant from a micellar solution onto a clean interface is for the micelles to **directly** adsorb onto the surface. In this transport route, when the surfactant density on the surface is very low, the micelles adsorb onto the surface and monomer disassociates from the micelles to populate the interface. As the surface density of the monolayer increases, the adsorption of the micelles will be reduced, and at equilibrium we can envision a steady state consisting of a small population of micelles adsorbed to the surface, with micelles disassociating and associating onto the surface. The direct

adsorption onto a hydrophobic solid surface from an aqueous micellar solution to form a hemimicelle on the surface has been demonstrated by molecular dynamics simulations.

The objectives of this thesis are twofold. The first is to develop a model for the direct adsorption of micelles onto the surface, and demonstrate that the model can explain the increased rate of dynamic tension reduction for adsorption of micellar solutions to a clean interface as the bulk concentration of surfactant increases. The second is to provide direct experimental evidence of the direct adsorption. To these ends, a direct kinetic model for micelle adsorption will be formulated. This model will be used to obtain equilibrium distributions of micelles on a surface, and to model the dynamic adsorption. The model will be shown to be able to explain the accelerated dynamic tension reduction by the fitting of the model constants. In addition, to verify the direct adsorption route, experiments are undertaken in which the micelles are tagged with label which is tracked during the adsorption process by dynamic tension and fluorescence labeling. The tracking of the label provides insight into the mechanism of adsorption of surfactant from micellar solutions onto a clean interface and in particular provides strong evidence of the direct adsorption route. The thesis will focus on aqueous systems, and adsorption to an air/water interface. Spherical micelles will be studied, using a polyethoxylated surfactant $C_{14}E_6$, which forms spherical micelles, as the model surfactant.

An outline of this thesis is as follows. A literature review is presented in Chapter 2 which summarizes the research undertaken to date on transport of surfactant from sub-micellar and micellar solutions to a clean interface. In Chapter 3 the kinetic model of direct micelle adsorption is formulated, and the equilibrium distribution of micelles on the surface is calculated. Chapter 4 utilizes the kinetic model to develop a framework for

adsorption of surfactant from micellar solutions to a clean air/water interface, and obtains the constants of the model by comparison with dynamic tension experiments. These experiments are undertaken as part of this study. Chapter 5 undertakes the micelle labeling, tag tracking experiments to verify the direct micelle adsorption route. Finally, Chapter 6 suggests avenues for future research.

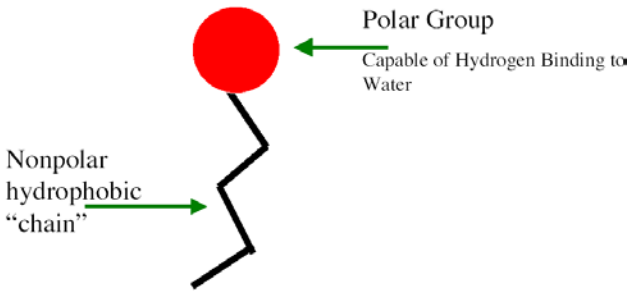

Figure 1.1: Schematic representation of the structure of a "Simple" Surfactant Molecule

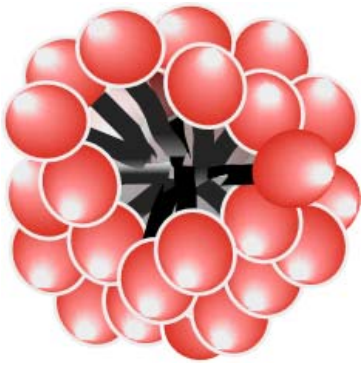

Figure 1.2: Schematic representation of the structure of a spherical micelle.

Chapter 2

Literature Review

2.1 Introduction

The aim of this chapter is to review the research undertaken on surfactant transport from a surfactant solution below CMC and above CMC, including both theoretical models and experimental methods. This chapter begins by describing mathematical models for the surfactant transport from a surfactant solution below CMC onto a clean air/water interface, followed by the experimental methods to measure the surface tension of an interface with a surfactant monolayer. The comparison of simulation results of the mathematical model with the experimental data carried out to determine the kinetic constants for the monomer adsorption are also reviewed here. Also discussed in this chapter are theories and models on multicomponent equilibrium adsorption isotherms. The theories and experiment on the transport of surfactant onto a clean air/water interface from aqueous solutions above critical micellar concentration are reviewed in this chapter too.

2.2 Theories and Experiments on the Transport of Surfactant onto a Clean Air/Water Interface from Aqueous Solutions below the Critical Micellar Concentration

2.2.1 Background

The dynamic adsorption of nonionic surfactant form an aqueous surfactant solution containing only surfactant monomer onto a water-air interface has been studied for several decades and is well understood and the modeling of this process is well established[1-5]. The surfactant transport involves kinetic adsorption/desorption of

monomers from the sublayer adjoining the surface onto the surface to form a monolayer, followed by diffusion of monomers from the bulk to the subsurface. This process is shown in Figure 2.1.

Since the monomer concentration is low, the diffusion of the monomers can be modeled by Fick's law, and the kinetic exchange is most generally formulated using the Frumkin rate law expression. In this model, adsorption is proportional to the surface area unoccupied by surfactant multiplied by an Arheninus factor describing the activation energy for adsorption that is assumed independent of surface coverage. The desorption is proportional to the surface concentration and an Arheninus activation energy factor which is assumed linear in the surface concentration. This linear dependence describes the effect of interaction between the adsorbed molecules on the desorption process[6], thus

$$\frac{d\Gamma}{dt} = \beta\Gamma_\infty C_s\left[1-\frac{\Gamma}{\Gamma_\infty}\right] - \alpha\Gamma e^{K\Gamma/\Gamma_\infty} \tag{2.1}$$

where C_s is the sublayer concentration, Γ is the surface concentration, α and β are kinetic rate constants for desorption and adsorption respectively, Γ_∞ is the maximum packing concentration, and K is a (nondimensional) parameter accounting for the effect of intermolecular interactions.

The equilibrium adsorption isotherm obtained from Equation (1) is:

$$\frac{\Gamma_e}{\Gamma_\infty} = \frac{\left[\beta C_o/\alpha\right]}{\left[\beta C_o/\alpha\right] + e^{K\Gamma_e/\Gamma_\infty}} \tag{2.2}$$

where C_0 is the bulk surfactant concentration and Γ_e is the surface concentration when equilibrium is reached.

The (equilibrium) equation of state describes the dependence of the surface tension on the surface concentration $(\gamma(\Gamma))$. The Gibbs thermodynamic treatment of an interface provides a relationship between the tension and the surface and bulk concentration for solution below the CMC where it is assumed that the concentration of surfactant is dilute, leading to the Gibbs-Duhem equation:

$$\Gamma = -\frac{1}{nRT}\frac{d\gamma}{d\ln(C_0)} \tag{2.3}$$

where Γ is the equilibrium surface concentration, C_0 is the bulk concentration, R is the gas constant, T is the Kelvin temperature. n=1 for non-ionic surfactants, neutral molecules or ionic surfactants in the presence of excess electrolyte, and n=2 for 1:1 ionic surfactants, assuming the interface is of electrical neutrality, n=3 for bis-(quaternary ammonium) surfactants. In the case of non-ideal solutions, the bulk concentration C_0 is replace by the activity. Integrating equation (2.3) yields the equation of state:

$$\gamma = \gamma_c + RT\Gamma_\infty\left\{\ln\left[1-\frac{\Gamma}{\Gamma_\infty}\right]-\frac{1}{2}K\left[\frac{\Gamma}{\Gamma_\infty}\right]^2\right\} \tag{2.4}$$

where γ_c is the clean tension and RT the thermal energy. When K is set to zero and intermolecular interactions are not included, the Langmuir rate law expression, Langmuir adsorption isotherm and equation of state are obtained, respectively:

$$\frac{d\Gamma}{dt} = \beta\Gamma_\infty C_s\left[1-\frac{\Gamma}{\Gamma_\infty}\right]-\alpha\Gamma \tag{2.5}$$

$$\frac{\Gamma_e}{\Gamma_\infty} = \frac{[\beta C_o/\alpha]}{[\beta C_o/\alpha]+1} \tag{2.6}$$

$$\gamma = \gamma_c + RT\Gamma_\infty\ln\left[1-\frac{\Gamma}{\Gamma_\infty}\right] \tag{2.7}$$

Furthermore, at the low limit of surface concentration, Henry rate law, Henry adsorption isotherm and a linear equation of state follow:

$$\frac{d\Gamma}{dt} = \beta C_s \Gamma_\infty - \alpha\Gamma \tag{2.8}$$

$$\frac{\Gamma_e}{\Gamma_\infty} = \beta C_0 / \alpha \tag{2.9}$$

$$\gamma = \gamma_c - RT\Gamma \tag{2.10}$$

The theoretical framework of this mass transfer begins with the formulation for the diffusion of the monomers in the bulk to the sublayer and mass balance at interface. We illustrate this formulation for a planar interface (at z=0) and with no effect of convection:

$$\frac{\partial C}{\partial t} = D\frac{\partial^2 C}{\partial^2 z} \tag{2.11}$$

$$\frac{d\Gamma(t)}{dt} = D\frac{dC(z,t)}{dz}\Big|_{z=0} \tag{2.12}$$

with the initial and boundary conditions:

$$\mathrm{C(z, t = 0) = C_0} \tag{2.13}$$

$$\Gamma(t = 0) = 0 \tag{2.14}$$

$$C(z = \infty, t) = C_0 \tag{2.15}$$

$$C(z = 0, t) = C_s(t) \tag{2.16}$$

where C(z,t) is the monomer concentration, Γ is the surface concentration, t is the time, D is the monomer diffusion coefficient, z is the distance from the surface, C_0 is the initial bulk concentration and C_s is the sublayer monomer concentration. By Laplace transform, the solution to the above equations can be expressed in term of the unknown term $C_{s:}$

$$\Gamma(t) = 2C_0\left(\frac{Dt}{\pi}\right)^{1/2} - \left(\frac{D}{\pi}\right)^{1/2}\int_0^t \frac{C_s(0,\tau)}{(t-\tau)^{1/2}}d\tau \tag{2.17}$$

Equation (2.17) is known as the classical solution of Ward and Tordai for the unsteady diffusion toward an initially clean planar surface[7].

Equation (2.17) together with equation (2.4) (with isotherm rate law plugged in) has to be solved numerically. Solutions have been carried out for the case in which the kinetics exchange at the interface is infinitely fast and the sublayer and surface are in equilibrium (diffusion limit), and the case is finite. These two cases will be discussed separately below.

2.2.2 Diffusion Limited Model

In this model, the diffusion process form the bulk to the subsurface is the rate-controlling step, assuming the kinetic exchange at the interface is infinitely fast (or adsorption rate constant $\beta \to \infty$). What also assumed is that the surface concentration is always at equilibrium with the sublayer concentration C_s, which changes as diffusion occurs. If the linear quasi-equilibrium isotherm $\Gamma = k_H Cs$ where $k_H = \frac{\beta\Gamma_\infty}{\alpha}$ (by assuming the bulk concentration is small) is solved together with the Ward and Tordai expression, an analytical solution can be obtained using Laplace transform:

$$\frac{C(0,t)}{C_0} = 1 - \exp\left(\frac{DtC_0^2}{k^2\Gamma_\infty^2}\right)erfc\left(\frac{\sqrt{Dt}C_0}{k\Gamma_\infty}\right) \tag{2.18}$$

What we can also get is:

$$\frac{\Gamma(t)}{\Gamma_e} = 1 - \exp\left(\frac{DtC_0^2}{k^2\Gamma_\infty^2}\right)erfc\left(\frac{\sqrt{Dt}C_0}{k\Gamma_\infty}\right) \tag{2.19}$$

By considering the limiting behavior of the exponential and complementary error functions, the short and long-time approximations for equation (2.18) follow easily:

Short-time approximation:

$$\frac{\Gamma(t)}{\Gamma_e} = \frac{2}{k_H}\left(\frac{Dt}{\pi}\right)^{1/2}\left[1 - \frac{(\pi D)^{1/2}}{2k_H}t^{1/2} + \ldots\right] \tag{2.20}$$

Long-time approximation:

$$\frac{\Gamma(t)}{\Gamma_e} = 1 - \frac{k_H}{(\pi D)^{1/2}}t^{-1/2}\left(1 - \frac{k_H}{2Dt} + \ldots\right) \tag{2.21}$$

For the higher bulk concentration, the thermodynamic equilibrium isotherm and Ward and Tordai expression have to be solved numerically together due to the nonlinearity of the Langmuir or Frumkin adsorption isotherms.

2.2.3 Mixed Diffusion/kinetic Model

In this model which is also called mixed kinetic model, the adsorption kinetics are not infinitely fast and time length scale of the kinetic adsorption is comparable with the one of the diffusion of monomers.

Sutherland[8] was the first one to solve the mixed kinetic model with linear Henry isotherm (equation (2.8)). The surface concentration $\Gamma(t)$ is given by:

$$\frac{\Gamma(t)}{\Gamma_e} = 1 - \frac{B}{B-A}\exp(A^2 Dt)erfc[A(Dt)^{1/2}] + \frac{A}{B-A}\exp(B^2 Dt)erfc[B(Dt)^{1/2}] \tag{2.22}$$

where

$$\mathbf{A} = \frac{-\sqrt{(\beta\Gamma_\infty)^2 - 4\alpha D} + \beta\Gamma_\infty}{2D} \tag{2.23}$$

$$B = \frac{\sqrt{(\beta\Gamma_\infty)^2 - 4\alpha D} + \beta\Gamma_\infty}{2D} \tag{2.24}$$

Considering the limiting behavior of the exponential and complementary error function can also get the short-time and long-time approximations:

Short-time approximation:

$$\frac{\Gamma(t)}{\Gamma_e} = \frac{\beta\Gamma_\infty t}{k_H}[1 - \frac{4\beta\Gamma_\infty}{3(\pi D)^{1/2}} t^{1/2} + ...] \tag{2.25}$$

Long-time approximation:

$$\frac{\Gamma(t)}{\Gamma_e} = 1 - \frac{k_H}{(\pi D t)^{1/2}}[1 - \frac{k_H^2}{2Dt} + \frac{k_H}{\beta\Gamma_\infty t} + ...] \tag{2.26}$$

For the higher concentrations, the mixed diffusion/kinetic transport has to be solved numerically. The work by several authors has been reviewed by Franses and Miller[1, 9-11].

2.2.4 Timescales Associated with the Transport

Two timescales are associated with the equilibration in the absence of the aggregates. The first, τ_k, is the kinetic time necessary for monomer in the sublayer to come to equilibrium in the absence of diffusion; this scale can be obtained form equation (2.1) by setting K=0 and C_s=C_0 and is given by $\tau_k = (\beta C_0 + \alpha)^{-1}$. The second, $\tau_D^{monomer}$, is the time diffusion of monomer in the bulk to reestablish a uniform spatial concentration for rapid surface kinetics. The amount of surfactant adsorbed onto the surface at equilibrium (Γ_e) can be viewed as diffusion from a bulk layer underneath the surface of thickness h that contains an equal amount of surfactants as that adsorbed at equilibrium on the surface[12].

Therefore $h = \frac{\Gamma_e}{C_o}$ and $\tau_D^{monomer} = \frac{h^2}{D} = \frac{\Gamma_e^2}{C_o^2 D}$ where D is the monomer diffusion coefficient.

Increasing the bulk concentration increases the kinetic and diffusional fluxes and (as reflected in the expressions for τ_k and $\tau_D^{monomer}$) decreases the tension relaxation timescale.

2.2.5 Experimental Methods for Measuring Equilibrium and Dynamic Surface Tensions

There are several methods for measuring equilibrium tensions at the air/liquid interface. Wilhelmy plate, drop weight, the shape analysis of pendant drops and bubble and the spinning drop, the maximum bubble pressure and oscillating jet methods, can all, in principle, be used to measure equilibrium surface tension as well as dynamic surface tension as surfactants adsorb onto the an initially clean interface.

These methods can be classified into three categories: force, shape, and pressure methods. With force methods one directly measures the surface tension as a "pull" or attractive force (or a "push" or repulsive force) on a partially immersed solid object, such as Wilhelmy plate. The major limitation of such methods is the uncertainty in the estimation of the contact angel between the immersed object and the solution, which is often assumed to be zero. Shape methods, such as the pendant or sessile drop, the sessile or captive bubble, and the spinning drop or bubble, indirectly measure the surface tension through knowledge of the surface shape in gravity or in a centrifugal field. The Laplace-Young equation is then used to relate the tension to the known pressure difference across the curved interface and the interfacial shape. In pressure methods, such as the bubble method or the maximum bubble pressure method, the Laplace-Young equation is used directly with the assumption that the bubbles are small enough to remain essentially spherical in gravity. For detailed description on surface tension measurement methods, see Refs[13, 14].

2.2.6 Determination of Kinetic Constants from Simulation and Experimental Data

For clean interface adsorption and re-equilibration, by modeling the kinetic exchange, and the bulk diffusive and convective transport (for measurements that involve

flow), the surface adsorption as a function of time can be predicted as a function of the surfactant transport parameters. The model prediction of the tension relaxation can be computed from the equation of state and, ideally, the kinetic constants and the diffusion coefficient can be inferred from a comparison of the model with the experimental results. The interpretation of the surface tension relaxation begins by assuming that kinetic exchange is very fast, and that the transport is diffusion controlled over the time scale (or frequency) of the experiment. An apparent monomer diffusion coefficient can be calculated with this assumption. In order to avoid the difficulty of measuring separately the diffusion coefficient of surfactant monomers by independent methods such as light scattering because of the very low monomer concentration, the apparent value is usually compared to the value obtained from the Stokes-Einstein equation (assuming some value for the hydrodynamic radius based on molecular considerations); if the apparent value is in reasonable agreement with the Stokes-Einstein value then no further interpretation of the experiment is done, the apparent value is considered as the diffusion coefficient, and the kinetic constants remain unresolved. If the apparent differs greatly from the Stoke-Einstein expectation, the transport process is either modeled as kinetic controlled, and comparison with data yields the kinetic parameters, or as mixed, kinetic constants and diffusion coefficients are derived from a fit of the data. Recently, research has shown in particular that by using high bulk concentrations of surfactant, the kinetic scale becomes progressively slower relative to diffusion, and kinetic effects can be ascertained and their kinetic measured.

Song et al. [15] determined the kinetic constants of the poly (ethylene glycol) alkyl ether surfactant $C_{14}E_6$ ($CH_3(CH_2)_{13}(OCH_2CH_2)_6OH$) by measuring the equilibrium and

dynamic surface tension below CMC, using the pendant bubble method. A schematic of the pendant bubble apparatus is shown in Figure 2.2. The pendant bubble technique can also be used as a film balance to obtain an accurate equation of state. In this method, a bubble is formed in a surfactant solution, and is allowed until equilibrium is reached. The bubble is then rapidly expanded or contracted, and the tension is simultaneously measured during the area change as described above, obtaining plots of the tension as a function of the area, which can be normalized to the initial area. For insoluble surfactants directly deposited on a pendant drop, the initial amount of surfactant is known, and the tension as a function of the surface concentration can be obtained[16, 17]. For soluble surfactants adsorbed from solution, the rapid expansions and contractions provide relative dilation rates much greater than those on a conventional planar trough, and thereby minimize exchange with the bulk. Consequently, plots of the tension as a function of the relative area can be reinterpreted as tension as a function of relative surface concentration[18].

2.2.7 Equilibrium Adsorption and Equation of State Measurements

The Frumkin adsorption model (Cf. Equation 2.1) including the intermolecular interaction can describe the $C_{14}E_6$ adsorption below CMC very well. Usually the model parameters are obtained by matching the equilibrium adsorption isotherm $\frac{\Gamma_e}{\Gamma_\infty} = \frac{[\beta C_o / \alpha]}{[\beta C_o / \alpha] + e^{K\Gamma_e / \Gamma_\infty}}$ and the equation of state (Cf. equation 2.4) for Frumkin rate law. But the difficulty of this approach arises due to the large amount of parameters, and the fitting is not unique and different sets of parameters can fit the experimental data equally well. Qing Song[15] used an alternate procedure in which the pendant bubble is used as a Langmuir trough to measure the equation of state directly, and then the equilibrium

parameter α / β is evaluated by fitting the absorption isotherm to the equilibrium surface tension versus log bulk concentration curve. This approached is given by Pan et al. in detail and will be summarized here[18]. At a given bulk concentration C_0, a pendant bubble is formed and then allowed to reach equilibrium with an equilibrium surface concentration Γ_e and surface tension γ_e. The bubble is then rapidly expanded and subsequently compressed (or compressed and then expanded). The tension $\gamma(t)$ is recorded as a function of the relative surface concentration Γ (t)/ Γ (γ =65 dyne/cm), where Γ (γ =65 dyne/cm) is the surface concentration corresponding to a surface tension at 65 dyne/cm. For the accuracy of the data, experiments are undertaken at different bulk concentration and repeated several times at the bulk concentration. It is shown that the correlation of all experimental data into one line verifies the conservation of mass and the fact that the equation of state is an instantaneous function of surface concentration. By fitting the experimental data to the Frumkin equation of state, $\Gamma_\infty = 3.32 \times 10^{-6}$ mol/m^2 and K=7.12 (indicating repulsion dominance) were found. It is also shown that the Frumkin model prediction agrees with the experimental data much better than the Langmuir model. The Frumkin model takes into consideration the parameter K, the effect of cohesive interactions between hydrocarbon chains, and the repulsive interactions of the ethoxylate headgroups. A negative K indicates that repulsion between the ethoxylated groups predominates over cohesion in monolayer.

Equilibrium surface tension measurement as a function of bulk concentration is carried out to find the kinetic constants ratio α / β by fitting the experimental data to Frumkin equilibrium adsorption isotherm (c.f. Equation 2.2). Instead of using the apparent concentration (C_{app}, the surfactant concentration in the solution poured into the

dish or cell), the corrected concentration (C_{app}-Γ_e(A/V)) is used when plotting the equilibrium surface tension as a function of bulk concentration, where A and V are the air/water interface area and solution volume respectively in the dish or cell. It is found $\alpha / \beta = 2.068 \times 10^{-6}$ mol/m^3 for Frumkin adsorption isotherm.

2.2.8 Dynamic Surface Tension Measurements and Determination of the Kinetic Constants

To determine the individual kinetic constants, the dynamics surface tension measurement is undertaken. Qing Song[15] detailed this measurement. As surfactant adsorbs onto the initially clean surface of an impulsively created pendant bubble, the surface tension relaxes. In predicting the relaxation, the unknowns are the monomer diffusion coefficient and the adsorption rate constant β (the equilibrium measurements provide the adsorption/desorption constants ratio α / β and therefore α once β is known; the maximum packing concentration and the intermolecular constant K are obtained from the fit of pendant bubble Langmuir trough data).

To model the relaxations, we should note first that in this pendant bubble technique, the bubble is created impulsively in less than a tenth of a second. Second, the hydrodynamic cleans after one second. The mass transfer after this one-second is modeled. The theoretical framework of the mass transfer below CMC is resolved in spherical coordinate:

$$\frac{\partial C}{\partial t} = D \frac{1}{r^2} \frac{\partial}{\partial r} (r^2 \frac{\partial C}{\partial r}) \tag{2.27}$$

$$\frac{d\Gamma(t)}{dt} = D \frac{dC(r,t)}{dr}\Big|_{r=a} \tag{2.28}$$

with the initial and boundary conditions:

$$C(r, t = 0) = C_0 \tag{2.29}$$

$$\Gamma(t = 0) = 0 \tag{2.30}$$

$$C(r = \infty, t) = C_0 \tag{2.31}$$

$$C(r = a, t) = C_s(t) \tag{2.32}$$

where C(r,t) is the monomer concentration, Γ is the surface concentration, t is the time, D is the monomer diffusion coefficient, r is the distance from the spherical surface, C_0 is the initial bulk concentration and C_s is the sublayer monomer concentration, a is the pendant bubble radius. By Laplace transform, the solution to the above equations can be expressed in term of the unknown term C_s:

$$\Gamma(t) = 2\sqrt{\frac{D}{\pi}}\left[C_0\sqrt{t} - \int_0^{\sqrt{t}} C_s(t-\tau)d\sqrt{\tau} \right] + \frac{D}{a}\left[C_0 t - \int_0^t C_s(r = a, \tau)d\tau \right] \tag{2.33}$$

Equation (2.33) is solved together with Frumkin rate law expression (Cf. equation (1)) numerically to obtain surface concentration $\Gamma(t)$ and C_s(t) as functions of time. The equation of state for Frumkin adsorption isotherm (Cf. equation 2.4) is then used to obtain the dynamic tension relaxation. In predicting the relaxation, the unknowns are the monomer diffusion coefficient and the adsorption rate constant β. Simulation are run varying D and β until the predicted relaxations fit the experimental data at all the bulk concentrations. The result is shown in Figure 2.3. D=6.0 $\times 10^{-10}$ m^2/s and β =4.0 $m^3/(mol \cdot s)$ are obtained when the theoretical simulations fits the dynamics relaxation best.

2.3 Theories and Models on Multicomponent Equilibrium Adsorption Isotherms

2.3.1 General Criteria for Thermodynamically Consistent Multicomponent Equilibrium Adsorption Isotherms for Ideal Solution

Though Langmuir isotherm and sets of improved Langmuir isotherms like Frumkin isotherm and generalized Langmuir isotherms are the most popular adsorption isotherms used nowadays, these equations for multicomponent systems have been reported by several authors to be thermodynamically inconsistent, meaning Gibbs adsorption isotherm is not satisfied. These isotherms do not account for the difference of the adsorbing molecule size and adsorption capacities, thus they could introduce error for multicomponent adsorptions of different molecular size and adsorption rate.

Levan and Vermeulen [19] used an integral method to determine whether the isotherm is thermodynamically consistent or not. A general criteria was developed by Franses et al. for testing binary isotherms for necessary conditions for thermodynamic consistency for ideal solutions[20]. The criteria are briefly described here.

For a dilute solutions of two components 1 and 2 in a solvent, the solution is assumed to be ideal and Gibbs adsorption isotherm which relates the surface tension γ with Γ_1, Γ_2, C_1 and C_2 as follows:

$$-\frac{d\gamma}{RT} = \Gamma_1 d\ln C_1 + \Gamma_2 d\ln C_2 = \frac{\Gamma_1}{C_1} dC_1 + \frac{\Gamma_2}{C_2} dC_2 \tag{2.34}$$

where Γ_1 (C_1) and Γ_2 (C_2) is the adsorbed solute concentration at equilibrium with bulk concentrations C_1 and C_2. The Gibbs adsorption rests on the foundation of classical surface thermodynamics and is consistent with the Gibbs-Duhem equation. The fact that

sum $\frac{\Gamma_1}{C_1}dC_1 + \frac{\Gamma_2}{C_2}dC_2$ must be an exact (or total) differential of the state function -γ/RT requires that the mixed second partial derivatives of any differentiable function must be equal, that is:

$$\frac{\partial^2 \gamma}{\partial C_1 \partial C_2} = \frac{\partial^2 \gamma}{\partial C_2 \partial C_1} \tag{2.35}$$

From Equations (2.34) and (2.35), the general criteria for thermodynamic consistency of the equilibrium adsorption isotherm for ideal solution follows:

$$\frac{\partial}{\partial C_1}\left[\frac{\Gamma_1(C_1, C_2)}{C_2}\right] = \frac{\partial}{\partial C_2}\left[\frac{\Gamma_1(C_1, C_2)}{C_1}\right] \tag{2.36}$$

If the functions Γ_1 (C_1) and Γ_2 (C_2) do not satisfy Equation (2.36), then the expression -dγ/RT is an inexact differential, meaning that γ is not a state function and does depend on the integration path, which of course is false. Thus, if Equation (2.36) is not satisfied, then Γ_1 (C_1) and Γ_2 (C_2) violate the combined first and second law of thermodynamics from which the Gibbs adsorption isotherm is derived, which means Γ_1 (C_1) and Γ_2 (C_2) are thermodynamically inconsistent.

2.3.2 Binary/multicomponent Adsorption Equilibrium Isotherms for Ideal Adsorption Solution

Multicomponent adsorption at air/water interface has attracted the interest of researchers over the decades because of its practical importance in foams, emulsions, catalysis, detergency and certain separation techniques[21-24]. For the milticomponent systems of molecules of different molecule size, the description of equilibrium adsorption is quite difficult. The simplest and most convenient way is that the adsorption equilibrium isotherm is represented by explicit equations. That is why the most widely used models

are those based on the Langmuir adsorption and have only two or three parameters. Since the Langmuir isotherm, or the modified form is only valid when each molecule is only associated with one site, and molecules occupying different sites do not interact, the Langmuir based isotherm for multicomponent adsorption contains only parameters of the single component isotherm, without introducing additional mixing parameters. This is usually preferred if those forms can be shown to be both realistic and theoretically valid and it is not necessary to experimentally obtain any multicomponent parameters.

2.3.2.1 Adsorption Isotherms of Single Component System

For single-component system, the Langmuir and Freundlich isotherms are the most popular two-parameter isotherm equations. The Langmuir isotherm is written here as:

$$\Gamma = \Gamma_{\infty} \frac{KC}{1 + KC} \tag{2.37}$$

where Γ_{∞} is the maximum surface concentration and K is equilibrium Langmuir constant.

The Freundlich isotherm is given here as:

$$\Gamma = K' C^{n} \tag{2.38}$$

where K′ and n are Freundlich isotherm constants.

2.3.2.2 Langmuir-based Equilibrium Adsorption Isotherm for Binary/multicomponent Systems

The generalized Langmuir isotherm obtained by Bulter and Ockrent[25] and Markhan and Benton[26] on the basis of kinetic consideration alone is the widely used isotherm for multicompnent systems. For binary system with solute 1 and 2 in solvent, the surface concentration of the two species are given as explicit function of bulk concentration C_1 and C_2:

$$\Gamma_1 = \Gamma_{\infty 1} \frac{K_1 C_1}{1 + K_1 C_1 + K_2 C_2} \tag{2.39}$$

$$\Gamma_2 = \Gamma_{\infty 2} \frac{K_2 C_2}{1 + K\ C_1 + K_2 C_2} \tag{2.40}$$

where $\Gamma_{\infty 1}$ and $\Gamma_{\infty 2}$ are the maximum surface concentration, K_1 and K_2 are equilibrium Langmuir constant of single components 1 and 2, respectively. Using the criteria Equation (2.36), the generalized Langmuir Isotherm is thermodynamic consistent only if:

$$\Gamma_{\infty 1} \frac{K_1 K_2}{(1 + K_1 C_1 + K_2 C_2)^2} = \Gamma_{\infty 2} \frac{K_1 K_2}{(1 + K_1 C_1 + K_2 C_2)^2} \tag{2.41}$$

This equation is only valid if $\Gamma_{\infty 1} = \Gamma_{\infty 2}$, which obviously would not be true if the adsorbing molecules are of different size of adsorption capacities, $\Gamma_{\infty 1} = \Gamma_{\infty 2}$. Thus the generalized Langmuir isotherms Equations (2.39) and (2.40) are thermodynamically inconsistent.

Utilizing the integral method, Levan and Vermeulen[19] developed the two- and three-term binary Langmuir adsorption isotherms. For two-term, surface concentration of component 1 is

$$\Gamma_1 = \frac{\overline{\Gamma_m} K_1 C_1}{1 + K_1 C_1 + K_2 C_2} + \Delta L_2 \tag{2.42}$$

surface tension is

$$\gamma = \gamma_0 - RT\overline{\Gamma_m} \ln(1 + K_1 C_1 + K_2 C_2) \tag{2.43}$$

where $\overline{\Gamma_m} = \dfrac{\Gamma_1 K_1 C_1 + \Gamma_2 K_2 C_2}{1 + K_1 C_1 + K_2 C_2}$ (2.44)

$$\Delta L_2 = (\Gamma_1 - \Gamma_2) \frac{K_1 C_1 K_2 C_2}{(K_1 C_1 + K_2 C_2)^2} \ln(K_1 C_1 + K_2 C_2) \tag{2.45}$$

The expressions for component 2 can be obtained by interchanging the component subscript in Equations (2.42) - (2.45). Since, the integral method bases on the Gibbs adsorption isotherm, isotherm Equation (2.42) is thermodynamically consistent.

Franses et al.[20] applied the ideal adsorbed solution theory of Myers and Prausnitz[27], and assume there is no area change upon mixing. The framework of this theory satisfies the thermodynamic consistency criteria. The surface concentration of component 1 and 2 depending on the bulk concentration c_1 and c_2 are obtained as

$$\frac{\Gamma_1\left[\Gamma_1 + K_1C_1(\Gamma_1+\Gamma_2)\right]}{\Gamma_{\infty 1}K_1C_1} + \frac{\Gamma_2\left[\Gamma_2 + K_2C_2(\Gamma_1+\Gamma_2)\right]}{\Gamma_{\infty 2}K_2C_2} = \Gamma_1 + \Gamma_2 \tag{2.46}$$

and

$$1 + K_2C_2\left(\frac{\Gamma_1+\Gamma_2}{\Gamma_2}\right) = \left[1 + K_1C_1\left(\frac{\Gamma_1+\Gamma_2}{\Gamma_1}\right)\right]^{R_\Gamma} \tag{2.47}$$

where $R_\Gamma=\Gamma_{\infty 1}/\Gamma_{\infty 2}$

The function $\gamma(C_1, C_2)$ and surface equation of state $\gamma(\Gamma_1, \Gamma_2)$ can also be obtained. These solutions cannot be put in an explicit analytical form.

2.3.2.3 Freundlich-based Equilibrium Adsorption Isotherm for Binary/multicomponent System

Digiano et al. used the ideal adsorbed solution theory to obtain such an isotherm in the case that all components have the same Freundlich exponent. For binary system, their result can be written as

$$\Gamma_i = \frac{K_i'^{1/n}C_i}{(K_1'^{1/n}C_1 + K_2'^{1/n}C_2)^{1-n}} \qquad (\text{i=1 or 2}) \tag{2.48}$$

Using criterion Equation (2.36), it can be easily shown that the Freundilich binary isotherm is valid only if $n_1=n_2$. This result is also obtained with the integral method by Rudisill and Levan[28].

The ideal adsorbed solution theory was also used to predict binary adsorption equilibria by a trial- and-error procedure of species obeying the pure component equations. Myers and Moser [29] used this method for the Langmuir isotherm. Fritz and Schlunder[30] used it for a piecewise continuous Freundlich isotherm.

Sheindorf et al.[31] derived a multicomponent Freundlich isotherm by assuming that an exponential distribution of adsorption energies exists for each component. For a binary system, their result can be written as

$$\Gamma_1 = \frac{K_1' C_1}{(C_1 + a_{12} C_2)^{1-n_1}} \tag{2.49}$$

$$\Gamma_2 = \frac{K_2' C_2}{(a_{12}^{-1} C_1 + C_2)^{1-n_2}} \tag{2.50}$$

Using criterion Equation (2.36), this binary adsorption isotherm is valid only if $n_1=n_2$ and $a_{12}=(K_2' / K_1')^{1/n}$, which reduces to Digiano's result. This result is also obtained with the integral method by Levan and Vermeulen[19].

Utilizing the integral method, Levan and Vermeulen[19] developed the two- and three-term binary Freundlich isotherm. The two-term is

$$\Gamma_1 = \frac{\bar{n} K_1' C_1}{(K_1' C_1 + K_2' C_2)^{1-\bar{n}}} + \Delta F_2 \tag{2.51}$$

$$\gamma = \gamma_0 - RT\ (1 + K_1' C_1 + K_2' C_2)^{\bar{n}} \tag{2.52}$$

where $$\bar{n} = \frac{n_1 K_1' C_1 + n_2 K_2' C_2}{K_1' C_1 + K_2' C_2} \tag{2.53}$$

$$\Delta F_2 = (n_1 - n_2)\frac{K_1' C_1 K_2' C_2}{(K_1' C_1 + K_2' C_2)^{2-\bar{n}}} \ln(K_1' C_1 + K_2' C_2) \tag{2.54}$$

Similarly, the isotherm for component 2 can be obtained by interchanging the component subscripts in Equations (2.51)-(2.54). The isotherms are thermodynamically consistent by the virtue of the integral method.

2.3.2.4 Scaled Particle Theory Isotherms

The Scaled particle theory isotherms were derived based on kinetic and molecular theory considerations, using the scaled-particle theory for two component mixture of hard circular disks of diameters σ_1 and σ_2 with 2 as the larger disk. Equilibrium adsorption isotherms are obtained as

$$C_1 = \frac{\theta_1 \exp A}{K_1(1-\theta_1-\theta_2)} \tag{2.55}$$

$$C_2 = \frac{\theta_2 \exp B}{K_2(1-\theta_1-\theta_2)} \tag{2.56}$$

where $R_\sigma \equiv \frac{\sigma_2}{\sigma_1}$, $\theta_1 = \frac{\Gamma_1}{\Gamma_{\infty 1}}, \theta_2 = \frac{\Gamma_2}{\Gamma_{\infty 2}}$

$$A(\theta_1,\theta_2) = \frac{3\theta_1 + \frac{1}{R_\sigma}\left(\frac{1}{R_\sigma}+2\right)\theta_2}{1-\theta_1-\theta_2} + \frac{\left(\theta_1 + \frac{1}{R_\sigma}\theta_2\right)^2}{(1-\theta_1-\theta_2)^2} \tag{2.57}$$

$$B(\theta_1,\theta_2) = \frac{3\theta_2 + R_\sigma(R_\sigma+2)\theta_1}{1-\theta_1-\theta_2} + \frac{(\theta_2 + R_\sigma\theta_1)^2}{(1-\theta_1-\theta_2)^2} \tag{2.58}$$

These equations account kinetically and molecularly for the available areas for disks of different sizes (R_σ) and the exponential terms account better for steric effects at high coverage. After some algebra manipulation (the derivation is omitted here), it can be shown that the Scaled Particle theory isotherms Equations (2.55) and (2.56) satisfy the

general criteria Equation (2.36) and are thermodynamically consistent with the Gibbs adsorption isotherm.

For one component, or setting θ_2=0, the modified Langmuir isotherm is obtained as

$$KC = \left(\frac{\theta}{1-\theta}\right)\exp\left(\frac{3\theta}{1-\theta}+\frac{\theta^2}{(1-\theta)^2}\right) \tag{2.59}$$

and the corresponding equation of state

$$\Pi(\theta) = RT\Gamma_\infty^*\left[\frac{\theta}{(1-\theta)^2}\right] \tag{2.60}$$

where $\theta = \Gamma/\Gamma_\infty^*$, the superscript * is used to differentiate the generalized Langmuir parameter Γ_∞^* from the Langmuir parameter Γ_∞ since they are generally different. Using the framework of ideal adsorbed solution theory together with the modified Langmuir adsorption isotherm Equation (2.59), Franses et al. [20] derived the ideal adsorbed solution model for binary component as

$$K_iC_i^o = \left(\frac{\theta_i^o}{1-\theta_i^o}\right)\exp\left(\frac{3\theta_i^o}{1-\theta_i^o}+\frac{\theta_i^{o2}}{(1-\theta_i^o)^2}\right) \tag{2.61}$$

and

$$\Pi_i^o = RT\Gamma_{\infty i}^*\left[\frac{\theta_i^o}{(1-\theta_i^o)^2}\right] \tag{2.62}$$

where $\theta_i^o = \frac{\Gamma_i^o}{\Gamma_{\infty i}^*}$, $\Gamma_i^o = \Gamma_{\infty i}^*\left(\frac{K_iC_i^o}{1+K_iC_i^o}\right)$, (i=1, 2)

$C_i^o(\Pi_i^o)$ is the concentration of pure component i at the same surface pressure $\Pi_1^o = \Pi_2^o = \Pi$ as the mixed solution.

2.4 Theories and Experiments on the Transport of Surfactant onto a Clean Air/Water Interface from Aqueous Solutions above the Critical Micelle Concentration

2.4.1 Background

In the surfactant solution with concentration above the CMC, the monomer concentration is approximately constant, and excess surfactant is incorporated into the aggregates. The fact that the monomer concentration remains fixed for C_o>CMC and yet the tension relaxation continues to shorten indicates that micelles are accelerating the transport of surfactant to the clean interface. In a mixture solution of monomers and micelles, monomers and micelles are in dynamic equilibrium. Upon the creation of a clean interface in the micellar solution, the adsorption of the surfactant monomers from the sublayer upsets the local micelle-monomer equilibrium, causing the micelles to dissociate. This results in a diffusive flux of micelles to the surface to restore the equilibrium. At the mean time, monomers from the monolayer can desorb from the surface. The diffusive transport of micelles and monomers, kinetic adsorption/desorption of monomers, as well as the kinetic of micellar break-up, determine the rate of dynamic surface tension reduction. A general picture of surfactant monomer and micellar diffusive transport and kinetic exchange above the CMC is shown in Figure 2.4.

2.4.2 Micellization Kinetics

2.4.2.1 Structure of Micelles

The forces between the amphiphilic molecules are very important in determination of structure of aggregates in the solutions. The attractions between the hydrophobic groups induce the molecules to associate, while the repulsion between the hydrophilic groups restrain the growth of aggregates. Out of these two interactions, one tends to decrease and

the other tends to increase the interfacial area per molecule. So the repulsive head group forces and attractive hydrophobic interfacial forces will determine the optimum head group area.

Israechivili [32]examined the shapes of micelles based on the molecular packing consideration. The geometry or packing properties of these molecules depend on their optimal area a, the volume v of their hydrocarbon chain or chains, and the maximum effective length that chains can extend. This length is called critical chain length l_c, which is of the same order as, though somewhat less than, the fully extended molecular length of the chains l_{max}. The critical chain length l_c sets a limit on chain extension. The fully extended molecular length is given by Tanford for a saturated hydrocarbon chain with n carbon atoms:

$$l_c \le l_{\max} \approx (0.154 + 0.1265n) \text{ nm and } v \approx (27.4 + 26.9n) \times 10^{-3} \text{ nm}^3 \quad (2.64)$$

Once the optimal surface area a, hydrocarbon chain volume v and critical length l_c are specified for a given surfactant molecule, the structure which molecules could pack into consistent with these geometric constraints will be determined. a, v and l_c could be measured or estimated. What Israelachivili[33] had also shown is that the value of the dimensionless packing parameter or shape factor, $\frac{v}{al_c}$ will determine whether they will form spherical micelles ($\frac{v}{al_c} < \frac{1}{3}$), cylindrical micelles ($\frac{1}{3} < \frac{v}{al_c} < \frac{1}{2}$), vesicles or bilayers ($\frac{1}{2} < \frac{v}{al_c} < 1$), planer bilayers ($\frac{v}{al_c} \approx 1$), or the inverted structures ($\frac{v}{al_c} > 1$).

The micelle aggregation number is usually measured by light scattering, diffusion, sedimentation velocity, sedimentation equilibrium, ultrasonic absorption, and time-

resolved fluorescence. Generally, the greater the "dissimilarity" between the surfactants and solvent is, the greater the aggregation number is. Thus for polyoxyethylenated nonionic surfactants, the aggregation number tends to increase with the increasing length of the hydrophobic groups, and decreases in the number of oxyethylene units surfactants. The temperature has a great effect on the aggregation too. An increase in temperature can cause a large increase in the aggregation number for this kind of surfactants. As to the ionic surfactants, the binding of the counterions to the micelles will contribute to the aggregation number, and the addition of neutral electrolytes also increases the aggregation number. The temperature has a small influence in the aggregation number for this kind of surfactants.

2.4.2.2 Experiment and Theory on Micellization Kinetics

The micelle population density is polydisperse in the number of monomer per micelles, with a rather sharp distribution that can be approximated by a Gaussian function. Experiments applying fluorescence and light scattering techniques[34] have shown that the monomer number per micelle range from roughly 10 to 100.

In the mixture solution of monomer and micelle, the molecules in micelles are constantly being exchanged with monomers in the bulk solution, and micelles are in dynamic equilibrium with the monomers in the bulk solution.

To incorporate the release of monomer from aggregates when the equilibrium is perturbed, the step-wise association model has been used. In this model, aggregates are built up by the sequential addition of monomer to form a polydisperse population with aggregate species S_i containing *i* monomers per aggregate:

$$S_i + S \underset{\mathbf{k_{-i}}}{\overset{\mathbf{k_i}}{\rightleftharpoons}} S_{i+1}; i = 1,2... \tag{2.65}$$

where k_i and k_{-i} are the rate constants for the forward and backward steps of the addition of monomer to species S_i to form S_{i+1} and are different for each association step. The aggregation is cooperative when the equilibrium constant $K_i = \frac{k_i}{k_{i-1}}$ increases with i, and anti-cooperative when K_i decreases with i. Cooperativity is due to the hydrophobic effect and is responsible for the formation of large aggregates rather than molecular clusters, and anti-cooperativity, is due to the repulsion in the headgroups, and insures that the micelle size remains finite[35-38]. This competition gives rise to a characteristic size distribution curve (Figure 2.5) consisting of monomers and oligomers ($1<i<S_1$), a region abundant in micelles ($S_2<i<S_3$) centered about a maximum with aggregation number σ, and a region in-between in aggregate space ($S_1<i<S_2$) in which the concentrations of aggregates are small.

Experimental measurements of the micelle assembly and disassembly in the absence of transport gradients (i.e. uniform concentrations) have been widely undertaken, and interpreted using the step wise model to obtain the kinetic constants of the model. Experimental techniques disturb equilibrium concentrations of the aggregates (spatially uniformly) by subjecting an equilibrium solution to either a temperature or pressure jump or an ultrasonic disturbance, or by dilution by mixing with a solution below the CMC as in a stopped-flow experiment (for a review, see Kahlweit and Teubner[39]). The re-equilibration of aggregate and monomer concentrations is followed by conductivity measurements (for ionic surfactants) or for nonionic surfactants by fluorescence or extinction coefficient measurements of dye molecules partitioning between the micellar and solution phases. These experiments usually fit the micelle and monomer concentration relaxations to exponential profiles, and first obtain characteristic time

constants. Most studies find that the re-equilibration time is characterized by two time constants, a fast relaxation (τ_F) which is in the range of 10^{-6}-10^{-3} sec and a slow relaxation (τ_{SL}) which is in the range of 10^{-3}-10 sec. In the fast relaxation process, the number of micelles does not change. However, due to the imposed disturbance, single monomers exchange with the micelles, leading to the change of micellar size either by incorporating or releasing monomers (Figure 2.6.a). In the slow relaxation process, micelles breakdown or form by releasing or adding monomers, leading to the change of the micellar number (Figure 2.6.b).

Aniansson and Wall [40-42] have shown how the existence of these two relaxation times can be understood in terms of the step-wise aggregation model. When equilibrium is disturbed the kinetic fluxes to restore equilibrium scale as $k_i[S_i][S]$ and $k_{-i}[S_{i-1}]$. In the abundant micelle region, the concentrations are large compared to the rare aggregate region and therefore the kinetic exchange is much faster in this region. As a result, the first kinetic response of the system to a dilution perturbation (as for example in a stop flow experiment) is the release of monomers from the abundant micelles and the shift of the distribution to the edge of the rare aggregate space with the number of aggregates in this region remaining constant. The fast time constant observed experimentally is then the rapid release of single monomers from the abundant micelles. The second response of the system is the slow cascading breakdown of the abundant micelles through the space of the rare aggregates with the abundant micelle space remaining in a quasi-equilibrium state (Figure 2.7). The experimentally observed slow time constant reflects this slow, step-wise, complete break-up of the abundant micelles through the rare-aggregate stage.

Aniansson and Wall have obtained analytical expressions for the fast and slow time steps for small perturbations from equilibrium in terms of the rate constants of the elementary steps, and these have been used to obtain the rate constants of these steps by comparison with the perturbation experiments. They applied the step-wise model for the kinetic processes of micelle formation and disintegration. Given the concentration of the species C_s, the kinetic equations for the bulk concentration of the species $C_s(t)$ are:

$$\frac{dC_1}{dt} = -2J_2 - \sum_{s=3}^{s3} J_s \tag{2.66}$$

$$\frac{dC_s}{dt} = J_s - J_{s+1}, \qquad \text{s=2,3,4…s}_3 \tag{2.67}$$

where $J_s(t)$ is the total rate of the s-th reaction:

$$J_s = k_x^+ C_1 C_{s-1} - k_s^- C_s \qquad \text{s=2,3,4…s3} \tag{2.68}$$

At equilibrium $J_s=0$ and above equation gives following relation:

$$k_s^+ / k_s^- = \overline{C}_s / (\overline{C_1}\,\overline{C_{s-1}}) \tag{2.69}$$

The mass balance of free and aggregated monomer is:

$$\sum_{s=1}^{s=s_3} sC_s = \overline{C} \tag{2.70}$$

Introducing the relative deviation from the equilibrium concentration:

$$\xi_s(t) = \frac{C_s - \overline{C_s}}{\overline{C_s}}, \qquad \text{s=1,2,3…s3} \tag{2.71}$$

So the flux could be expressed as:

$$J_s = k_s^- \overline{C_s}\left[\xi_1(1+\xi_{s-1}) + \xi_{s-1} - \xi_s\right] \tag{2.72}$$

Aniansson and Wall also analyzed the re-equilibrium process from small deviations from equilibrium. Using the above formulation, the relaxation time for the slow process was obtained as:

$$\frac{1}{\tau_{sl}} = \frac{1}{R\overline{C_1}\beta_m} \frac{n_2\beta_n + m_2\beta_m}{n_2\beta_n + \sigma_m^2\beta_m} \tag{2.73}$$

Here $m_2 = m^2 + \sigma_m^2 = \sum_{s_2+1}^{s_3} s^2 \overline{C_s} / \overline{C_m}$ (2.74)

$$n = \sum_{1}^{s_1} s\overline{C_s} / \overline{C_n} \tag{2.75}$$

$$n_2 = n^2 + \sigma_n^2 = \sum_{1}^{s_1} s^2 \overline{C_s} / \overline{C_n} \tag{2.76}$$

$$\overline{C_n} = \sum_{1}^{s_1} \overline{C_s} \tag{2.77}$$

$$R = \sum_{s_1+1}^{s_2} (k_s^- \overline{C_s})^{-1} \tag{2.78}$$

Where m_2 and n_2 are the second moments of the micelle and bloomer size distributions; σ_n and n are the dispersion and the mean aggregation number of the bloomers; $\overline{C_n}$ is the total bloomer concentration; $\beta_n = \overline{C_n} / \overline{C_1}$; R is termed the resistance of the transition region.

In order to derive an expression for the fast process relaxation time, Aniasson and Wall assumed that the size distribution of the abundant micelles is broad enough to be considered as continuous. They assume the following Gaussian size distribution:

$$C_s = C_{\max} \exp(-\frac{(s-m)^2}{2\sigma_m^2}) \tag{2.79}$$

where m is the mean aggregation number and σ_m is the dispersion. Using this distribution, Aniansson and Wall showed that:

$$\frac{1}{\tau_F} = \frac{k_m^-}{\sigma_m^2}(1+\sigma_m^2\beta_m) \tag{2.80}$$

$$\text{where } k_m^- = \sum_{s_2+1}^{s} k_s^- \overline{C_s} / \overline{C_m} \tag{2.81}$$

$$\overline{C_m} = \sum_{s_2+1}^{s_3} \overline{C_s} \tag{2.82}$$

$$m = \sum_{s_2+1}^{s_3} s\overline{C_s} / \overline{C_m} \tag{2.83}$$

$$\beta_m = \overline{C_m} / \overline{C_1} \tag{2.84}$$

k_m^- is the mean dissociation rate constant of the micelles; $\overline{C_1}$ is the concentration of the free monomers (for non-ionic surfactants $\overline{C_1} = CMC$); $\overline{C_m}$ is the total concentration of the micelles ($\overline{C_m} \approx \left(\overline{C} - \overline{C_1}\right)/m\overline{C_1}$); $\overline{C_s}$ is the s-mer concentration; $\overline{C}$ is the total surfactant concentration; m is the mean aggregation number of the abundant micelles. (The bars indicate equilibrium values).

From above equations, we can see that there is a linear relationship between $1/\tau_F$ and the total surfactant concentration, which is in agreement with experiments. In practice, as the total surfactant concentration increases, the number of micelles increases which results in a decrease in intermicellar distance. So, the time period for a monomer to colloid with a micelle is shorter at higher surfactant concentration. The magnitude of

τ_F depends on the length of the hydrocarbon chain of the surfactant: the shorter the chain length, the faster is the relaxation time, since the micelles are moving loosely packed structures for shorter chain surfactants.

2.4.3 Theories and Experiments on the Transport of Surfactant onto a Clean Air/water Interface from Aqueous Solutions above Critical Micelle Concentration

2.4.3.1 Nth Order Reaction and Mono-dispersed Micelle Scheme

There has been limited work on the kinetic of adsorption from micellar solutions both theoretically and experimentally. Several researchers have attempted to use the stepwise model to formulate reaction diffusion equation to describe the influence of the micelles on the transport. The simplest is to focus only on the slow step of the process (i.e. to model the breakdown of the abundant micelles through the rare aggregate cascade), and model this breakdown (and reformation) by assuming an Nth order reaction scheme: $NS \underset{k_{-N}}{\overset{k_N}{\rightleftarrows}} S_N$ where N is the aggregate number for the largest micelle. In this framework, the micellar solution is considered to be composed of monomer and a mono-dispersed distribution of micelles with aggregation number N, and the diffusive-kinetic conservation equations for the monomer and the micelle are solved using the Nth order reaction rate formulation; thus for the rate of production of monomer $\mathrm{R} = \mathrm{k}_{-\mathrm{N}}[\mathrm{S}_\mathrm{N}] - \mathrm{k}_\mathrm{N}[\mathrm{S}]^\mathrm{N}$. Lucassen[43] used this approach and made the first attempt to describe quantitatively the transport from a micellar solution to an oscillating bubble interface from micellar solutions. Later, Miller[44] used this approach to a clean interface and solved the respective diffusion equations for the monomers and the monodisperse micelles using the same model. Both Henry adsorption isotherm and Langmuir adsorption isotherm were used in computation, and the numerical results demonstrated

that the adsorption relaxation in the presence of micelles is faster that that of below the CMC.

Joos and J. Van Hunsel [45]applied the same approach for the interpretation of the experimental data for the dynamic surface tension of micellar solution, in which the effect of the micelles is accounted for by an effective diffusivity of the monomers. Joos et al[46] attended to account for the micellization kinetic by adding an additional term proportional to the deviation of the monomer concentration from the equilibrium value in the diffusion equation of monomer. This approach is equivalent to the pseudo-first-order reaction (PFOR) model, which is widely used in the chemical kinetics. Under the assumption that the diffusion of the micelles could be neglected, they solved the respective boundary value problem using the concept of a diffusion penetration depth.

2.4.3.2 Models for System With Small Departure from Equilibrium

Fainerman[47] first attempted to use the mathematical framework of the Annianson and Wall theory to develop in a consistent way conservation equations for monomers and micelles that account for bulk diffusion as well as the kinetics of micelle breakdown, assuming small deviations from equilibrium and an infinitely fast exchange of surfactant between the sublayer and surface. He examined two regimes, one in which the time scales for monomer and micelle diffusion are of the order of the slow micellization kinetic scale ($\frac{\tau_D^{monomer}}{\tau_{SL}} = O(1); \frac{\tau_D^{micelle}}{\tau_{SL}} = O(1)$) and one in which these scales are of the order of the fast micellization kinetic scale ($\frac{\tau_D^{monomer}}{\tau_F} = O(1); \frac{\tau_D^{micelle}}{\tau_F} = O(1)$). For the case in which $\frac{\tau_D^{monomer}}{\tau_{SL}} = O(1); \frac{\tau_D^{micelle}}{\tau_{SL}} = O(1)$ Fainerman (see also Dushkin and Ivanov[48-50] and

Noskov [51]) showed that the conservation equation for a small deviation of the monomer concentration from equilibrium ($\xi_1 = \frac{C_1 - C^*}{C^*}$) can be written in the form of a pseudo first order reaction (PFOR) as: $\frac{d\xi_1}{dt} = D\frac{\partial^2 \xi_1}{\partial x^2} - \frac{1}{\tau_{SI}}\xi_1$ where τ_{SL} is Aniansson and Wall's analytical expression for the timescale for the slow kinetic process. The slow time scale equations were used to describe surfactant transport from micellar solutions to an expanding bubble in the maximum bubble pressure method; comparison of the simulations with measurements of the tension reduction provided a measurement of τ_{SL}, and were shown to compare favorably with direct measurements of τ_{SL} [52-54]. A similar approach has been used by Danov et al to describe transport to an interface whose equilibrium monolayer has been perturbed[55].

2.4.3.3 Models for System With Large Departure from Equilibrium

Most of the research on dynamic adsorption from micellar solutions have been based on the experiment measuring dynamic surface tension, where the creation of a clean interface from surfactant micellar solution definitely leads to significant deviations from equilibrium, and consequently to non-linear process in the system.

The application of the step-wise model to systems far from equilibrium is much more complex than its application to the case when the monomer-micelle equilibrium experiences a small deviation since the entire nonlinear kinetics has to be specified rather than its small deviation approximation. One approach, is to solve the transport equations with a simplified model for the nonlinear kinetics; this approach has begun with the study of Franses, Basaran and coworkers [56].

Qing Song, rather than specify the nonlinear kinetics, took a different approach to the transport modeling which does not require the specification of the kinetics and yet will be capable of predicting tension reductions specifically in the industrial relevant cases of high micellar concentration. This approach will be summarized here.

The assumptions that micellar breakup is infinitely fast compared to the monomer and micellar diffusion and that the micellar breakup is not the limiting step, are made and verified. Consider a clean interface adsorption to a planar surface from a micellar solution in which the monomer concentration is maintained at CMC and micellar concentration is $C^0_{Micelle}$. The maximum rate, at which bulk monomer diffusion proceeds, is obtained when the sublayer concentration remains zero; the adsorption under these condition is given by $\Gamma(t) = 2C_{CMC}\sqrt{\frac{Dt}{\pi}}$ and the time for an equilibrium monolayer to form is therefore $\tau^{Monomer}_{Diffusion} = \pi\frac{\Gamma_e^2}{4DC_{CMC}^2}$. Similarly, the diffusion time scale for the micelle is $\tau^{Micelle}_{Diffusion} = \pi\frac{\Gamma_e^2}{4(\sigma C^0_{Micelle})^2 D_{Micelle}}$. The rate at which kinetics exchange alone delivers material to the surface can be obtained by integrating the adsorption isotherm for the sublayer concentration equal to CMC (i.e. no bulk diffusion); for the Langmuir equation the kinetic adsorption is given by $\Gamma(t) = \Gamma_e(1 - e^{-(\alpha+\beta C_{CMC})t}$, and the characteristic time to achieve equilibrium is given by $\tau^{Monomer}_{Kinetic} = \frac{1}{(\alpha + \beta C_{CMC})}$. By applying the parameters for $C_{14}E_6$, above characteristic time scales are given in Table 2.1.

As we can see from Table 2.1, the time scale for micelle breakup is smallest compared to the diffusion of the monomers and the micelle, as well as kinetic exchange.

Thus the assumption that the micelle breakup is infinitely fast compared to the monomer and micelle diffusion as well as kinetics.

With the infinitely fast micellar kinetics, micelles act as reservoirs to maintain the monomer concentration at CMC; thus if micelles are present in a region of solution domain, the monomer concentration is kept at CMC value; if micelles are not present, the monomer concentration is less than CMC.

Table 2.1: Characteristic Time Scales of Nonionic Surfactant at Different Surfactant Concentrations for $C_{14}E_6$

Surfactant Concentration (mol/m^3)	1.27 CMC	2.0 CMC	3.0 CMC	4.0 CMC
$\tau_{Diffusion}^{Monomer} = \pi \frac{\Gamma_e^2}{4DC_{CMC}^2}$ (s)	205.2	205.2	205.2	205.2
$\tau_{Diffusion}^{Micelle} = \pi \frac{\Gamma_e^2}{4(\sigma C_{Micelle}^0)^2 D_{Micelle}}$ (s)	11261.88	821	205.25	91.22
$\tau_{Kinetic}^{Monomer} = \frac{1}{(\alpha + \beta C_{CMC})}$ (s)	27.4	27.4	27.4	27.4
$\tau_{Micelle}^{Breakup}$ (s)	4~10	4~10	4~10	4~10
Whole dynamic surface tension relaxation time scale (s)	400	150	100	80

Song et al. examined the case at lower bulk micellar concentration, the micelle diffusive flux is slower than the kinetic exchange and the micelle bulk diffusion can not "keep up" with the kinetic adsorption of monomers from the sublayer to the surface. Thus

after an induction period all micelles are consumed near the surface and a micelle-free zone forms at the surface and gradually moves into the bulk phase. The thickness of this zone, measured from the interface, is denoted as $\delta(t)$. At the boundary of the micelle-free zone with the bulk solution, micelles break-up to supply surfactant monomers and keep the monomer concentration at the CMC. Within the micelle-free zone, monomer diffuses from the front to the surface where the concentration of monomer is decided by the kinetic equation and is below the CMC. Within the region between the micelle-free zone front and the bulk phase, the monomer concentration is equal to the CMC, and micelles diffuse from the bulk phase to the front of the micelle-free zone to supply micelles breaking down at the front. As adsorption onto the surface proceeds and the surface becomes saturated, the kinetic flux to the surface decreases. The concentration gradient of monomer across the micelle-free zone is reduced and the front begins to move back towards the interface. The micelle diffusion gradient also relaxes as the monomer flux in the micelle free zone decreases. At equilibrium the front arrives back at the interface and the bulk solution is once again a uniform micellar solution. The computed dynamic tensions agree well with the data with nonadjustable parameters, affirming the treatment of the infinitely fast micelle with respect to diffusion and kinetic adsorption. Furthermore, fluorescence microscopy method is used to verify the existence of the micelle free zone successfully.

The case Song et al. has examined in which the micelle breakdown is much faster than the rate of its bulk diffusion towards the surface will be the case as long as the micellar concentration is not too high. This kinetic limit model works well for the surfactant concentration up to the critical value of 4.25 CMC for $C_{14}E_6$. The theory

predicts that once the surfactant concentration is higher than the critical value, i.e. $C_T > 4.25C_{CMC}$, the dynamic surface tension relaxation is determined only by the kinetics. Since in this case, micelles exist everywhere in the solution and the monomer concentration is constant, the rate-limiting step to adsorption is the kinetic one, and the dynamic relaxation in concentration is given by integrating the Frumkin kinetic equation, with the relaxation in tension obtained from the equation of state. This is a limiting relaxation determined only by kinetics, and valid in principle for all bulk concentrations greater than the critical value. But the experimental data which are plotted in Figure 2.8 show that the dynamic surface tension relaxation become faster with increasing surfactant concentration. What we should note is that, as long as the surfactant concentration is above CMC, no matter what the surfactant concentration is, the surface tension (or surface concentration) reached at equilibrium is the same as what can be reach with surfactant concentration of CMC. The suspected reason for the discrepancy is that surfactant transport through monomer adsorption route is not enough to explain the accelerated surface tension reduction observed and the micelle direct adsorption route, in which micelles adsorb directly onto the surface, break up and release monomer onto the surface monolayer are proposed in this study to explain the fast surface tension reduction achieved by micellar solutions.

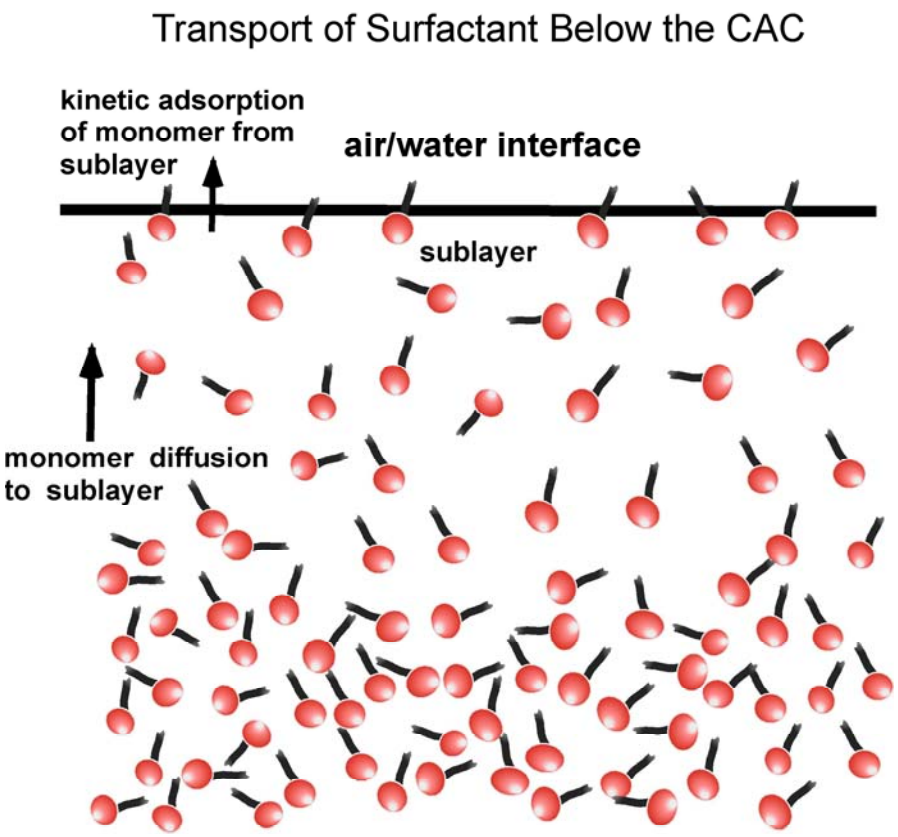

Figure 2.1: Transport of surfactants to an initially clean interface from a solution with a bulk solution C_o below the CMC.

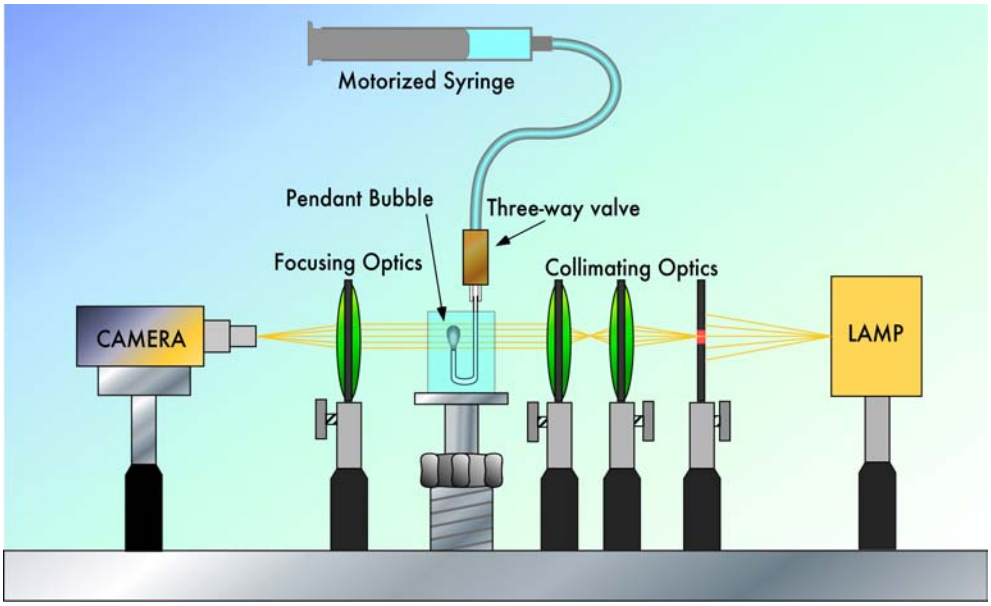

Figure 2.2: Schematic representation of Pendant Bubble Tensionmetry, enhanced by video-image digitization.

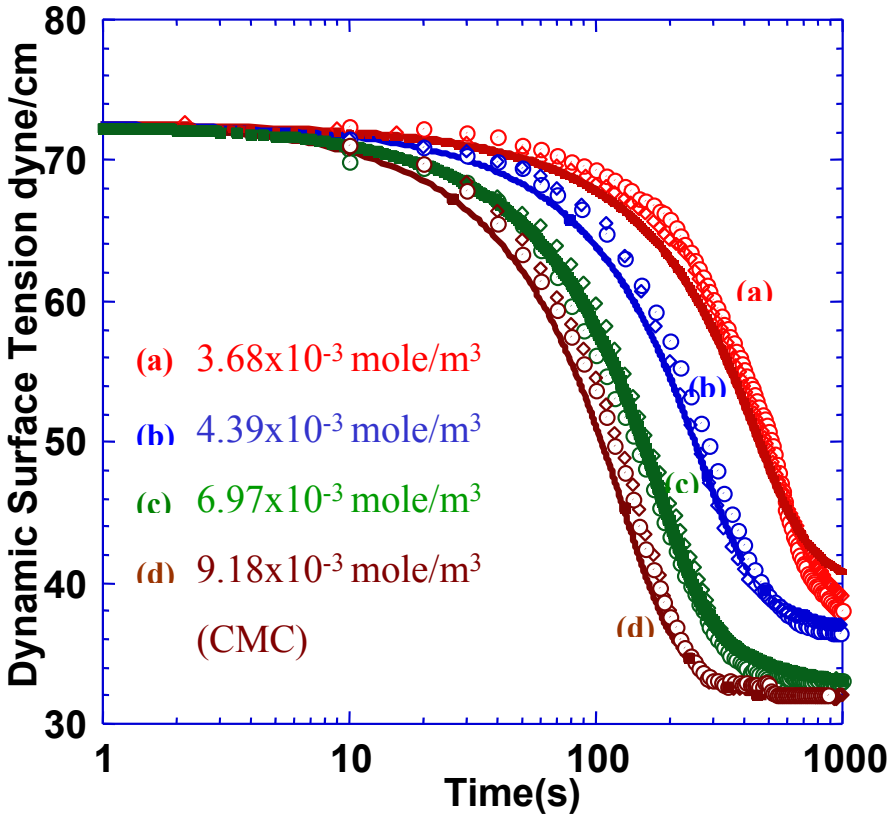

Figure 2.3: Comparison of simulations of tension relaxation and experimental relaxations for bulk concentrations less than the CMC with $D=6.0 \times 10^{-10}$ m^2/s and $\beta=4.0$ $m^3/(mole.s)$

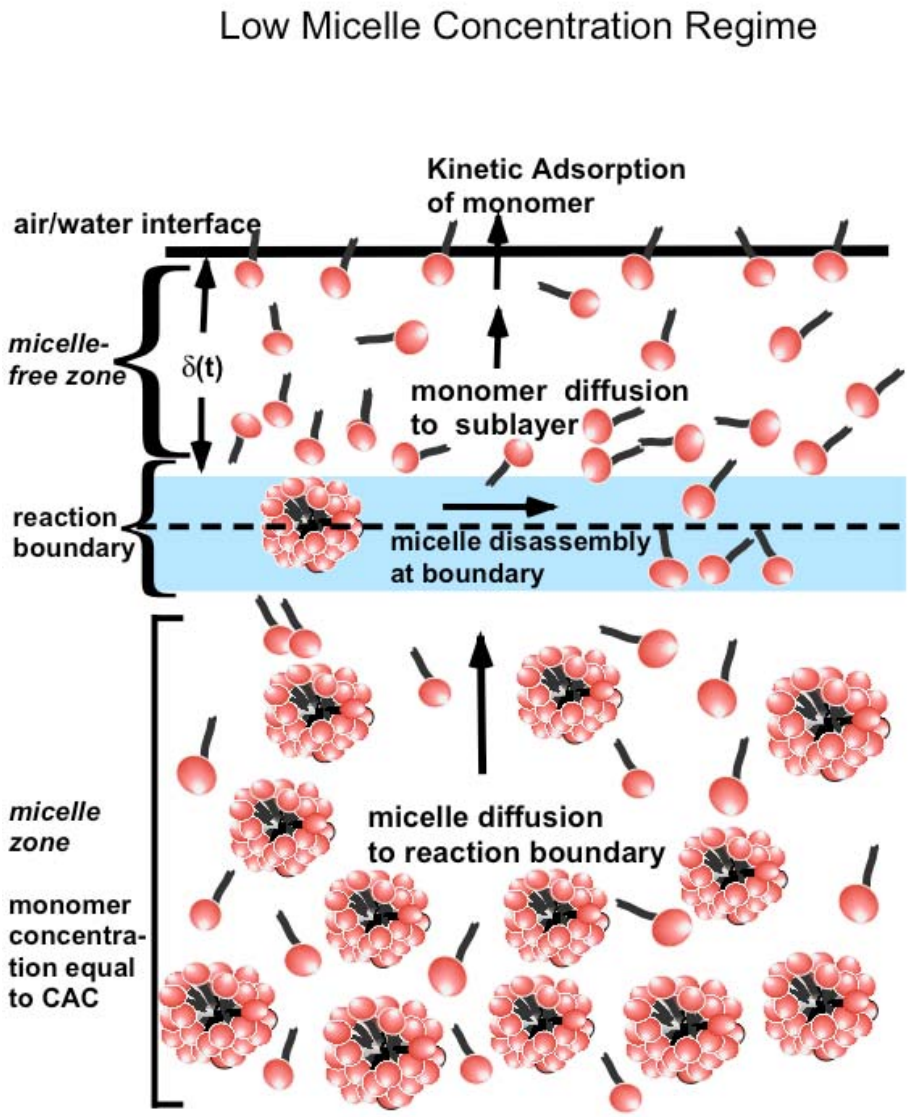

Figure 2.4: Schematic representation of surfactant transport from micellar solution

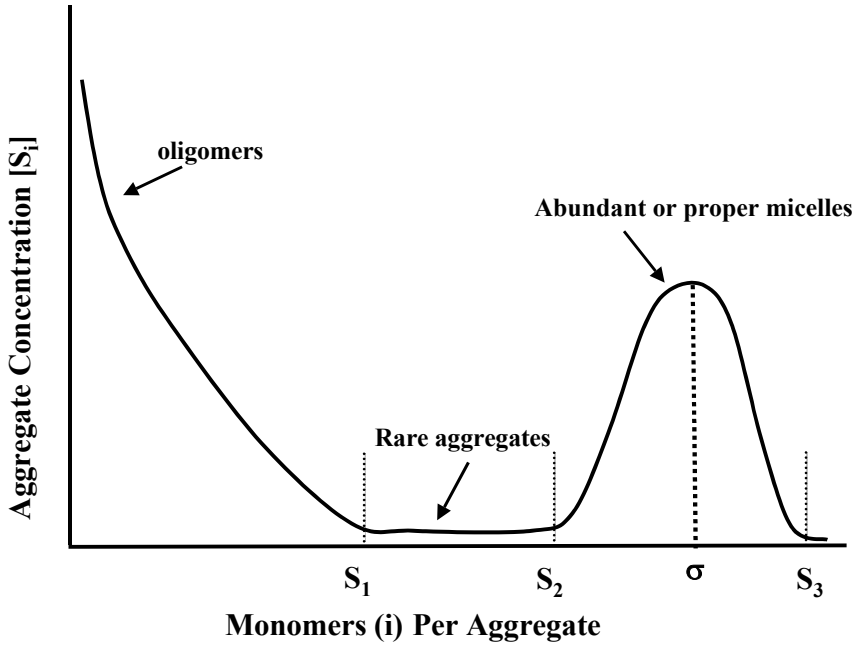

Figure 2.5: Size distribution of micelles in the stepwise model indicating oligomers, rare aggregates and abundant micelles.

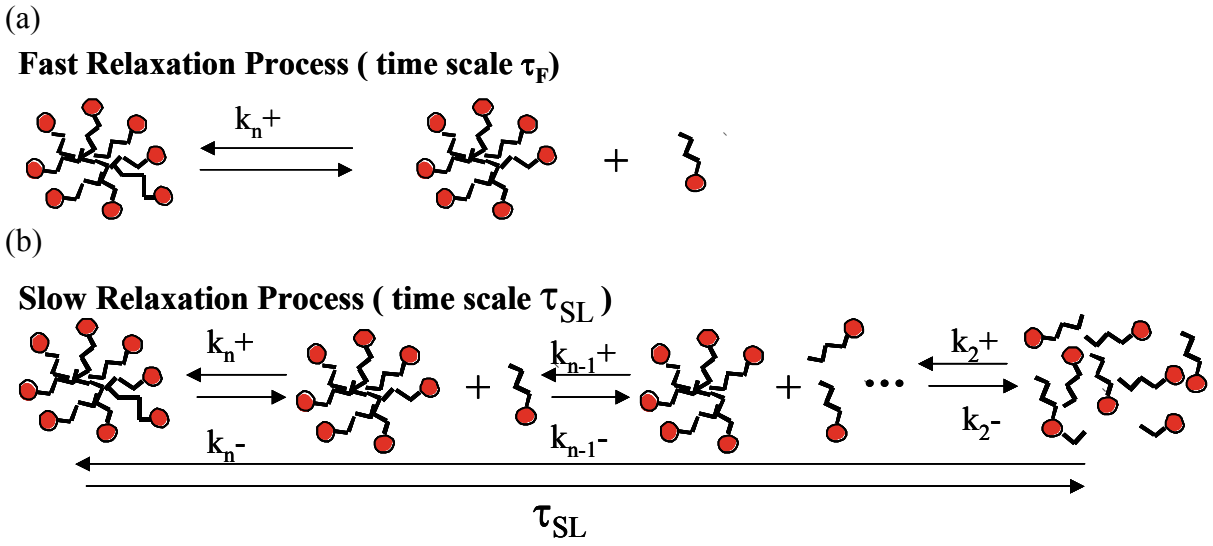

Figure 2.6: (a) Fast relaxation process of single monomer exchange; (b) The slow relaxation process of micellar formation or breakdown.

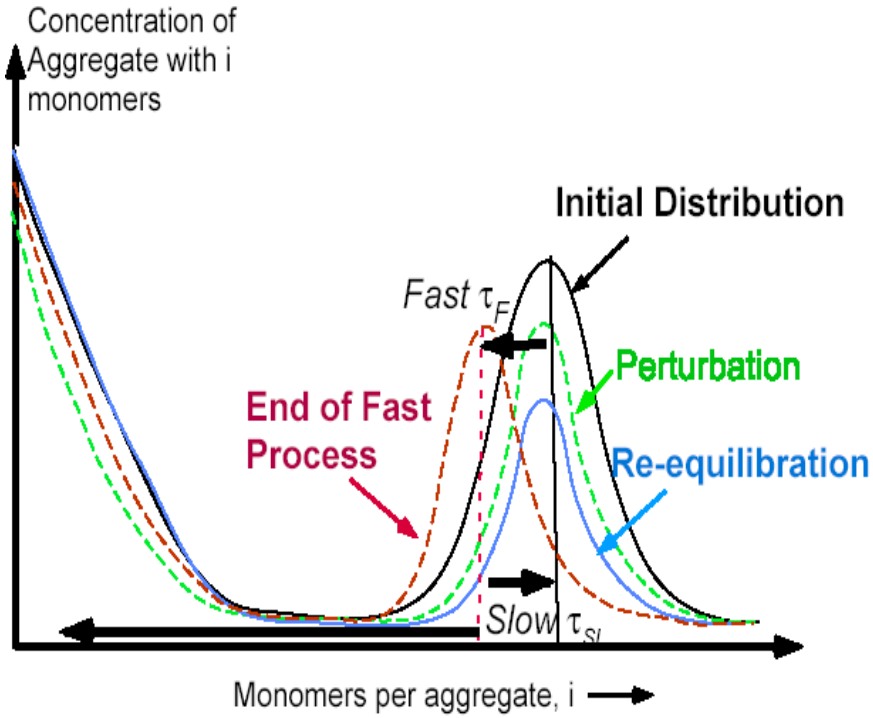

Figure 2.7: Size distribution of micelles in the stepwise model indicating oligomers, rare aggregates and abundant micelles, subject to perturbation.

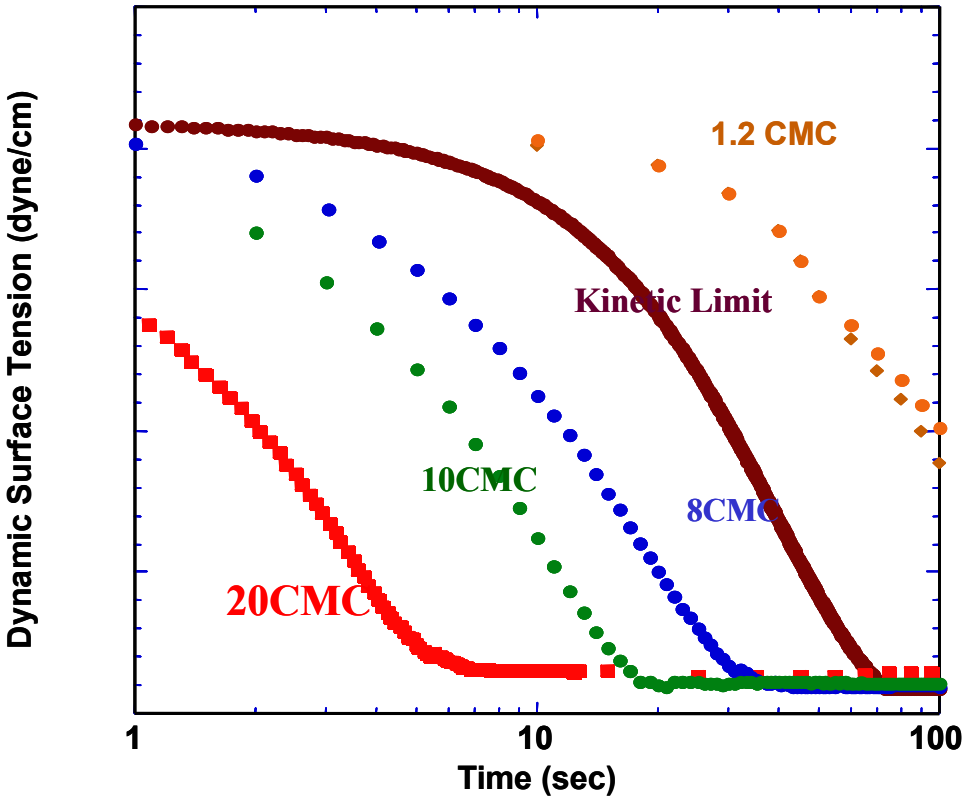

Figure 2.8: Experimental dynamic surface tension curves of $C_{14}E_6$ at different micelle concentration plotted together with theoretical kinetic limit curve.

Chapter 3

Theoretical Formulation of the Direct Adsorption of Micelle onto the Surface and Equilibrium Adsorption Isotherms

3.1 Introduction

The aim of this chapter is to outline a theoretical framework which accounts for the adsorption of micelle as well as monomer from bulk solution phase to an air water interface. In section 3.2, a simplified model is adopted to describe the kinetics of bulk micellization and equilibrium distribution of micelles. In section 3.3, a kinetic expression is proposed for the direct adsorption of micelle onto the surface and is used to compute the equilibrium concentration of monomer and micelle on the surface and in the bulk. In section 3.4, these equilibria are used along with Gibbs–Duhem equation to determine a new equation of state which accounts the existence of micelle on the surface at equilibrium. These equations then will be used in chapter 4 as the starting point of describing the dynamic adsorption of micelle onto the surface.

3.2 Simplified Micellization Kinetics in a Micellar Solution

We treat the micelle as a monodispersed species with one aggregation number (the number of surfactant molecules contained in one micelle) from the center of the aggregate distribution, and note this approximation should be reasonably valid since the aggregates distribution usually remains narrow.

The intermediate steps in the step-wise micellization model are merged together to give simpler micellization kinetics in the bulk, which describe the micellization kinetics

in one reversible reaction step (Figure 3.1). K_1 and K_2 are the reaction rate constants. The micellization kinetics in a micellar bulk solution can be written as:

$$r_{micellization} = K_1 C_m - K_2 (C_1)^{\sigma} \tag{3.1}$$

where K_1 and K_2 are the reaction rate constants for the forward and backward reactions, C_1 is the monomer bulk concentration, C_m is the micelle bulk concentration and σ is the aggregation number. For bulk solution, where micellization equilibrium is reached, the equilibrium constant K_N can be obtained as:

$$\frac{C_m}{(C_1)^{\sigma}} = \frac{K_2}{K_1} = K_N \tag{3.2}$$

Experiments identify the CMC as concentration at which added surfactant preferentially starts entering aggregate. A good measurement is the equal probability law, which states that a surfactant molecule added to the solution is as likely to enter a micelle as to remain in the solution. So that K_N can be express as[1]:

$$(C_1)_{CMC}^{1-\sigma} = \left(\sigma^2 K_N\right)^{-1} \tag{3.3}$$

where $(C_1)_{CMC}$ is the monomer concentration at the CMC. The CMC refers to the total concentration given by:

$$\text{CMC} = \sigma (C_m)_{CMC} + (C_1)_{CMC} = \sigma K_N (C_1)_{CMC}^{\sigma} + (C_1)_{CMC} \tag{3.4}$$

where $(C_m)_{CMC}$ is the micelle concentration at the CMC. Combining Equations (3.3) and (3.4) gives a expression of K_N in term of experimentally determined CMC and average aggregation number σ:

$$K_N = \left(\frac{CMC}{1/\sigma + 1} \right)^{1-\sigma} \frac{1}{\sigma^2} \tag{3.5}$$

K_N is usually a large value since the CMC is much smaller than 1 and aggregation numbers are from a few tens and a few hundreds. Taking the logarithm and dividing both sides of Equation (3.3) by aggregation number σ leads to $\frac{1}{\sigma}\ln C_m = \frac{1}{\sigma}\ln(\frac{1}{K_N}) + \ln C_1$. Taking into consideration that C_1 is usually much bigger or of the same order of magnitude as C_m, and σ is a large value varying from a few tens to a few hundreds, $\frac{1}{\sigma}\ln C_m$ will be negligible. It is usually estimated that when the total concentration of surfactant solution is at or below C_{CMC}, all surfactant molecules exist as singly dispersed monomer. Micelle starts to exist when the total surfactant concentration is larger than C_{CMC}.

This estimation can also be made using the chemical potential analysis. Since the surfactant concentration range of interest is dilute, the bulk solution is treated as an ideal solution. Thus the chemical potentials of monomer and micelle in the ideal bulk solution are:

$$\mu_1 = \mu_1^0 + kT\ln C_1 \tag{3.6}$$

$$\mu_m = \mu_m^0 + kT\ln C_m \tag{3.7}$$

where μ_1^0 and μ_m^0 are the standard state chemical potentials for monomer and micelle in the bulk, k Boltzmann's constant and T the absolute temperature. When micelleization kinetics reaches equilibrium in the bulk, the chemical potential of a singly dispersed bulk monomer is equal to the chemical potential per surfactant molecule of a micelle, or the bulk monomer chemical potential is 1/σ of the chemical potential of micelle with an aggregation number σ, hence:

$$\mu_1^0 + kT\ln C_1 = \frac{1}{\sigma}\mu_m^0 + \frac{1}{\sigma}kT\ln C_m \tag{3.8}$$

The term $\frac{1}{\sigma}kT\ln C_m$ will be negligible, thus $\mu_1 = \mu_1^0 + kT\ln C_1 \approx \frac{1}{\sigma}\mu_m^0 \approx \mu_m \approx const.$ and monomer concentration in a micellar solution can be approximated to be a constant value. The excess will be incorporated to form micelles, which are interpreted to constitute a pseudo-phase in equilibrium with the singly dispersed monomer molecule. Thus the All-or-Nothing theory for the bulk equilibrium can be written as:

$C_1=C_{total}$, $C_m=0$; when $C_{total}\leq C_{CMC}$ (3.9)

$C_1=C_{CMC}$, $Cm=(C_{total}- C_{CMC})/\sigma$; when $C_{total}>C_{CMC}$ (3.10)

The constant monomer concentration, usually known as critical micelle concentration C_{CMC} can be experimentally identified and denotes the concentration at which the pseudo-phase separation occurs[2].

3.3 Equilibrium Adsorption Isotherms for a Micellar Solution

3.3.1 Kinetic Express for Monomer and Micelle Adsorption from a Micellar Solution

Direct adsorption of micelle onto the interface and the presence of micelle in the monolayer on the surface require that the monomer exchange between surface and sublayer to be revised to take into the consideration that the available spots on the surface can also be taken by adsorbed micelle besides monomer. Correspondingly, the kinetic exchange of monomer on the surface is rewritten as:

$$j_{monomer} = \beta C_s \Gamma_\infty \left(1 - \frac{\Gamma}{\Gamma_\infty} - \Gamma^* \cdot \Delta A\right) - \alpha\Gamma e^{K\Gamma/\Gamma_\infty} \tag{3.11}$$

where Γ^* is the micelle surface coverage and ΔA is the area needs to be swept free of surfactant so that the micelle can adsorb. $\Gamma_\infty\left(1-\frac{\Gamma}{\Gamma_\infty}-\Gamma^*\cdot\Delta A\right)$ stands for the available spots for monomer adsorption after occupation of the micelle and monomer on the surface. Similar construction of the clean surface area has been utilized by Talbot et al. [3] in modeling multicomponent adsorption kinetics and Franses[4] in adsorption isotherms for mixtures of different-size molecules.

Micelle exchange on the surface is:

$$j_{micelle}=\frac{\beta^* C_{MS}}{\Delta A}e^{-\Pi\Delta A/RT}-\alpha^*\Gamma^* \tag{3.12}$$

Where C_{MS} is the micelle sublayer concentration, β^* and α^* are adsorption and desorption rate constants respectively both of which are independent of the surfactant surface concentration, Π is the surface pressure (which is the difference between the clean air/water surface tension and reduced interfacial tension due to surfactant adsorption), ΔA is the area to be swept free of surfactant so that the micelle can adsorb, T is the Kelvin temperature. Hence, ΠΔA/RT is the work needed to be done against the surface pressure to clear area for micelle adsorption. The adsorption of micelle is proportional to sublayer micelle concentration and activation energy written in the exponential term depending on the surface pressure. Desorption of micelle is proportional to the micelle surface concentration and interaction between adsorbed micelles are ignored since monomer will be the dominant species in the monolayer and adsorbed micelle surface concentration at the air/water interface is small.

3.3.2 Equilibrium Adsorption Isotherms for Monomer and Micelle Adsorption

Setting the net exchange of monomer and micelle at surface to be zero introduces the equilibrium adsorption isotherms for the two components:

Monomer equilibrium isotherm:

$$\frac{\theta_e e^{K\theta_e}}{1-\theta_e-\theta_e^*} = \frac{C_{1e}}{a} \tag{3.13}$$

Micelle equilibrium isotherm:

$$\frac{\theta_e^*}{e^{\left(-\Pi\frac{\Delta A}{RT}\right)}} = \frac{C_{me}}{a^*} \tag{3.14}$$

where $\theta_e = \frac{\Gamma_e}{\Gamma_\infty}$, $\theta_e^* = \Gamma_e^* \cdot \Delta A$ are nondimensionalized equilibrium surface concentrations, C_{1e} and C_{me} are equilibrium monomer and micelle bulk concentration, $a=\alpha/\beta$ and $a^*=\alpha^*/\beta^*$ are the ratio of desorption rate constant and adsorption rate constant for monomer and micelle.

These two equilibrium isotherms together with bulk equilibrium between monomer and micelle (Equation 3.3) will lead to the micelle breakup equilibrium on surface, which can reduce to the equation correlates equilibrium monomer and micelle surface concentration:

$$K_s e^{(-\sigma K\theta_e)} = \frac{\theta_e^\sigma}{\left(1-\theta_e-\theta_e^*\right)^\sigma}\frac{\exp\left(-\Pi\Delta A/RT\right)}{\theta_e^*} \tag{3.15}$$

where constant $K_s = \frac{a^*}{K_N a^\sigma}$.

3.4 New Equation of State Incorporating Micelle Surface Concentration

To describe the chemical potentials of adsorbed monomer and micelle in the surface monolayer, the potential distribution method of Widom[5] to relate the available surface function to the residual chemical potential of the component in the two dimensional mixture are adopted here. Thus the chemical potentials of adsorbed monomer and micelle in the surface monolayer can be written as:

$$\mu_1^S = \mu_1^{S0} + RT \ln \frac{\theta}{1-\theta-\theta^*} + KRT\theta \tag{3.16}$$

$$\mu_m^S = \mu_m^{S0} + RT \ln \frac{\theta^*}{e^{-\Pi \Delta A / RT}} \tag{3.17}$$

where the superscript "s" refers to the surface monolayer and the standard chemical potential μ_1^{S0} and μ_m^{S0} which are independent of surface tension. Adsorption isotherm also can be obtained by equating the bulk chemical potential to the surface chemical potential:

$$\mu_1^0 + RT \ln C_1 = \mu_1^{S0} + RT \ln \frac{\theta}{1-\theta-\theta^*} + KRT\theta \tag{3.18}$$

$$\mu_m^0 + RT \ln C_m = \mu_m^{S0} + RT \ln \frac{\theta^*}{e^{-\Pi \Delta A / RT}} \tag{3.19}$$

From Equations (3.18) and (3.19) and the adsorption isotherm Equations (3.13) and (3.14) follow with

$$a = \exp\left(\frac{\mu_1^{s0} - \mu_1^0}{RT}\right) = \frac{\alpha}{\beta} \text{ and } a^* = \exp\left(\frac{\mu_m^{s0} - \mu_m^0}{RT}\right) = \frac{\alpha^*}{\beta^*}.$$

Equation (3.15), relating the equilibrium surface concentrations of monomer and micelle relation can also be obtained by using $\mu_m^s = \sigma\mu_1^s$ with $K_s = \exp\left(\frac{\mu_m^{s0} - \mu_1^{s0}}{RT}\right) = \frac{a^*}{K_N a^\sigma}$.

Adsorption Gibbs equation given below is used to relate the change of the surface tension with the change of the surface concentration:

$$-d\gamma = d\Pi = \Gamma_1 d\mu_1^S + \Gamma^* d\mu_m^S = \Gamma_1\left\{RTd\ln\frac{\theta}{1-\theta-\theta^*} + KRTd\theta\right\} + \Gamma_m RTd\ln\frac{\theta^*}{\exp(-\Pi\Delta A/RT)} \qquad (3.20)$$

The above differentials are exact since the monomer surface concentration θ and micelle surface concentration θ^* are at equilibrium on the surface. Thus the new equation of state which incorporates monomer surface concentration and micelle concentration is then thermodynamically consistent[4]. The equilibrium adsorption isotherms of monomer and micelle (Equations (3.13) and (3.14)) are thermodynamically consistent too.

Equations (3.15) and (3.20) are solved numerically together to give surface pressure or surface tension as an implicit function of monomer surface coverage θ or micelle surface coverage θ^*. When it comes to dynamic surface tension of a surface monolayer which has both monomer and micelle adsorbing, the assumption that the transient configurations of adsorbed particles can be approximated by the corresponding equilibrium configuration is usually used. Thus, the calculated correlation from the equilibrium isotherm will be used to numerically interpret the dynamic surface tension of a surface monolayer having both micelle and monomer adsorption.

The All-or-Nothing theory is extended for the surface monolayer having both monomer and micelle too. When the adsorption equilibrium is established between the surface surfactant monolayer and bulk solution, the chemical potential of the surfactant in

the surface monolayer equals to that of a bulk monomer. It easily follows that the chemical potential of the surface monomer stays constant (is equal to constant bulk monomer chemical potential) when the surface adsorption equilibrium is reached in a micellar solution. Further assumption can be made that the intact micelle imbedded in the surface monolayer has constant chemical potentials, considering the chemical potential of the intact or partial surface micelle equals the number of the surfactant molecules multiplies the chemical potential of surface monomer. Using the Gibbs-Duhem equation for two species on the surface, the surface tension doesn't change after a critical surface tension.

$$-d\gamma = d\Pi = \Gamma_1 d\mu_1^S + \Gamma^* d\mu_m^S = 0 \tag{3.21}$$

Thus, safe assumption can be made that with the increasing surfactant bulk concentration bigger than C_{CMC}, the equilibrium surface tension keeps as the same as the one can be achieved by the surfactant solution of concentration C_{CMC}. When the bulk concentration is smaller than C_{CMC}, equation of state for Frumkin isotherm can be used to calculate surface tension as function of monomer surface concentration. After equilibrium surface tension $\gamma_e(C_{CMC})$ with a bulk concentration at C_{CMC} is reached, surface tension can be assumed to stay constant at $\gamma_e(C_{CMC})$. This assumption is also valid given that the intact or partial micelle population in the surface monolayer will be very small, and their small surface concentration compared to monomer one will not effect the equilibrium surface tension much.

With this assumption, the equilibrium adsorption isotherms for micellar solution can be simplified by replacing the surface pressure Π in Equation (3.14) with constant surface

pressure $\Pi_e(C_{CMC})=\gamma_c- \gamma_e(C_{CMC})$. Monomer and micelle surface concentrations can be easily calculated from the modified isotherms.

3.5 Equilibrium Adsorption Isotherms Simulation Results

3.5.1 Evaluation of Equilibrium Parameters and Equilibrium Surface Tensions Simulation

For the simulation results reported here, the CMC value of $C_{14}E_6$ is 0.00912 mole/m^3 [6], and the average aggregation number of $C_{14}E_6$ is chosen to be 100, which falls into the right rang of 50-120 for most C_iE_j surfactants[7-11]. Equilibrium constant K_N for micellization kinetics can be calculated according to Equation (5). The values of monomer parameters $\Gamma_\infty=3.32\times10^{-6}$ mole/m^2, $a=\alpha/\beta=2.068\times10^{-6}$ mol/m^3, K=7.12, and β=7.0 m^3/(mol·s) obtained from below the CMC regime are used. The prediction of equilibrium surface tension using the new equilibrium isotherm requires the micelle equilibrium parameter $a^*=\alpha^*/\beta^*$ and ΔA. The values of a^* and ΔA are changed simultaneously until the equilibrium surface tension predicted by the equilibrium isotherms of monomer and micelle (Equations (3.13), (3.14) and equation of state numerically interpreted from Equation (3.20)) matches the experimental data obtained using pendant bubble apparatus. The simulation shows that the equilibrium surface tension curve is not sensitive to the value of ΔA. And ΔA is believed to be of the order of $1/\Gamma_\infty$ to induce the micelle adsorption. $a^*=\alpha^*/\beta^*$ =0.005 mol/m^3 is found for good agreement between the prediction of equilibrium surface tension and the experimental data (Figure 3.6). The monomer and micelle bulk concentration and surface concentration predicted from the equilibrium adsorption isotherms are also plotted in Figure 3.4 and

Figure 3.5. A change in the slop of monomer bulk concentration indicates that the total bulk concentration is becoming higher than the CMC and micelle starts appearing in the solution. Correspondingly, the initially micelle bulk concentration will start increasing from zero. The change in the slop of monomer surface concentration is a sign for micelle appearance in the surface monolayer. The low value of the nondimensional micelle surface concentration indicates that the there are few intact micelles in the surface monolayer. Most of the micelle adsorbed onto the surface will break into monomer, which will be incorporated into the monolayer. The surface micelle concentration was plotted as a function of the surface monomer concentration in Figure 3.5, in which the abrupt turning point indicated that the intact micelle starts existing in the surface monolayer which becomes crowded enough so that the adsorbed micelle doesn't have chance to breakup.

The simulation results using the simplified All-or-Nothing assumption are also plotted in Figures (3.7), (3.8) and (3.9), and verified that the All-or-Nothing theory are good enough to predict the bulk concentration, surface concentrations and surface tension of a equilibrated system.

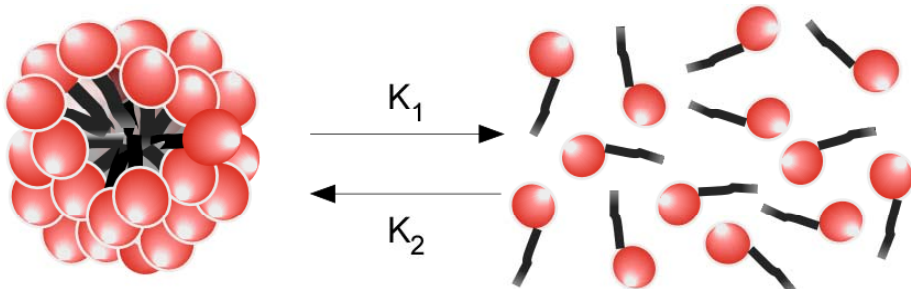

Figure 3.1: Schematic representation of simplified bulk kinetics in a micellar solution.

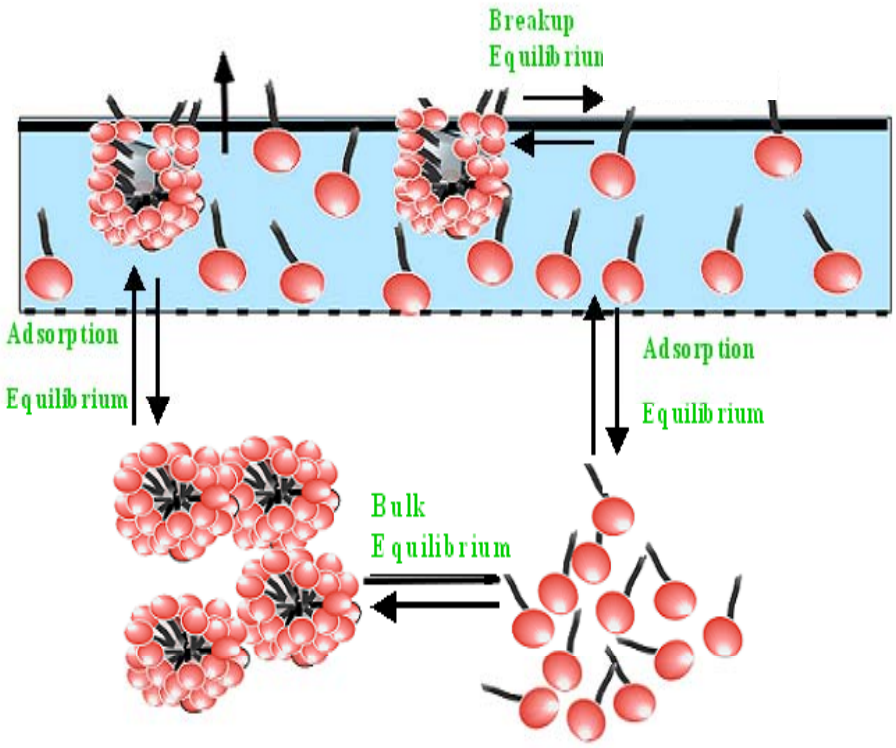

Figure 3.2: Four equilibrium relations in bulk-surface equilibrium system.

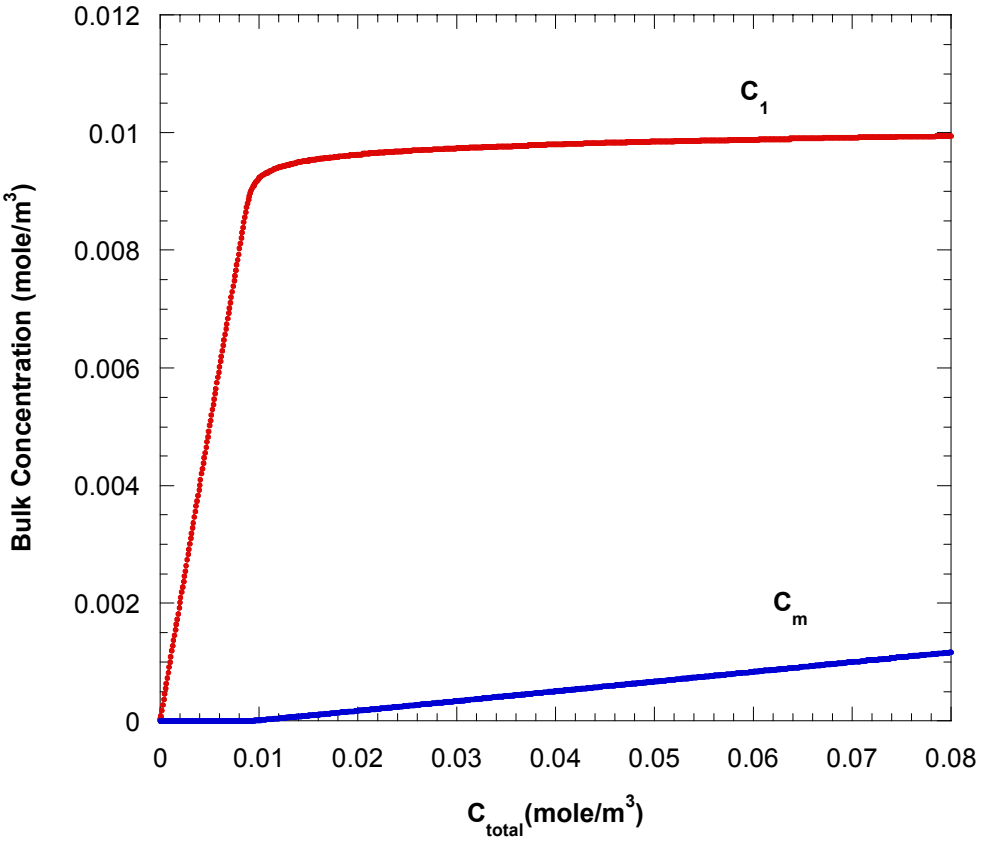

Figure 3.3: Monomer (red) and micelle (blue) bulk concentrations distribution.

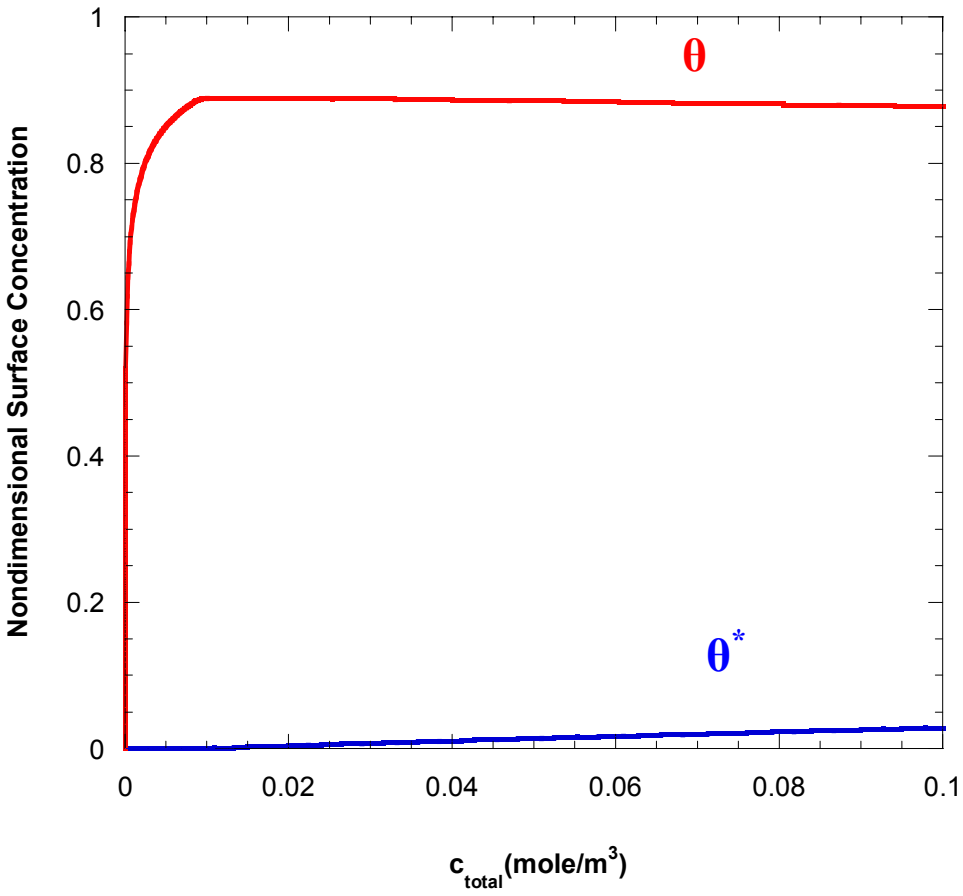

Figure 3.4: Nondimensional monomer (θ) and micelle (θ^*) concentrations prediction from equilibrium adsorption isotherms.

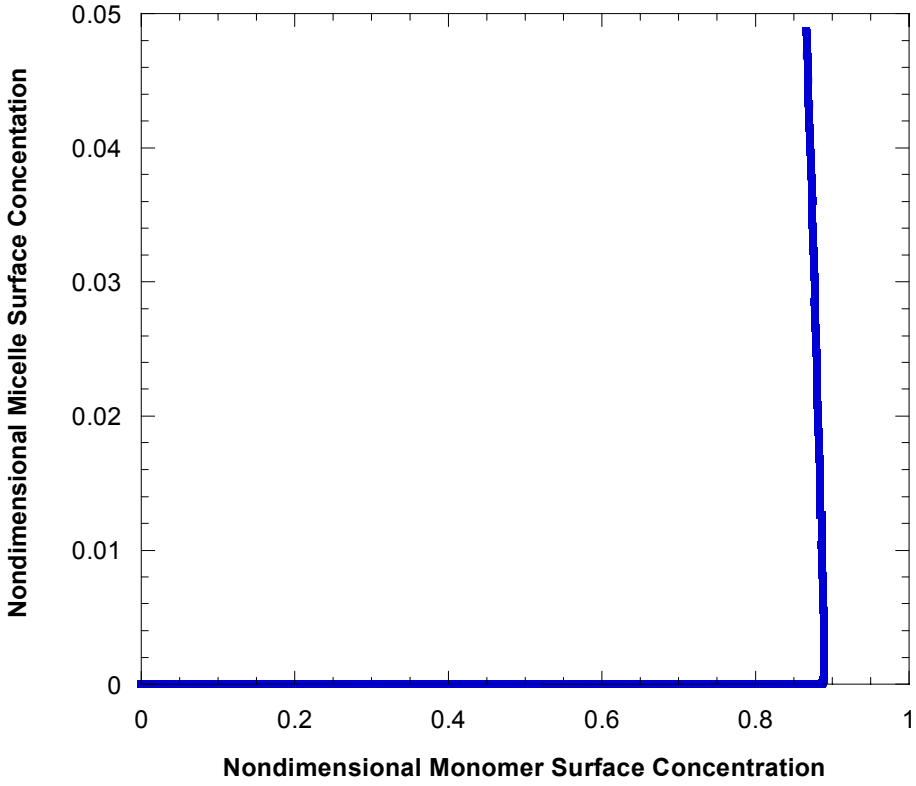

Figure 3.5: Nondimensional micelle surface concentration plotted vs nondimensional monomer surface concentration.

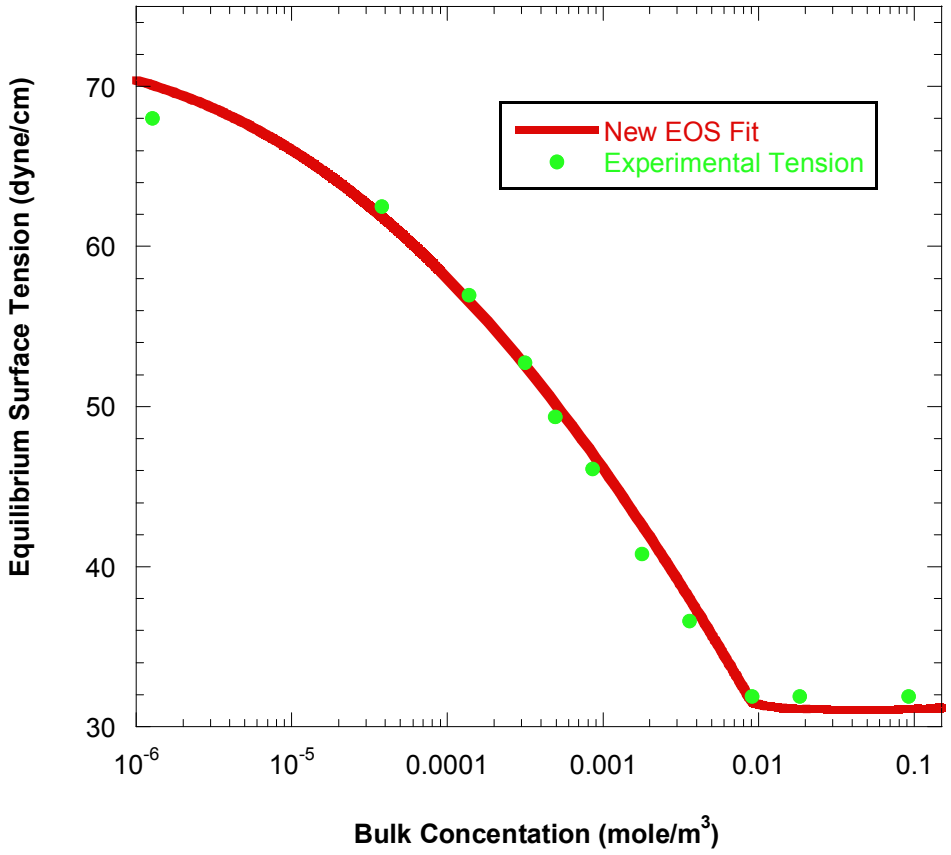

Figure 3.6: Experimental equilibrium surface tension prediction using new equilibrium isotherms of monomer and micelle, and new equation of state with $a^{*}=\alpha^{*}/\beta^{*}=0.005$ mol/m^3 and $\Delta A=(1/\Gamma_{\infty})$.

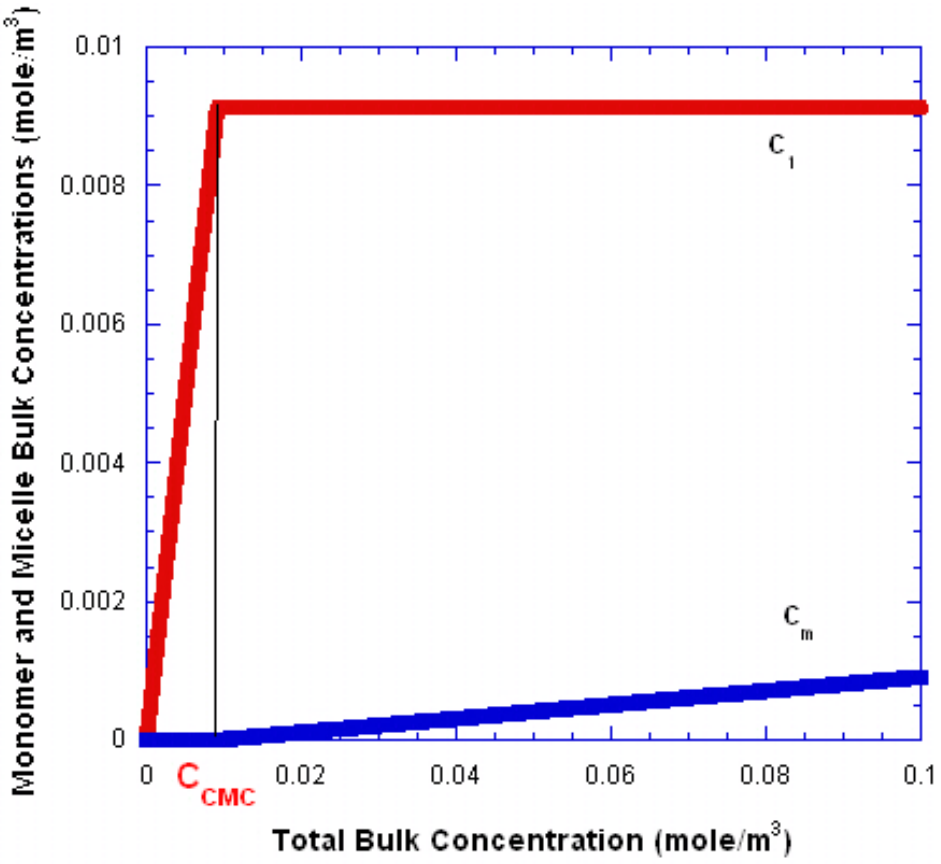

Figure 3.7: Monomer (C_1) and micelle (C_m) bulk concentrations estimated from the All-Or-Nothing hypothesis.

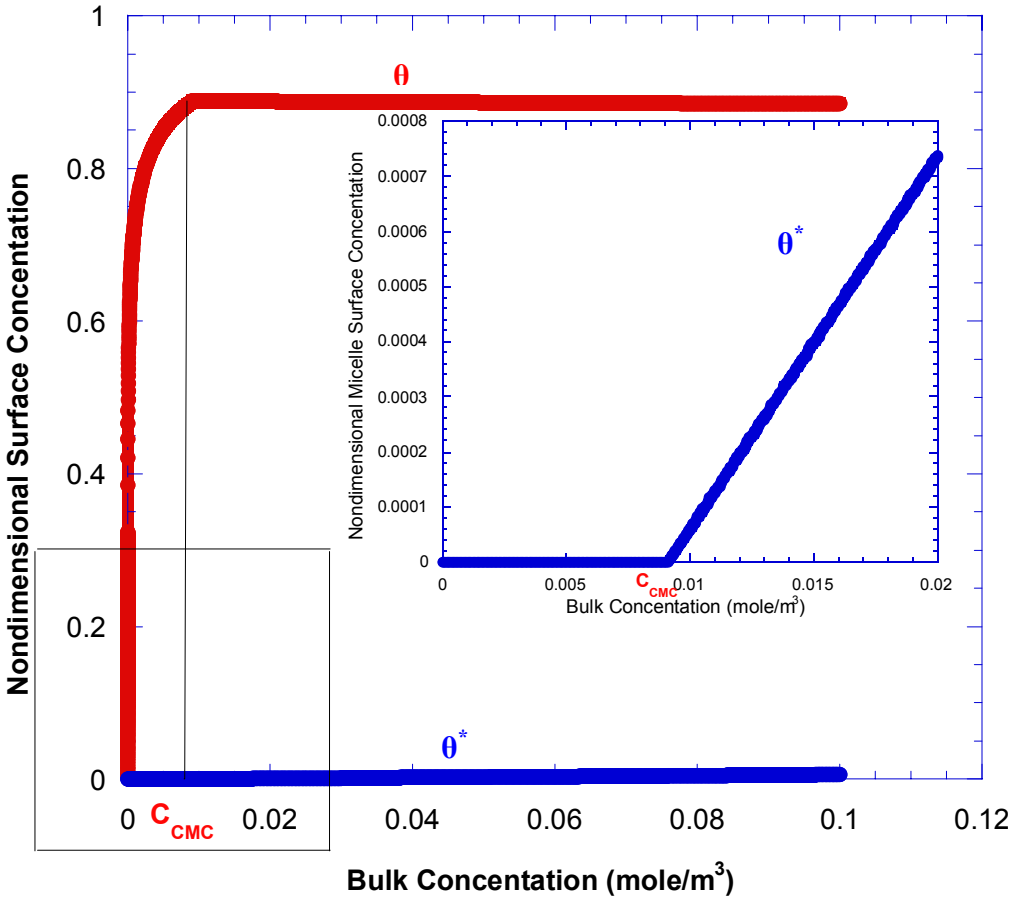

Figure 3.8: Nondimensional monomer surface concentation ($\theta=\Gamma/\Gamma_\infty$) and micelle surface concentration ($\theta^*=\Gamma^*\Delta A$) predicted from equilibrium adsorption isotherms with $a^*=1.0\times10^{-3}$ mol/m^3, $\Delta A=1/\Gamma_\infty$ from All-Or-Nothing hypothesis.

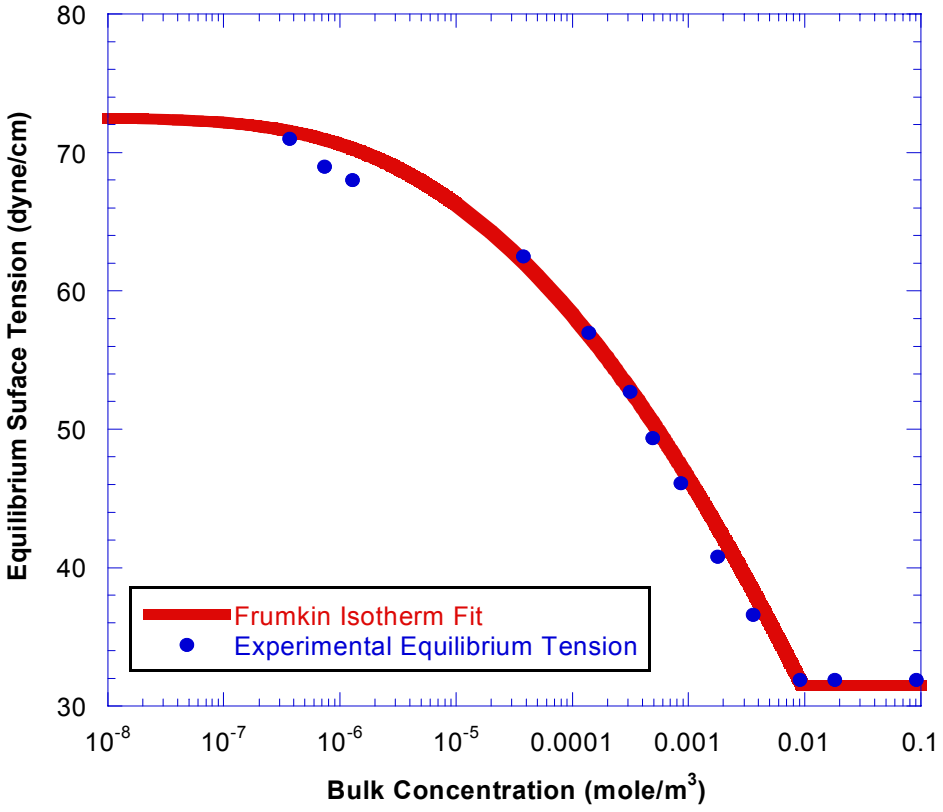

Figure 3.9: Experimental equilibrium surface tension and Frumkin Isotherm fit with $\Gamma_\infty=3.32\times10^{-6}$ mole/m^2, a $=\alpha/\beta=2.068\times10^{-6}$ mol/m^3 and K=7.12 from All-Or-Nothing hypothesis.

Chapter 4

Theory and Models for Surfactant Transport from a Micellar Solution onto a Clean Air/water Interface

4.1 Introduction

Surfactant transport route by adsorption of monomer onto an air/water interface is a well-recognized and documented process. For surfactant transport from a high concentration solution containing monomer and aggregates (spherical aggregate is usually called micelle), sole monomer adsorption route fails to predict the fast tension relaxation since there is a limit imposed by the sole monomer adsorption route. The focus of this chapter is to study of the mechanisms of transport of surfactant molecules from an aqueous micellar solution onto an initially clean air/water interface. Generally, upon the creation of a clean interface in the micellar solution, monomers from the sublayer just underneath the surface will kinetically adsorb onto the interface, followed by the diffusion of the monomers from the bulk to the surface to replenish the monomer concentration in the sulbayer that is depleted of the monomer due to adsorption. Micellar aggregates in the bulk phase can augment the adsorption process by two routes. First of all, the adsorption and diffusion of monomer disturbs the bulk micellization equilibrium and micelles can kinetically break-up and release monomers, which can then diffuse to the sublayer and kinetically adsorb onto the surface. Secondly, micelles can directly adsorb onto the surface and then surfactant molecules in micelles are released into the surfactant monolayer. As the surface monolayer becomes more and more crowded, monomer and micelle kinetic adsorption through these two routes respectively and the breakup of the adsorbed micelle will slow down and equilibrium will be established

between the surface and bulk finally. Very low surface concentration of intact or partial micelles in the surface monolayer is expected.

Theoretical transport model is developed for micellar solutions of nonionic surfactant hexaoxyethylene tetradecyl ether ($C_{14}E_6$) and supporting experiments are carried out correspondingly to verify the model. We analyzed the model for a wide concentration range. For a low micellar concentration solution (below a critical micellar concentration), the micelle break up time scale is smaller than the micelle diffusion time scale, thus a micelle-free zone will emerge in the sublayer and move into the bulk. For a high micellar concentration solution (above a critical micellar concentration), the micelle breakup time scale is bigger than the micellar diffusion time scale so there is no micelle-free zone developed during the transport process and micelle will be present all through the solution.

Numerical solutions of the monomer and micelle surface concentrations, sublayer monomer and micelle concentrations, bulk monomer and micelle distributions, and dynamic surface tension as a function of time are obtained. Experimentally, we use the pendent bubble technique to measure the dynamic surface tension, and compared the theoretical prediction of transport model to the experimental data to verify our models. The excellent agreements between the theoretical model and experimental data are demonstrated for a wide concentration range.

4.2 Diffusion Process in the Bulk Solution

When the concentration gradients of monomer and micelle are developed in the bulk due to surface adsorption, monomer and micelle will diffuse to the surface, driven by the

concentration gradients. The local mass balance of monomer and micelle in the bulk can be written as:

$$\frac{\partial C_1(r,t)}{\partial t} = \frac{D_1}{r^2}\frac{\partial}{\partial r}\left\{r^2 \frac{\partial C_1(r,t)}{\partial r}\right\} + r^{Bulk}_{micellization}(C_1, C_m) \tag{4.1}$$

$$\frac{\partial C_m(r,t)}{\partial t} = \frac{D_m}{r^2}\frac{\partial}{\partial r}\left\{r^2 \frac{\partial C_m(r,t)}{\partial r}\right\} - r^{Bulk}_{micellization}(C_1, C_m) \tag{4.2}$$

where $C_1(r,t)$, $C_m(r,t)$ are monomer and micelle bulk concentrations, D_1 and D_m are monomer and micelle diffusivities, $r^{Bulk}_{micellization}$ which is expressed in Equation (4.1) is the conversion between micelle and monomer in the bulk due to equilibrium disturbance. If the bulk concentration is below the critical micelle concentration, the estimation Equation (3.9) will be used so that there is only monomer in the bulk solution, $r^{Bulk}_{micellization}$ in Equations (4.1) and (4.2) follows naturally to be zero and there will be only monomer diffusion in the bulk. For a high micellar solution of the studied $C_{14}E_6$ surfactant, the time scale of monomer diffusion is much longer than time scale of slow micellization process in the step-wise micellization model, quasi-equilibrium estimation used by Qing Song is adopted here for bulk micellization so that monomer concentration will always be kept at the critical micelle concentration with the presence of micelle and the micellization rate in Equation (4.2) will be set to zero (Cf. Section 2.2.3.3).

4.3 Direct micelle adsorption route

When a clear air/water interface is created in a micelle solution, both the monomer and micelle in the bulk will adsorb onto the surface. The adsorption of micelle through the direct micelle adsorption route and the presence of micelle in the monolayer on the

surface require that the monomer exchange between surface and sublayer to be revised to take into the consideration that the available spots on the surface can also be taken by micelle besides monomer. Correspondingly, the mass balance of monomer on the surface is composed of two parts, first, the monomer exchange between surface and bulk, and second the micelleziation between the adsorbed micelle and monomer in the surface monolayer. Thus the surfacee mass balance of monomer is rewritten as:

$$\frac{d\Gamma}{dt} = \beta C_s \Gamma_\infty \left(1 - \frac{\Gamma}{\Gamma_\infty} - \Gamma^* \cdot \Delta A\right) - \alpha \Gamma e^{K\Gamma/\Gamma_\infty} + r_{micellization}^{surface}(\Gamma, \Gamma^*) \tag{4.3}$$

where Γ^* is the micelle surface coverage and ΔA the area to be swept free of surfactant so that the micelle can adsorb, $r_{micellization}^{surface}(\Gamma, \Gamma^*)$ is the conversation rate of adsorbed micelle into monomer in the surface monolayer. $\Gamma_\infty \left(1 - \frac{\Gamma}{\Gamma_\infty} - \Gamma^* \cdot \Delta A\right)$ illustrates the available spots for monomer adsorption after occupation of both monomer and micelle on the surface. Similar construction of the clean surface area has been utilized by Talbot et al.[1] in modeling multicomponent adsorption kinetics and Franses[2] in adsorption isotherms for mixtures of different-size molecules.

Similarly, the mass balance of adsorbed micelle on the surface is:

$$\frac{d\Gamma^*}{dt} = \frac{\beta^* C_{ms}}{\Delta A} e^{-\Pi \Delta A/RT} - \alpha^* \Gamma^* - r_{micellization}^{surface}(\Gamma, \Gamma^*)/\sigma \tag{4.4}$$

where C_{ms} is the micelle sublayer concentration, $\beta^*/\Delta A$ and α^* are the adsorption and desorption rate constants respectively both of which are independent of the surfactant surface concentration, Π is the surface pressure (which is the difference between the clean air/water surface tension and reduced interfacial tension due to surfactant adsorption $\Pi = \gamma_c - \gamma$), T is the Kelvin temperature. ΠΔA/RT is the work needed to be done

against the surface pressure to clear area for micelle adsorption. The adsorption of micelle is proportional to sublayer micelle concentration and activation energy written in the exponential term depends on the surface pressure. Desorption of micelle is proportional to the micelle surface concentration and interaction between adsorbed micelles are ignored since monomer will be the dominant species in the monolayer and the amount of the adsorbed micelle that remains intact in the surface monolayer is very small.

4.4 Surfactant Transport from a Micellar Solution

4.4.1 Surfactant Transport from a Micellar Solution with Concentration above the Critical Value

Generally, once a fresh air/water interface is created in surfactant solution containing both monomer and micelles, monomer and micelle in the sublayer will kinetically adsorb onto the interface. The adsorbed micelle on the surface will break up and release monomer into the monolayer. The adsorption will deplete monomer and micelle from the sublyer, which will results in concentration gradients of the two species. Thus, monomer and micelle in the far field will diffuse toward surface to restore monomer and micelle concentrations in the sublayer. The kinetic adsorption will also disturb the dynamic equilibrium between micelle and monomer, thus micelle in the bulk will disassemble into monomer to replenish monomer concentration in the bulk.

Surfactant	**CMC ($\times 10^5$) M**	$\tau_D^{monomer}(C_{CMC}) = \frac{\Gamma_\infty^2}{DC_{CMC}^2}$	**Slow Micellar Kinetic Step Time τ_{SL}**
$C_{14}E_6$	**0.912**	**331 Sec**	**~ 10 Sec**

Table 4.1: Time scales of $C_{14}E_6$ solution at the CMC.

For high concentration $C_{14}E_6$ solution, the assumption that the micellization kinetics is much faster compared to the diffusion of monomer so that the monomer concentration throughout the bulk would be kept at C_{CMC} is adopted here too. The assumption is based on the fact the diffusion time scale of monomer (calculated from the kinetic parameters of monomer) is much larger than the slow relaxation time scale in micellization kinetics (obtained by experimentally for C_iE_j surfactant [3]) of $C_{14}E_6$ (cf. Table 4.1).

Thus for $C_{14}E_6$, the monomer concentration is kept homogeneous as long as micelle is present in the solution, only micelle diffuses toward surface due to micellar concentration gradient. A schematic of surfactant transport from high $C_{14}E_6$ micellar solution onto an air/water interface is shown in Figure 4.1. So for the high concentration regime $n>n^*$, we have the diffusion of micelles which is governed by:

$$\frac{\partial C_m(r,t)}{\partial t} = \frac{D_m}{r^2}\frac{\partial}{\partial r}\left\{r^2\frac{\partial C_m(r,t)}{\partial r}\right\}, \quad r>b \tag{4.5}$$

where $C_m(r,t)$ is the micelle bulk concentration, D_m is the micelle diffusivity, which is assumed to be constant and independent of the concentration value, b is the radius of the spherical bubble. Equation (4.5) is subject to the first boundary condition that surface concentration is related to the diffusion flux at the interface via the mass balance equation:

$$\frac{d(\Gamma+\sigma\Gamma^*)}{dt} = D_m\frac{\partial(\sigma C_m(r,t))}{\partial r}\Big|_{r=b} \tag{4.6}$$

and also the second boundary condition that the concentration of micelle in the far field is not disturbed and fixed to the bulk initial micelle concentration:

$$\sigma C_m(r\to\infty,t) = \sigma C_m^o = (n-1)C_{CMC} \tag{4.7}$$

The initial condition for C_M is

$$\sigma C_m(r,t=0) = \sigma C_m^o = (n-1)C_{CMC} \tag{4.8}$$

and sublayer micelle concentration:

$$C_m(r=b,t) = C_{ms}(t) \tag{4.9}$$

where C_T=nC_{CMC} is the total concentration of surfactant solution, C_m^o is the initial and far-field micellar bulk concentration and C_{MS} is the micelle sublayer concentration.

The kinetic exchange of monomer and micelle on the surface is governed by:

$$\frac{d(\Gamma+\sigma\Gamma^*)}{dt} = \beta C_{cmc}\Gamma_\infty\left(1-\frac{\Gamma}{\Gamma_\infty}-\Gamma^*\Delta A\right)-\alpha\Gamma e^{K\Gamma/\Gamma_\infty}+\sigma\left[\frac{\beta^* C_m}{\Delta A}\exp\left(\frac{-\Pi\cdot\Delta A}{RT}\right)-\alpha\Gamma^*\right] \tag{4.10}$$

The calculation of Equations (4.5)-(4.10) will be simplified using a similar All-or-Nothing strategy that was used for bulk solution. If the monomer surface concentration is smaller than the critical monomer surface concentration $\Gamma_e(C_{CMC})$ (which is obtained when the surface is in equilibrium with a bulk solution of concentration C_{CMC}), all the adsorbed micelles are assumed to breakup completely into monomer, leaving no intact micelle in the monolayer (Γ^* in Equations (4.6) and (4.10) are set to be zero). Thus Equations (4.6) and (4.10) are replaced with the following two equations respectively:

$$\frac{d\Gamma}{dt} = D_m\frac{\partial(\sigma C_m(r,t))}{\partial r}\Big|_{r=b} \tag{4.11}$$

$$\frac{d\Gamma}{dt} = \beta C_{cmc}\Gamma_\infty\left(1-\frac{\Gamma}{\Gamma_\infty}\right)-\alpha\Gamma e^{K\Gamma/\Gamma_\infty}+\sigma\left[\frac{\beta^* C_m}{\Delta A}\exp\left(\frac{-\Pi\cdot\Delta A}{RT}\right)\right] \tag{4.12}$$

Equation of state for Frumkin adsorption isotherm (Equation (2.4)) will be used to compute the surface tension for monolayer only containing monomers.

After the critical monomer surface concentration $\Gamma_e(C_{CMC})$ is reached, the monomer surface concentration is kept constantly at $\Gamma_e(C_{CMC})$, and intact micelle will start

accumulating in the surface monolayer. Thus Equations (4.6) and (4.10) will be modified to:

$$\frac{d\Gamma^*}{dt} = D_m \frac{\partial (C_m(r,t))}{\partial r}\Big|_{r=b} \tag{4.13}$$

$$\frac{d\Gamma^*}{dt} = \frac{\beta^* C_m}{\Delta A} \exp\left(\frac{-\Pi_e(C_{CMC})\cdot \Delta A}{RT}\right) - \alpha\Gamma^* \tag{4.14}$$

The surface tension of the surface monolayer containing monomer surface concentration at $\Gamma_e(C_{CMC})$ and intact micelle will be kept at $\gamma_e(C_{CMC})$ (cf. Equilibrium surface tension of a monolayer having both monomer and micelle).

Control-volume formulation will be used after scaling the radial coordinates with bubble radius b, the micelle concentration by the far-field bulk concentration $(n-1)C_{CMC}/\sigma$, time with monomer diffusion time $\frac{\Gamma_\infty^2}{D(C_{CMC})^2}$, monomer surface concentration by maximum monomer coverage Γ_∞, micelle surface concentration by ΔA. The micelle distribution in space and time $C_m(r, t)$, time dependence of monomer surface concentration $\Gamma(t)$, micelle surface concentration $\Gamma^*(t)$ and surface tension $\gamma(t)$ will be calculated.

4.4.2 Surfactant Transport from a Micellar Solution below a Critical Concentration

If the concentration of the micellar solution is below a critical value $n<n^*$, the sublayer concentration of micelle remains above zero until a particular time t_d, at which the sublayer concentration of micelle is zero and a micelle-free zone starts developing, emerging from the sublayer and moving into bulk. For $t \le t_d$, the solutions to Equations (4.5)-(4.10) provide the micelle distribution and surface monomer and micelle concentrations in time. At $t=t_d$, micelle sublayer concentration is zero. For $t>t_d$, the

micelle-free zone appears and then moves into the bulk solution. The boundary of this micelle free zone is denoted as r-b=δ(t). As the surface monolayer gets more and more populated with the adsorbed monomer and micelle, micelle direct adsorption slows down, allowing the micelle diffusion catches up, the micelle free zone narrows and the boundary will move back to the interface until it disappears completely. Mass transfer of monomer in the micelle-free zone is formulated:

$$\frac{\partial C_1(r,t)}{\partial t} = \frac{D_1}{r^2}\frac{\partial}{\partial r}\left\{ r^2 \frac{\partial C_1(r,t)}{\partial r} \right\}, \qquad b<r<b+\delta(t) \tag{4.15}$$

Mass transfer of micelle in the micelle zone is given:

$$\frac{\partial C_m(r,t)}{\partial t} = \frac{D_m}{r^2}\frac{\partial}{\partial r}\left\{ r^2 \frac{\partial C_m(r,t)}{\partial r} \right\}, \qquad r> r<b+\delta(t) \tag{4.16}$$

Kinetic exchange at the bubble interface is governed by monomer adsorption and desorption:

$$\frac{d\Gamma}{dt} = \beta\Gamma_\infty C_1(r=0,t)\left[1-\frac{\Gamma}{\Gamma_\infty}\right] - \alpha\Gamma e^{K\Gamma/\Gamma_\infty} \tag{4.17}$$

At the bubble interface, the monomer diffusive flux is equal to the kinetic rate adsorption of monomer to the surface:

$$D\frac{\partial C_1(r,t)}{\partial r}\bigg|_{r=b} = \frac{d\Gamma}{dt} \tag{4.18}$$

At the micelle-free zone boundary, the monomer diffusive flux must be equal to the micelle diffusive flux multiplied by the aggregate number, micelles at the boundary all break up into monomers:

$$D\frac{\partial C_1(r,t)}{\partial r} = \sigma \cdot D_m \frac{\partial C_m(r,t)}{\partial r}, \qquad r=b+\delta(t) \tag{4.19}$$

$$C_m(r=b+\delta(t),t) = 0 \tag{4.20}$$

$$C_1(r = b + \delta(t), t) = C_{CMC} \tag{4.21}$$

Far-field boundary:

$$C_m(r \to \infty, t) = C_m^0 \tag{4.22}$$

Equations (4.15)-(4.22) will be nondimensionalized using the same scales as described previously and will also be solved using control-volume formulation to give monomer bulk distribution $C_1(r<b+ \delta(t), t>t_d)$, micelle bulk distribution $C_m(r>b+ \delta(t), t>t_d)$, moving micelle-free zone boundary $\delta(t)$, monomer surface concentration $\Gamma(t)$, micelle surface concentration $\Gamma^*(t)$ and surface tension $\gamma(t)$.

4.5 Simulation Results

$\Gamma_\infty=3.32\times10^{-6}$ mole/m^2, $a=\alpha/\beta=2.068\times10^{-6}$ mol/m^3, K=7.12, and $\beta=7.0$ m^3/(mol·s) are obtained below the CMC regime by fitting the theoretical predications with experimental equilibrium and dynamic surface tension data (Cf. Appendix 1). The average value of micelle diffusion coefficient D_M is chosen to be 1.0×10^{-10} m^2/s at temperature of 22 ± 0.5 °C for the low concentration range (Note, the C_{CMC} value for $C_{14}E_6$ is approximately 4.36×10^{-3} kg/m^3, several C_{CMC} or even 20 CMC is still a low concentration.). This value of micellar diffusivity falls into the range of diffusivity of micelle of aqueous solutions reported by different researchers using dynamic light scattering[4], pulsed-gradient echo (PGSE)[5] and pulsed field gradient NMR[6] of nonionic C_iE_j surfactants. After applying All-or Nothing estimation on the surface monolayer, the only unknown parameters in the simulation are the micelle adsorption rate constant β^* (or α^*) and ΔA, for which we will try to find one universal value for each so that all the simulation results above C_{CMC} agree well with the experimental data. By

fitting the simulation results to the dynamic surface tension data obtained from pendant bubble experiment (Cf. Chapter 5) for surfactant solution at different concentrations, $\beta^*=7$ $m^3/(mole\cdot s)$, thus $\alpha^*=7\times10^{-3}$ s^{-1} from $a^*=\alpha^*/\beta^*$ $=0.001$ mol/m^3, and $\Delta A=1/\Gamma_\infty=3.01\times10^5$ $m^2/mole$. The overall agreement is very good between the simulation results and experimental data for all the studied bulk concentrations, ranging from 1.27 CMC to 4 CMC (Figure 4.3) for the regime with micelle-free zone developed at certain point, from 6 CMC to 20 CMC (Figure 4.4) for the regime without micelle-free zone.

The micellar sublayer concentrations predicted from the transport model are plotted in Figure 4.2. The micelle sublayer concentration starts dropping to a very low value rapidly at the early stage of adsorption, the kinetic adsorption of monomer as well as micelle are fast due to relatively clean surface. Disassemble of micelle to restore monomer concentration in the sublayer also lowers micelle concentration. The diffusion of micelle can't keep up with the fast depletion of micelle from the sublayer, thus micelle sublayer concentration reduces sharply. As the adsorption of monomer and micelle goes on, the surface becomes more and more crowed, which leads to the reduction of adsorption rate of monomer and micelle. Then, the diffusion of micelle catch up and restore the micelle sublayer concentration until it reaches an equilibrium value. The critical bulk concentration n^* at which the micelle free zone emerges is found to be 6.0 CMC. The moving boundaries for different bulk concentrations at time $t-t_d$ are plotted in Figure 4.5. Shortly after the creation of the clean air/water interface in the micellar solution, fast micelle adsorption as well as micelle disassembly into monomer in the bulk quickly depleted the micelle from the bulk, leading to a micelle free zone developed in the bulk. The boundary between the zone having micelle and the micelle-free zone will depart

from the surface and move into the bulk as the kinetic adsorption keeps removing micelle from the bulk. As surface becomes more and more crowded with populated surfactant, the kinetic adsorption slows down and the diffusion of the micelle from the far field will restore the micelle concentration by narrowing the micelle-free zone width and finally the micelle free zone will disappear completely as the micelle-free zone moves back to the surface. Thus a maximum micelle free zone width was observed from the prediction of the model. The bulk monomer and micelle concentration distribution are plotted in Figure 4.6 and Figure 4.7 for the C_{total}=3 CMC solution, during the process of the micelle-free zone development.

4.6 Conclusions

First of all, theoretical models of surfactant adsorption and transport in a bulk solution containing only singly dispersed surfactant monomer are reexamined in this article. Especially for nonionic polyethoxylated surfactant $C_{14}E_6$, using literature vale of C_{CMC}=0.00912 mole/m^3 for the critical micelle concentration, 100 for average aggregation number, diffusivity $D_1=1.0\times10^{-10}$ m^2/s estimated from experimental measured diffusivities of similar surfactants, monomer parameters $\Gamma_\infty=3.32\times10^{-6}$ mole/m^2, $a=\alpha/\beta=2.068\times10^{-6}$ mol/m^3, K=7.12, and β=7.0 $m^3/(mol\cdot s)$ are obtained below the CMC regime by fitting the theoretical predications with experimental equilibrium and dynamic surface tension data.

Secondly, for a micellar solution, besides the conventional surfactant transport route through monomer adsorption onto the surface at the mean time of monomer diffusion and micelle diffusion, another novel surfactant transport route through micelle direct

adsorption is proposed. In this new picture of surfactant transport, micelles expedite the surface tension reduction of the surface monolayer in two ways. The first well-understood one is that micelles break up into monomers in the sublayer initially, then the released monomers from the micelle in the sublayer adsorb onto the surface. The second way is that micelles in the sublayer direct adsorb onto the surface themselves and breakup into monomers later which can be incorporated into the surface monolayer to speed up the surface tension reduction. The mathematical equations of the surface kinetic exchange of monomer and micelle are proposed first, in which the adsorption rate of monomer is treated as proportional to the sublayer monomer concentration and unoccupied space area. The adsorption rate of micelle is taken as linear in the sublayer micelle concentration and adsorption energy expressed in term of work need to be done to swipe surface area free of surfactant so that micelle can start adsorbing. When set to zero, these kinetic exchange equations give rise of equilibrium adsorption isotherms of both monomer and micelle. These isotherms are analyzed for the chosen surfactant $C_{14}E_6$ to give surface tension of surface monolayer containing both adsorbed monomers and intact micelles. The contribution of intact micelle in the surface monolayer is not important given that the constant chemical potential of adsorbed monomer and also non-changing chemical potential of adsorbed micelle when the bulk concentration passes the critical micelle concentration. Thus, though intact micelle starts to appear in the monolayer when the bulk concentration is bigger than the critical micelle concentration, the surface tension is kept the same as the surface tension achieved with bulk concentration at the critical micelle concentration. For $C_{14}E_6$, since the surface monolayer is covered mostly with monomer and micelle surface concentration is very small (interpreted both from the

experimental data and simulation results), equilibrium isotherm (shape of the equilibrium surface tension vs. bulk concentration curve) is found not sensitive to the micelle equilibrium parameters a^* and ΔA. Based on physical analysis, the lower limit of ΔA is the cross section area of a single monomer ($1/\Gamma_\infty$), the up limit is 100 times the cross section area of a single monomer ($100/\Gamma_\infty$) since one C14E6 micelle contains up to 100 monomers. A small value a^* is proposed considering that it is not easy for the adsorbed bulky micelle to detach itself from the surface monolayer. The agreement between the simulation and experimental data is very good.

Third, when formulating the theoretical equations for surfactant transport from a micelle solution, the new general picture is that, upon the creation of a clean air/water interface in a micellar solution, both micelle and monomer in the sublayer just beneath the surface will kinetically adsorb onto surface. The adsorbed micelle will break up into monomer if surface is not too crowed. The kinetic adsorption of the two species will disturb the dynamic equilibrium between micelle and monomer, thus micelle in the sublayer will also disassemble into monomer to restore monomer concentration. At the mean time, monomer and micelle from far field will diffusion toward surface as the concentration gradients are developed due to depletion of micelle and monomer from sublayer. For the studied surfactant $C_{14}E_6$, the monomer diffusion in a high concentration micellar solution is ignored given the fast micellization time scale compared to monomer adsorption time scale and monomer diffusion time scale. Thus for high concentration $C_{14}E_6$ micellar solution, monomer concentration will be kept constantly at the critical micelle concentration with the presence of micelle in the vicinity. Thus the proposed formulation of the transport theory for $C_{14}E_6$ involves the kinetic adsorption of both and

micelle from the sublayer onto the surface, and the diffusion of micelle in the bulk to replenish the sublayer micelle concentration. The assumption that the adsorbed micelle on the surface always breakup completely into monomer when the surface is not crowded or the surface concentration of monomer is smaller than the critical value $\Gamma_e(C_{CMC})$, which is the monomer surface concentration when the surface is in equilibrium with bulk surfactant of concentration C_{CMC}. After $\Gamma_e(C_{CMC})$ is reached, adsorbed micelles don't break up completely and there will be a small amount of adsorbed micelles remain as intact in the surface monolayer.

Fourth, when the total micelle concentration is smaller than a critical value n^*, a zone depleted of micelle completely will emerge as the bulk micelle diffusion is not fast enough to keep up with the rapid kinetic adsorption at the surface. This micelle-free zone will expand into the bulk at the early stage of surfactant transport and retract back to the surface later when the surface adsorption slows down. The formulation of the micelle-free zone involving the micelle diffusion in the bulk containing micelle, monomer diffusion in the micelle free zone, micelle breakup into monomer completed at the micelle free zone boundary, and monomer kinetic adsorption at the surface boundary. The diffusion coefficient of $C_{14}E_6$ micelle is chosen to be 1.0×10^{-10} m^2/s. By matching the dynamic surface tension prediction and experimental results, the micelle kinetic parameters $\beta^* = 7$ $m^3/(mole\cdot s)$, and $\Delta A=1/\Gamma_\infty$ are obtained, and the critical bulk concentration n^* is found to be 6.0 CMC. ΔA value is the same as the cross section area of a single monomer indicates that it may not be necessary for the whole micelle to adsorb onto surface before surfactant molecule in the micelle can be released. A micelle in the sublayer can start releasing monomer one by one into the monolayer if a small

clear spot around the size of monomer is made in the surface monolayer. The flexible structure of micelle in the vicinity of a hydrophobic surface may also lead to bind a big micelle to a smaller space in the monolayer.

The good agreement between the simulation results and experimental data for a wide range of bulk concentration from 1.27CMC to 4CMC for micelle-free zone, 6 CMC to 20CMC for micelle zone, suggests that the proposed surfactant transport model is adequate enough to predict surfactant transport in a micelle concentration with universal monomer and micelle parameters. Few micelle in the surface monolayer is seen during the adsorption process and equilibrium state suggests that micelle contributes to the reduction of surface tension by adsorbing onto surface and almost completely breakup into monomer, which is also discussed by Daniel and Bain [7].

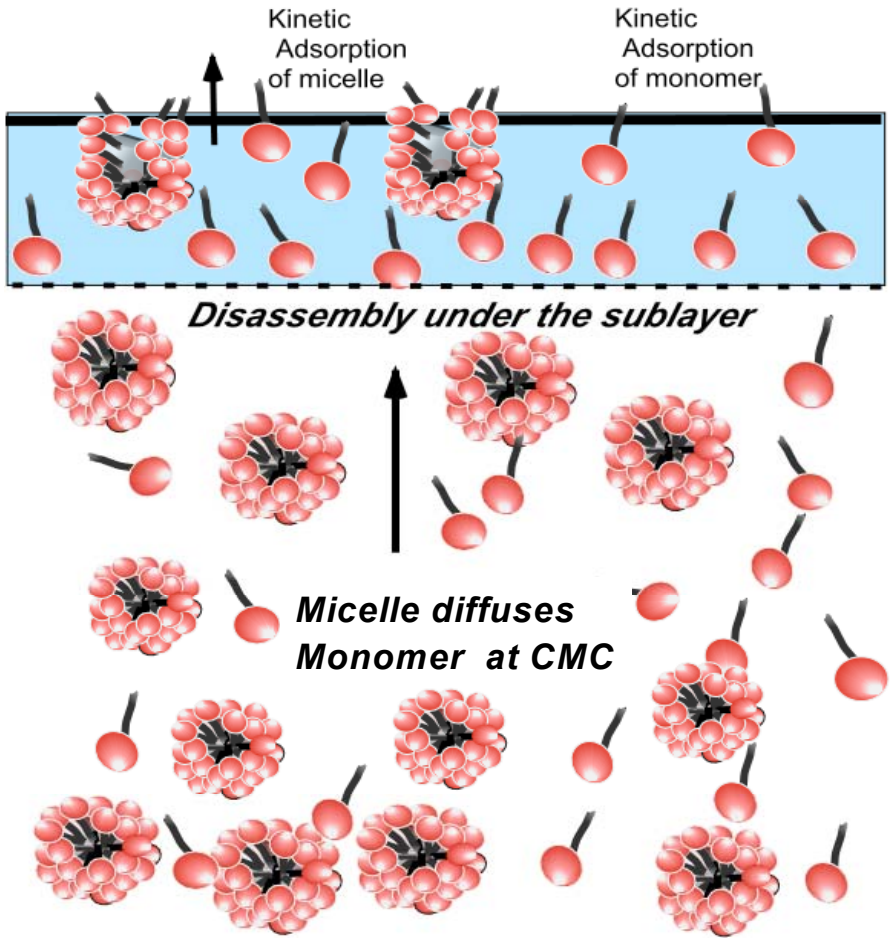

Figure 4.1: Schematic representation of surfactant transport from high $C_{14}E_6$ micellar solution onto an air/water interface via two routes.

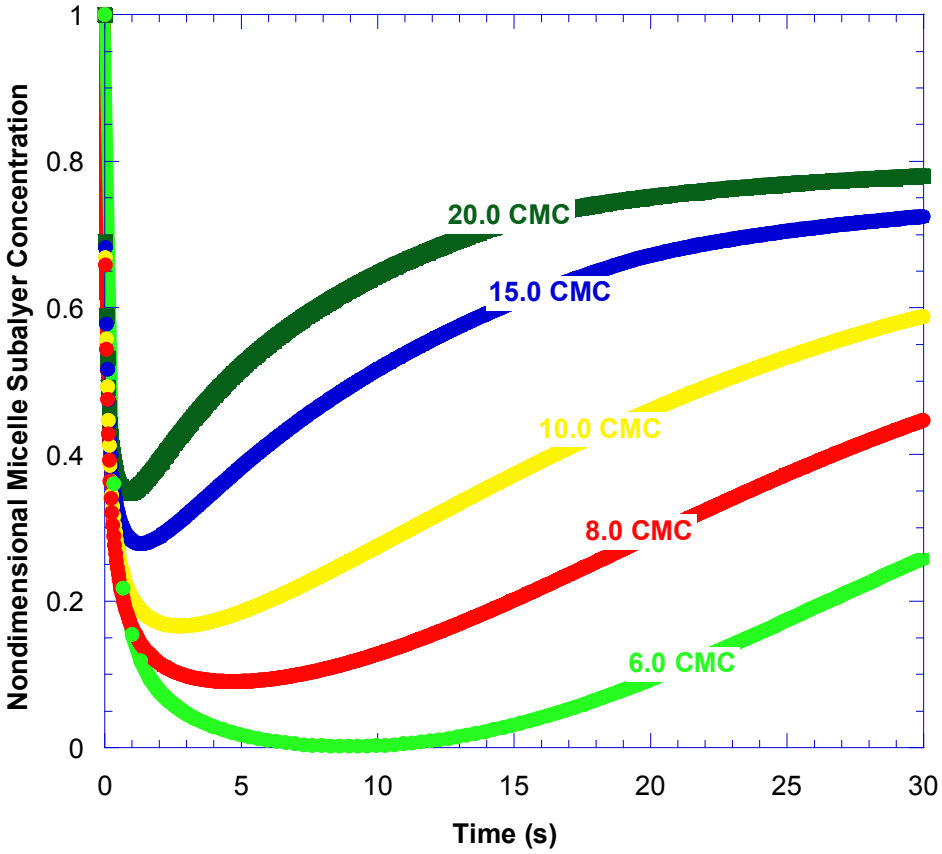

Figure 4.2: Sublayer micelle concentration of different bulk concentrations predicted from the model. Critical value for micelle-free zone is 6 CMC.

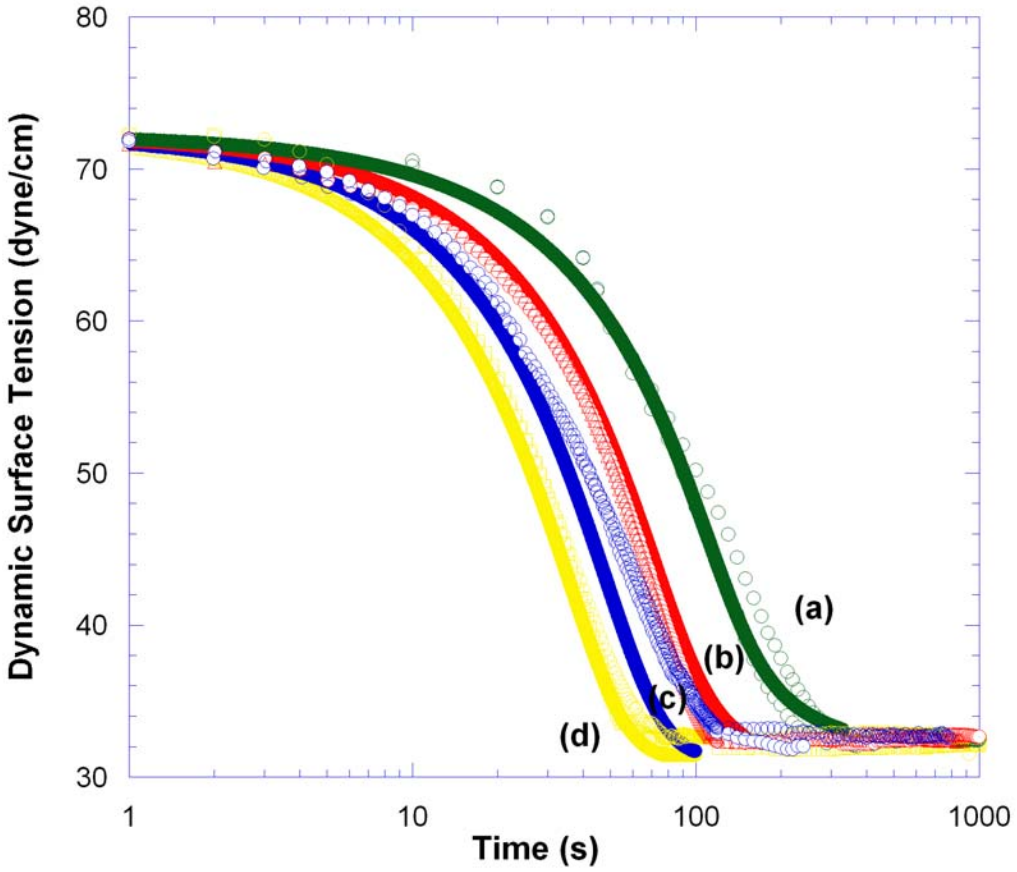

Figure 4.3: Dynamic surface tension predication for micelle-free zone regime with $D_M=1.0\times10^{-10}$ m^2/s, $\Delta A=1/\Gamma_\infty=3.01\times10^5$ m^2/mole, β^* = 7 $m^3/(mole\cdot s)$, $\alpha^*=7\times10^{-3}$ s^{-1}: (a) n=1.27 CMC; (b) n=2.0 CMC; (c) n=3.0 CMC; (d) n=4CMC;. Dashed curves are the experimental data and continuous curves are the simulation results.

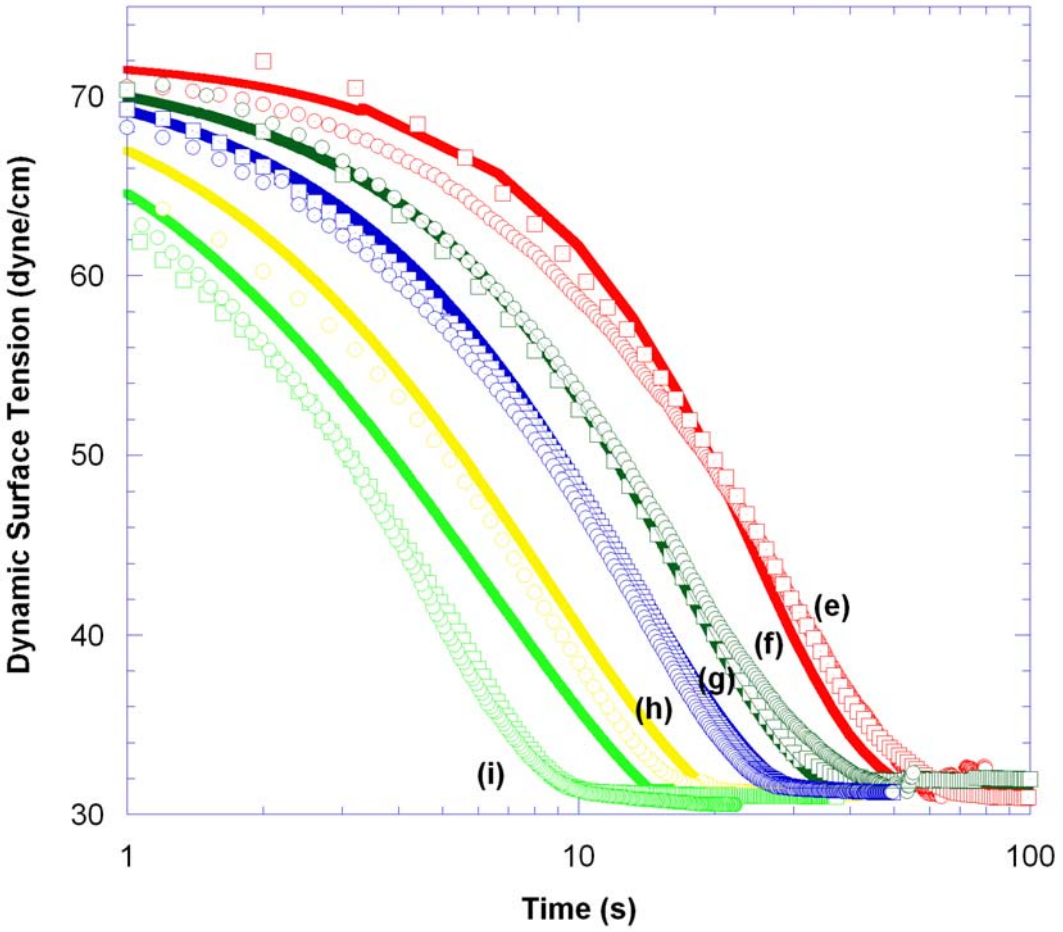

Figure 4.4: Dynamic surface tension predication for micelle-free zone regime with $D_M=1.0\times10^{-10}$ m^2/s, $\Delta A=1/\Gamma_\infty=3.01\times10^5$ m^2/mole, $\beta^* = 7$ $m^3/(mole\cdot s)$, $\alpha^*=7\times10^{-3}$ s^{-1}: (e) n=6 CMC; (f) n=8.0 CMC; (g) n=10.0 CMC; (h) n=15.0 CMC; (i) n=20.0 CMC. Dashed curves are the experimental data and continuous curves are the simulation results.

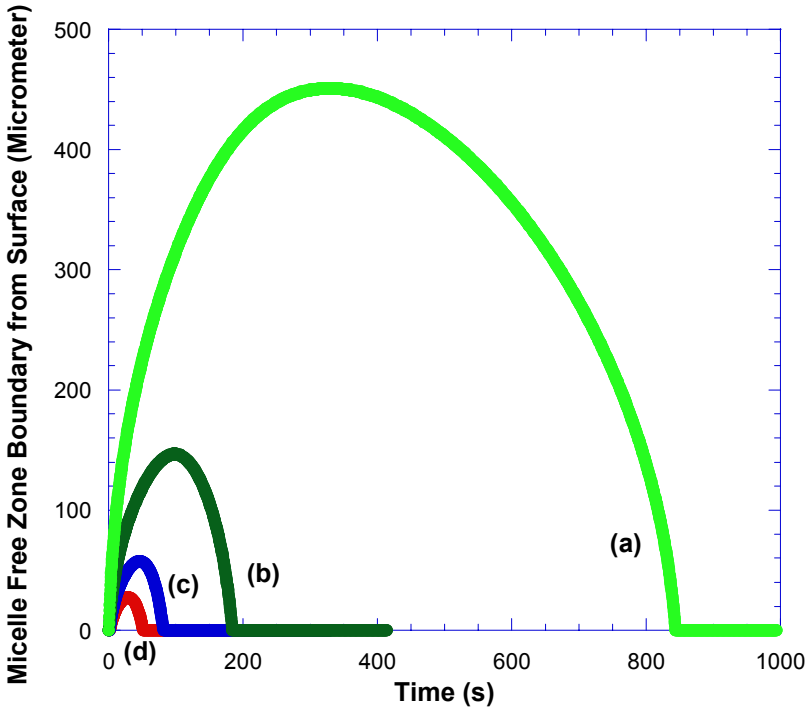

Figure 4.5: Moving boundary positions $\delta(t-t_d)$ in the bulk predicted from the model. (a) n=1.27 CMC; (b) n=2.0 CMC; (c) n=3.0 CMC; (d) n=4CMC.

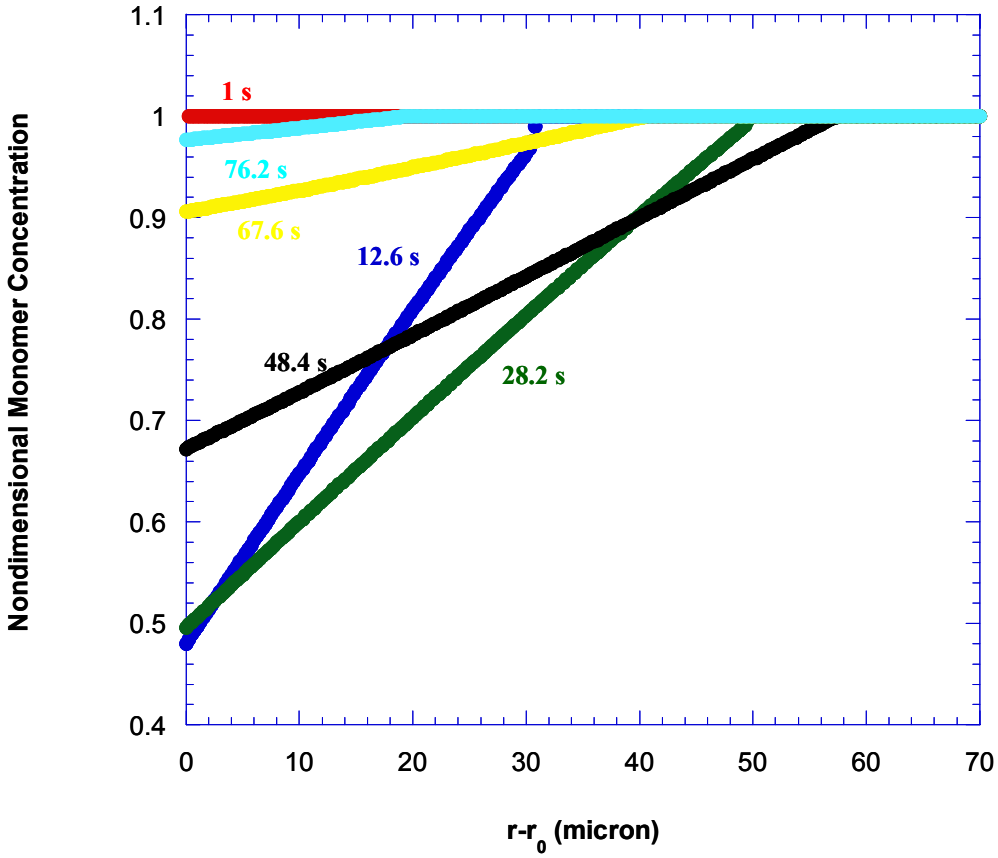

Figure 4.6: Monomer bulk concentration (nondimensionalized by CMC) distributions in the bulk through micelle-free zone development, C_{total} =3 CMC.

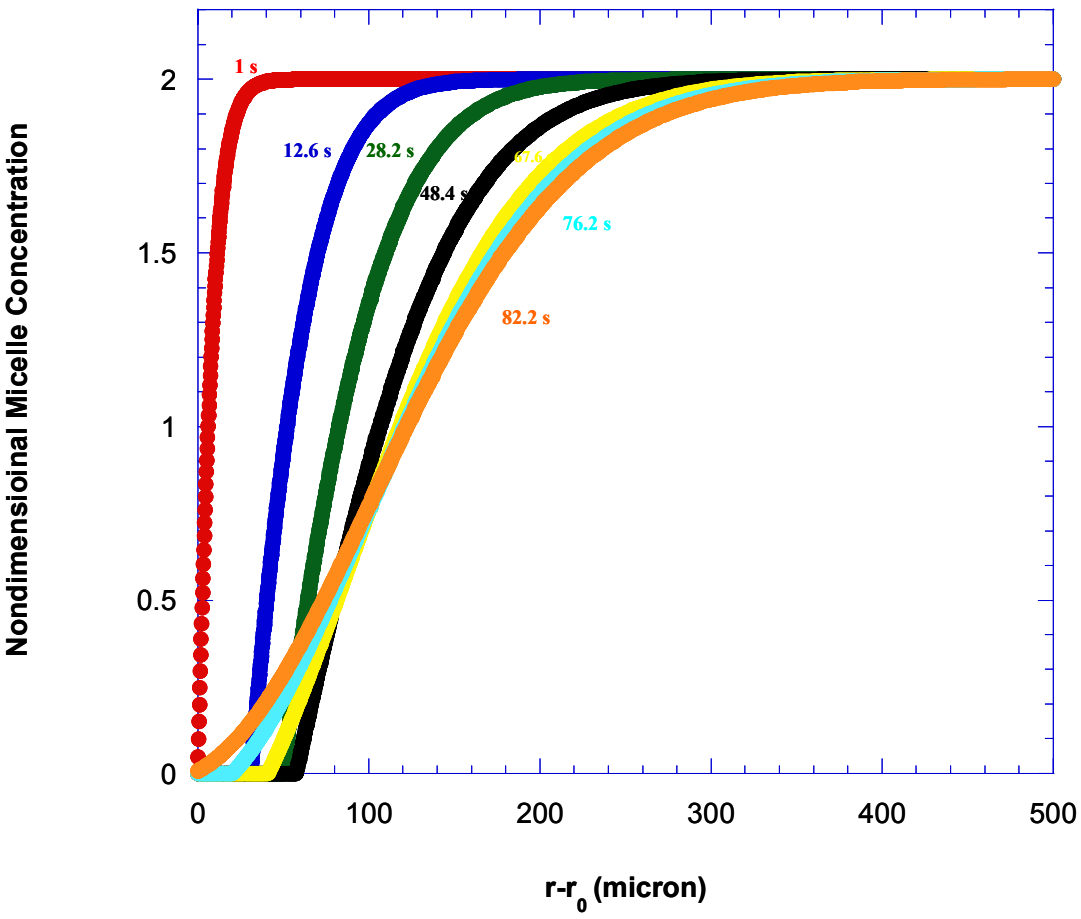

Figure 4.7: Micelle bulk concentration (nondimensionalized by (cn-1) CMC) distributions in the bulk through micelle-free zone development, cn=3, C_{total} =3 CMC.

Chapter 5

Experimental Evidence for the Direct Adsorption of Micelles onto an Air/water Interface

5.1 Introduction

This chapter details experimental evidence that spherical surfactant aggregates, present in a micellar aqueous solution, can adsorb ***directly*** onto a clean air/water interface from a bulk solution phase. To demonstrate this direct adsorption route, the aggregates in solution are tagged with a small, hydrophobic molecule which, when dissolved in an aqueous surfactant solution phase, incorporates itself preferentially into the hydrophobic core of the aggregate. The adsorption of the molecular tag to an air/water surface will be detected when a micellar solution of labeled micelles adsorbs onto a clean air/water interface. This adsorption will be compared to the adsorption of the tag from surfactant solutions below the critical micelle concentration (CMC), where it is dissolved at the same concentration as in the micellar solution, but because of the absence of aggregates, is present as free molecules. The comparison of the transport rates of the tag from these two solutions is used to provide insight into the transport of surfactant to a clean air/water interface from a micellar solution, and in particular to validate the direct micellar adsorption route. In the remainder of this introduction to this chapter, we first describe how the molecule tagging the micelles will be detected when it adsorbs onto an air/water interface (Sec. 5.1.1). We then describe (Sec. 5.1.2) the transport routes available to the tag for adsorbing onto the surface from sub-micellar and micellar solutions, and explain how the detection of the tag on the surface from both of these solutions can, in view of these routes, be used to validate the direct transport route. All the experiments detailed in

this chapter use the polyethoxylated surfactant $C_{14}E_6$ ($CH_3(CH2)_{13}(OCH_2CH_2)_6OH$) as the model surfactant. This surfactant forms approximately spherical micelles in aqueous solutions at room temperature. The materials and experimental methods are described in Sec. 5.2, and the results and discussion are given in Sec. 5.3

5.1.1 The Detection of the Tag on the Air/water Interface

The small hydrophobic molecule which is used to tag the micellar aggregates is Nile Red, a dye, whose structure is shown in Figure 5.1. The solubility of Nile Red in water is very low, less than 1 μg/ml and the concentration used in the experiments of this study, c, is .2 μg/ml. Aqueous solutions at this concentration shown no precipitation and stable adsorption and emission spectra indicating the dye to be solvated in solution. Nile Red is chosen for two reasons. First, as is well documented, when Nile Red is dissolved in an aqueous solution containing micelles, it preferentially incorporates itself into the hydrophobic interior of the aggregates leaving only trace amounts of free molecule in solution. Hence it is a discriminating tag of aggregates. Second, Nile Red contains a fluorescing chromophore, and advantage can be taken of this group on the molecule, to implement a fluorescence method for detecting Nile Red's adsorption onto an air/water interface. Two different methods are used to detect the adsorption of the Nile Red onto an air/water interface. The first, indirect method, is based on measuring the reduction in dynamic surface tension when surfactant solutions containing the dye adsorb onto the surface and comparing the tension relaxation to the case in which the surfactant solution does not contain the dye. The second, more direct method, takes advantage of the chromophore group on the Nile Red, and detects, the luminescent energy release from

Nile red when excited non-radiatively by Fluorescence Resonance Energy Transfer (FRET) from donor molecules localized on the surface.

In the dynamic surface tension method, the surface tension of a fresh interface created in a surfactant solution is measured as a function of time until equilibrium is achieved. The easiest method for undertaking this measurement is to impulsively create a pendant bubble at the tip of a needle and obtain the tension by imaging the shape of the interface. This experimental method is described in detail in Sec. 5.2. As surfactant adsorbs from solution to the interface of the bubble, the surface tension is reduced until equilibrium is achieved. When a small hydrophobic molecule is present on a surface containing an adsorbed monolayer of amphiphiles, the molecule can partition into the hydrophobic part on the monolayer where it effectively increases the surface pressure or decreases the surface tension as it expands the monolayer (Figure 5.2). Hence in the experiments to be discussed here, as the tag adsorbs onto the surface from a micellar solution (by whatever route), the dynamic and equilibrium tensions are altered in such a way that there is a reduction from reference values obtained in the absence of the dye, and the observation of a reductive difference can be used to infer the presence of the tag on the surface.

The second method used to detect the adsorption of Nile Red on the air/water surface is based on the detection of a luminescent emission of energy from the Nile Red, with the excitation for this emission originating from non-radiative fluorescence resonance energy transfer (FRET) from donor molecules localized on the surface. The donor molecule to be used is a phosphocholine phospholipid in which one acyl chain of the lipid is attached to a heterocyclic NBD chromphore (2-(12-(7-nitrobenz-2-oxa-1, 3-diazol-4-yl) amino) dodecanoyl-1-hexadecanoyl-sn-glycero-3-phosphocholine, NBD C_{12}-HPC, Figure 5.1)

As is usual for lipids, this labeled lipid dye is nearly insoluble in water. In our experiments they are directly spread onto the air/water interface of a thin film by dissolving the lipid in a volatile non-polar solution and spreading the solution onto the surface. After evaporation of the solvent, the lipids are anchored onto the surface. The adsorption spectrum of the NBD chromophore has an adsorption peak at approximately 458 nm, and the emission spectrum has a peak at approximately 540 nm. The emission peak of the NBD, at 540 nm, coincides with the region in the adsorption spectrum of the Nile Red chromophore where there is significant adsorption (Figure 5.3). The emission spectrum of the Nile red has a peak at 640 nm, significantly Stokes red shifted from its peak adsorption (Figure 5.3). The overlap ($J(\lambda)$) of the emission of the donor and the adsorption of the acceptor allows for strong non-radiative energy transfer. The non-radiative energy transfer is based on intermolecular resonance energy interactions between the transition dipoles of the donor and acceptor molecules. This transfer, since it is based on intermolecular interactions, is only effective when the molecules are within the Förester energy distance of approximately 10 nm or less. The resonance energy transferred from the donor (NBD C_{12}-HPC) is readmitted by the Nile red as luminescence in accordance with its emission spectrum which has a peak at 640 nm. When the surface is illuminated with light at the excitation adsorption peak of the NBD donor (approximately 450 nm), the presence of Nile Red emission at 640 nm confirms that Nile Red is directly on the surface (Fig. 5.4). In this study, the emission spectra at the surface will be recorded using Confocal Laser Scanning Microscopy (CLSM) on monolayers overlaying thin aqueous films situated in chambered cover glass. This technique is described in detail in Sec. 5.2

5.1.2 Transfer Routes of the Label to the Surface and Identifying the Signature of Direct Micelle Adsorption

Consider first the transport of the Nile red label at a concentration c (below its solubility limit) when the label is dissolved as a free solvated species in an aqueous surfactant solution below the critical micelle concentration, and a clean air/water interface is created in the solution (Figure 5.5). In this case, there is only one accessible route to the surface: The free dye diffuses to the surface and adsorbs onto the surface, simultaneous with the adsorption of the surfactant. The rate of transport is driven by the affinity of the Nile Red to the surface from the sublayer. When the surface is free of surfactant, the Nile Red does not have a strong tendency to adsorb to the surface since it is not amphiphilic. However, with the simultaneous adsorption of the surfactant, a hydrophobic layer comprised of the hydrocarbon chains of the surfactant builds on the surface and the affinity of the Nile Red to the surface increases as the dye can now adsorb into the layer. Thus as the adsorption of the Nile Red proceeds, the rate of transport of the dye to the surface increases until eventually equilibrium is approached and a steady adsorption of dye develops on the surface. The hydrophobic part of the monolayer acts as a reservoir for the dye, scavenging it from solution so that at equilibrium there is a steady dye on the surface and (for limited volumes of surfactant solution) a reduced amount of dye in the bulk. Hence the accumulation of the dye on the surface is an expected delayed response with adsorption increasing until eventually the adsorption levels off. This response represents the reference from which the transport of micelles to the surface will be compared.

When the bubble is created in a micellar solution in which the tag is embedded in the core of the micelles (at the same overall concentration c), there are three principal

adsorption routes to the surface. The first is the adsorption of free dye present in the solution at equilibrium, as in Figure 5.5. This route is negligible because the selective partitioning of the dye in the micelles insures that there is a negligible amount dye in the bulk at equilibrium. A second route arises as micelles disassociate into surfactant monomer due to the reduction in monomer concentration as a result of monomer adsorption to the surface. The micelle disassociation releases Nile Red into solution, and this charge to the solution provides a greater concentration of the dye to adsorb as a free molecule onto the surface (Figure 5.6). This route then resembles the adsorption to the first route, except that the monolayer assembles more quickly in this case because of the higher surfactant concentration and free dye can partition in neighboring micelles that have not disassembled. Hence for the same concentration of dye in the bulk as in the below CMC reference, if this is the principal route, what should be observed is that the Nole red should show up on the interface much earlier but at a much reduced level.

The third route for the adsorption of dye onto the surface is for the micelles to directly adsorb onto the surface and release the dye partitioned into their hydrophobic core (Figure 5.7). As this adsorption route is most important when the interface is clean, the adsorption of the Nile Red tag on the surface should exhibit an initial increase followed by a reduction in the rate of adsorption. Since the bulk concentrations of the dye in the reference and the micellar solutions are the same, this increase will depend on the diffusion and adsorption rates. The diffusion rate is slower because micelles diffuse slower than free monomer. But the adsorption rate of the micelles to the surface could be anticipated to be larger, making the adsorption and tag signal larger than in the reference.

In summary, the signature for direct micelle adsorption is the behavior of the adsorption of the dye at early times compared to the reference. If the early adsorption is much greater at early times relative to the reference, then micelles would be directly adsorbing with a higher adsorption rate than monomer. This would represent unequivocable proof of direct adsorption. If no initial adsorption of the dye is found, at early times (and for all times) then this would be strong evidence that the micelles cannot adsorb onto the surface, and their presence simply augments the adsorption by disassembly to release monomer. If the initial adsorption is of the order of the delayed adsorption then both neither route can be eliminated.

5.2 Experimental Section

5.2.1 Materials

2-(12-(7-nitrobenz-2-oxa-1, 3-diazol-4-yl) amino) dodecanoyl-1-hexadecanoyl-sn-glycero-3-phosphocholine (NBD C_{12}-HPC) and Nile Red were obtained from Invitrogen Corporation and stored in the refrigerator. The poly (ethylene glycol) alkyl ether surfactant $C_{14}E_6$ ($CH_3(CH_2)_{13}(OCH_2CH_2)_6OH$) was purchased from Nikko Chemical Company, Ltd. (Japan) and stored in a dark cabinet. Ethyl alcohol (ACS reagent grade) and chloroform (HPLC grade) were purchased from Spectrum Chemicals. Deionized (DI) water with resistivity at least 18MΩ·cm was obtained from a Millipore purification system (Millipore, MA). All chemicals were used as received without any further purification. Lab-Tek® II Chamber Coverglass™ with two chambers for an inverted microscope were purchased from Electron Microscopy Science and rinsed with deionized water before use in confocal microscopy. A gas-tight 10-μl microsyringe with flat-cut

needle tip and a 1000-µl microsyringe were purchased from Hamilton Cooperation. A flat-cut 25-gauge needle for the 1000-µl microsyrenge was bought from Vita Needle Company.

An aqueous 15 CMC $C_{14}E_6$ stock solution was made and diluted to desired concentrations. A 0.3 mg/ml Nile Red stock solution was made in ethanol and diluted to 0.2 µg/ml (the solubility of Nile Red in pure water is 0.3 µg/ml) in either water or surfactant solutions by vigorously stirring overnight. The solution was left still for a couple hours before use. A 7.58 mg/L NBD C_{12}-HPC stock solution in chloroform was made and 3µl of which is spread on the air/water interface using microsyringe to generate NBD C_{12}-HPC monolayer.

5.2.2 Experimental Techniques

Pendant Bubble Tensiometry

The pendant bubble tensiometry is a well-established and widely utilized method to measure the dynamic surface tension relaxation as the surfactants adsorb onto the surface due to its accuracy and reliability. A schematic illustration of this method is given in Figure 5.8. For the details of this method, refer to articles[1, 2]. Briefly, a pendant bubble is rapidly formed (in a few tenths of second) on the tip of an inverted needle that is immersed in surfactant solutions of known concentration. As surfactants absorb onto the interface, the tension is lowered, and the shape of the bubble, which is a balance between surface tension and buoyant forces, elongates. At any time, the shape of the bubble is governed by the Laplace-Young equation, which relates the pressure drop across the interface to the two radii of curvature. A digital image of the silhouette of the pendant

bubble (the insert) is used to obtain the loci of the pendant bubble. The experimental loci are compared with theoretical interface shape that is generated by the solution of the Young-Laplace equation. The surface tension, which determines the theoretical shape, is then varied until an optimum is achieved between the theoretical shape and the experimental loci. All experiments were taken at room temperature 22 ± 0.5 °C by placing a quartz curvette filled with surfactant solution in a thermostating chamber in which water from a recirculating bath set at 22°C thermostats the chamber. Measurements were begun after a temperature equilibrium is reached between the chamber and the surfactant solution. In each run, measurement is usually taken until equilibrium is reached.

The pendant bubble method is used to record the dynamic surface tension reduction accompanying the adsorption of Nile Red from an aqueous solution of concentration 0.2μg/ml, $C_{14}E_6$ monomer adsorption from an aqueous solution of concentration 0.17CMC (1.55×10^{-3} mole/m^3), the adsorption of $C_{14}E_6$ and Nile Red from a mixed solution which has 0.2μg/ml Nile Red and 0.17CMC $C_{14}E_6$, $C_{14}E_6$ adsorption from a 15CMC micellar solution, and the adsorption of Nile Red and $C_{14}E_6$ from a mixed solution which has 0.2μg/ml Nile Red and 15 CMC $C_{14}E_6$.

Spectrofluorimetry

A spectrofluorometer (FlouroMax-3, Horiba Jobin Yvon) was used to measure the excitation and emission spectra of the NBD C_{12}-HPC dissolved in chloroform, and Nile Red dissolved in either pure water or surfactant solutions. The excitation spectra were recorded with detection at 540 nm and 640 nm for 8.85×10^{-6} mole/L NBD C_{12}-HPC in chloroform solution and 0.2 μg/ml Nile Red in 15 CMC $C_{14}E_6$ aqueous solution with slit width of 1 nm respectively. Emission spectra of the NBD C_{12}-HPC (slit width of 1 nm)

and Nile Red (slit width of 2 nm) are obtained by exciting at 458 nm and 543 nm respectively.

Confocal Laser Scanning Microscopy (CLSM)

The main hardware parts of a confocal laser scanning microscope consists of multiple laser excitation sources, a scan head with optical and electronic components, electronic detectors (usually photomultipliers, PMT), and a computer for acquisition, processing, analysis, and display of images. Schematic representation of the beam path of a confocal microscope is shown in Figure 5.9. The light coming from the laser passes an excitation pinhole is reflected by a diachronic mirror, focused by a microscope objective and illuminates a small point on the focal plane on the sample. A fraction of the emitted photons is collected by the microscope objective and can pass through the dichroic mirror, and is subsequently focused onto the detector pinhole and imaged onto the detector.

Confocal Laser Scanning Microscopy can produce much more prominent and high-resolution optical images compared to traditional widefield fluorescence microscopy. In a widefield microscope, incident light from an incoherent mercury or xenon arc-discharge lamp is focused down to a sample by an objective, thus illuminating a large spot on the sample, leading to fluorescence generation from the entire depth of the illuminated spot and results in poor resolution along the depth of the sample. In a laser scanning confocal microscope, the source pinhole attenuates the incident beam size down to a few microns, which gets further focused down to a small spot (about 1 micron in diameter) on the sample. 3-D intensity variation a focused laser beam in CLSM, called the point-spread function (PSF) is assumed to be radically and axially Gaussian[3], which implies that there will be minimal excitation of the sample above and below the focal plane.

Additionally, by putting a pinhole in front of the detector blurring from out-of focus planes is greatly reduced. Hence, it is the combination of the source and detector pinhole improves the vertical resolution significantly. The sample is scanned point-by-point with a finely illuminated spot on the sample plane. Fluorescence single is accumulated on the PMT detector and image is reconstructed with a computer. The scan head controls the movement of the illuminated fine spot through galvanometer-based raster scanning mirror system.

Confocal Laser Scanning Microscope (CLSM, Leica TCS SP2® AOBS Laser Scanning Confocal Microscopic Imaging System, equipped with an acoustic-optical beam splitter and a prism spectrophotometer detector, 10× PL FLUOTAR N.A. 0.30) was used to study the phase behavior of NBD C_{12}-HPC monolayer on an air/water interface and the fluorescent emission spectra of the surface and the bulk. Beam Expansion 3, pin hole size 113.4 Airy units, PMT with a Gain (voltage) of 815.9 v and an Offset of -9.2, 1400 Hz scan speed were set to observe the phase behavior of NBD C_{12}-HPC monolayer on air/water interface. Line average and area average were chosen to be one to minimize the scanning time. For recording the fluorescence spectrum and FRET between NBD C_{12}-HPC and Nile Red in the surface monolayer, PMT is adjusted to a Gain of 1000 v and an offset of -9.2, with other settings remaining the same. 1 ml deionized water was injected into the chambered coverglass and on top of which, chloroform solution of NBD C_{12}-HPC was spread using a microsyringe. After waiting about one minute to allow chloroform to evaporate, the fluorescence images of the NBD C_{12}-HPC monolayer on the water layer was obtained by exciting with a 458 nm laser line, and with emission collecting window from 530 to 750 nm. Fluorescence images of the

surface were taken at different time to illustrate the first order phase transition from gaseous phase (G) to liquid expand phase (LE).

At least 20 minutes were allowed to let NBD C_{12}-HPC spread out and form an assumedly uniform monolayer on the surface. Then an emission collecting window from 468 to 750 nm with a slit width of 5 nm was used to obtain the emission spectrum of NBD C_{12}-HPC. 0.5ml surfactant solution either with or without Nile Red was injected underneath the surface monolayer using a 1000-μl microsyringe fitted with a flat-cut 25-gauge needle. The needle was kept at the bottom of the coverglass and the introduction spot of surfactant solution was right above the objective lens. The injection was usually completed smoothly within 15 seconds and the flow rate was kept small enough so that the injection would not disturb the NBD C_{12}-HPC surface monolayer and micelle would not be delivered to the surface monolayer due to the convection.

Another fluorescence experiment was carried out, in which, the NBD C_{12}-HPC surface monolayer was allowed to equilibrate with micelle solution so that surface monolayer with maximum $C_{14}E_6$ surface concentration with NBD C_{12}-HPC embedded will be formed on the surface. After introduction of micelle solution which had Nile Red incorporated in the micelle, the surface fluorescence spectrum was carefully monitored.

5.3 Results and Discussion

5.3.1 Dynamic Surface Tension Measurements

Results are first presented on the transport of the Nile Red dye from sub-micellar and micellar solutions to a clean air/water interface, as measured by the reduction in dynamic surface tension as surfactant from the solutions absorb to a clean interface. As an initial

reference experiment, the dynamic surface tension of a pendant bubble immersed in a Nile Red aqueous solution of concentration 0.2 μg/ml (which is below the solubility of Nile Red in water of 0.3 μg/ml) at 22 ± 0.5 °C without any surfactant (Figure 5.10) is measured, and indicates that the surface tension does not appreciably change from its initial value of 72.5 dyne/cm, which is the surface tension of a clean air/water interface. This result implies that at this dilute concentration, there is not enough Nile Red adsorption onto the clean air/water interface to change the surface tension from the value of the clean air/water interface tension. Nile red is a mostly hydrophobic molecule, and not very amphiphilic. Given that its character is not very amphiphilic, and since it is dissolved below its solubility limit in water, Nile Red does not have a strong driving force to adsorb by itself onto the air/water interface, particularly at low concentrations.

The adsorption characteristics are different when a surfactant monolayer is adsorbed on the surface, and the hydrophobic phase composed of the chains of the surfactant above the water offers a hosting environment for the Nile red. The dynamic surface tension relaxations of 0.17 CMC $C_{14}E_6$ solution and 0.17 CMC $C_{14}E_6$ with 0.2 μg/ml Nile Red solution are plotted together in Figure 5.11. All the Nile Red is freely dissolved in the bulk aqueous phase when the concentration of the surfactant solution is below the CMC. These dynamic tension results clearly show that, after an induction time, the Nile Red adsorbs to the surface. During the first tens of seconds of adsorption, both surfactant solutions with and without Nile red exhibit an identical induction period in the tension where the tension remains at approximately the clean interface value. During this period, the surfactant adsorbing onto the surface exists in co-existing gaseous (G) and liquid expanded (LE) phases, and as the adsorption proceeds the liquid expanded phase grows

at the expense of the gaseous phase. In the gaseous phase, the surfactant tails lie down on the surface and are separated from one another. This phase does not provide a good hosting environment for the Nile red since there is no hydrophobic domain on the surface. In the liquid expanded phase, the surfactant tails are above the surface forming a more continuous hydrophobic region which provides the proper hosting environment. The induction period in the surface tension ends when enough surfactant adsorbs onto the surface so that the monolayer is entirely in the liquid state, and further adsorption results in an increase in the surface pressure of the monolayer and a reduction in tension. As the liquid expanded state completely covers the surface, the adsorption of the dye becomes important and the data demonstrates that, after the end of the tension induction period, the tension of the dye surfactant solution becomes lower than that of the solution without the dye as the added presence of dye on the surface increases the surface pressure (Figure 5.2). At the end of the induction period, around 100 seconds after the creation of the surface, the dynamic surface tension of surfactant and Nile Red mixed solution departs from and stays below the tension achieved by the surfactant solution alone. Since the small Nile Red concentration is not believed to alter the adsorption property of $C_{14}E_6$, the difference in the dynamic surface tension reduction indicates that the affinity of Nile Red to hydrophobic environment could lead to the adsorption of Nile Red to the $C_{14}E_6$ surface monolayer, which acts as a hydrophobic shield for Nile Red from the aqueous bulk. The adsorption of both Nile Red and surfactant resulted in a mixed monolayer of Nile Red and $C_{14}E_6$ and reduced the surface tension of the mixed solution relative to the surfactant-only solution, with a ~ 2.5 dyne/cm difference from the one without Nile Red.

This difference persists to equilibrium. The equilibrium surface tension of the mixed solution is lower than the one of the surfactant-only solution implying that at equilibrium the adsorbed Nile Red in the surfactant monolayer remains in the surfactant monolayer and does not go back to the surfactant solution bulk. This is as expected, since the bulk solution contains no hydrophobic domains to sequester the dye, and the hosting of the dye in the hydrophobic part of the monolayer is an energetically preferable arrangement.

The difference in dynamic tension relaxations between the Nile Red/surfactant and surfactant-only solutions is completely different when the concentration of surfactant in both solutions is above the CMC, and this difference demonstrates clearly the direct micelle adsorption route. The dynamic surface tension relaxations of 15 CMC $C_{14}E_6$ miceller solution and a mixed 0.2 μg/ml Nile Red in 15 CMC $C_{14}E_6$ micellar solution are plotted in Figure 5.12. In the mixed solution of Nile Red in a surfactant micellar solution, the Nile Red partitions preferentially into the micelle which provides a hydrophobic environment for the Nile Red, and removes the Nile red from water. When a clean interface is created in a micellar solution, the adsorption of surfactant to the surface is much faster than in the case of a sub-micellar solution, and the induction period is less than a second. The data indicates that after one second, the amount of dye on the surface is already very large, with a difference in tensions at one second after the creation of the interface of approximately 5-7 dyne/cm, approximately double the largest difference obtained in the sub-micellar dynamic relaxations. Direct adsorption of micelles onto the surface during the induction period can account for this large difference in tensions, with the adsorbed micelle then breaking up and releasing monomer as well as the incorporated Nile Red onto the surface monolayer. During the induction period, regions of the surface

are in a gaseous state and micelles can easily adsorb to the surface, delivering the Nile red. If the Nile red did not adsorb to the surface by delivery through the direct adsorption of the micelles - but instead adsorbed to the surface by disassembly of the bulk micelles followed by adsorption of the liberated dye - the tension after one second between the micellar solutions with and without Nile red would not be very different. This is because, as we know from the prior experiment, free dye does not adsorb very well to the gaseous/liquid expanded interface during the induction period because of a lack of a hydrophobic hosting environment. And an additional consideration is that free dye liberated by micelle disassembly is more than likely adsorbed into remaining micelles in their vicinity, further decreasing the driving force for any adsorption of free dye to the induction period monolayer. The large difference in tension, in fact, represents an overshoot in the dye delivered to the surface; the previous experiment shows that free dye adsorbing to the monolayer retains an amount that accounts for a much smaller difference in tension.

This large amount of Nile Red initially adsorbed to the surface during the overshoot due to direct micelle adsorption is eventually removed to the bulk as the surfactant adsorption proceeds and the surface equilibrates. This removal is an essential difference between the transport of Nile Red between the bulk and the surface in the sub-micellar and micellar solutions, and provides further evidence of the direct micelle adsorption route. As the adsorption proceeds, the more surface-active surfactant replaces the less surface-active Nile Red in the monolayer, and the Nile Red on the surface desorbs to the bulk. The desorption is further driven by the presence of micelles in the bulk; Nile Red on the surface desorbs from the surface, dissolves in the bulk and partitions into the

hydrophobic domain of the micelles. The solubility in the bulk is enhanced greatly by the presence of bulk micelles since the bulk micelles provide more hydrophobic volume to incorporate Nile Red than the surface monolayer. The bulk micelles repartition the Nile Red from the surface monolayer into the bulk micelles until the tension of the micellar Nile red solution becomes equal to that of the micellar solution without Nile red. This indicates that the amount of Nile red on the surface is below the detection of tensiometric measurement. The removal of the Nile Red from the surface monolayer is reflected in the dynamic tension curves by their change in curvature as the surface tension gradually reaches the equilibrium surface tensions (see the insert of Figure 5.12). The removal of the Nile Red from the surface finally leads to the same equilibrium surface tension as the micellar solution without dye. This was not the case when the Nile Red was dissolved in sub-micellar solutions where the dye absorbed onto the surface remains on the surface since there are no micelles to provide a re-partitioning reservoir.

5.3.2 Photoluminescence Measurements of Dye Adsorption

In this section, results are presented on the transport of the Nile red dye from sub-micellar and micellar solutions to a clean air/water interface, as measured by the photoluminescence of the Nile Red due to nonradiative energy transfer from a donor fluorophore, NBD C_{12}-HPC, located on the surface. The fluorescence excitation and emission spectra of the Nile Red and NBD C_{12}-HPC are presented first (Sec. 5.3.2.1), and is followed by a study of the phase behavior and photoluminescence of the donor, by itself at the air/water interface (Sec. 5.3.2.2). The last subsection (5.3.2.3) presents the results on the adsorption of the Nile Red from the surfactant solutions to the air/water surface, and the relevance of the results to validating the direct micelle adsorption route.

5.3.2.1 Excitation and Emission Spectra of NBD C_{12}-HPC and Nile Red

The photoluminescence (PL) excitation and emission spectra of NBD C_{12}-HPC dissolved in chloroform and Nile Red in a micellar solution are characterized using a spectrofluorimeter and are summarized as given in Figure 5.3. NBD emission spectrum in chloroform is plotted in Figure 5.13. The excitation wavelength is 458 nm and the emission maximum (λ_{max}) is around 535 nm, which is very close to adsorption maximum of Nile Red around 540 nm. Figure 5.14 shows the emission spectrum of 0.2 μg/ml Nile Red in water, 0.5 CMC and 15 CMC $C_{14}E_6$ solutions. An appreciable λ_{max} shift of Nile Red is observed in going from an aqueous solution (λ_{max}=659.0nm), to Nile Red dissolved in a 0.5 CMC $C_{14}E_6$ solution (λ_{max}=651.0nm), and finally to Nile Red dissolved in a15 CMC $C_{14}E_6$ micelle solution (λ_{max}=637.0nm). Nile Red is soluble over a very wide range of solvents, and is a solvatochromic fluorescent probe which shows a large bathochromic absorbance shift (108nm from n-hexane to water)[4], and emission maximum shift (40.1nm from t-butanol to water)[5] with increasing solvent polarity. Since Nile Red is poorly soluble in water, there is a large preference to partition into micelles or other aggregates which offers a hydrophobic binding site. In a micelle, Nile Red has a general tendency to position at the interface owing to the large surface-to-volume ratio of the micelle [6]. However, some molecules are facing the water (a polar interface), whereas others are more located toward the hydrophobic tail of the amphiphiles (at a polar interface). The broad emission spectra are likely due to the coexistence of multiple populations in 15 CMC micelle solution and the spectrum can be deconvoluted into two spectra originating from the Nile Red's residence at the two interfaces. Though there is no micelle aggregate in the 0.5CMC solution, the divergence

between the spectra of 0.5CMC and water solutions may be due to the presence of preaggregates in 0.5 CMC solution, which partially shield the Nile Red from being completely exposed to water, resulting in a fluorescent emission intensity difference.

5.3.2.2 Fluorescence on an Air/water Interface of a Monolayer of the Donor NBD C_{12}-HPC alone and with Surfactant

The first fluorescence results presented in Figure 5.15 (a)-(f) were obtained by CLSM after spreading the NBD C_{12}-HPC chloroform solution onto a clean air/water interface. The inverse surface coverage of the NBD C_{12}-HPC was approximately 1500 $Å^2$ /molecule and was in the first order phase transition region, consisting of gaseous (G) and liquid expand (LE) states. Upon illumination, the dye doesn't fluoresce in the gaseous state because the NBD fluorophore is in contact with water and its fluorescence is thus quenched. In the LE state, the dye can fluoresce since the fluorophore is removed from the water surface and exists in a hydrophobic environment. The coexistence of G and LE phases was obvious about one minute after the spreading ((a) and (b)), showing large bright LE pockets with round dark (gaseous) domains in a mainly dark background. As time progresses, the bright LE regions increase at the expense of dark gaseous regions ((c) and (d), about three minutes after the spreading) until the background went from dark to bright, with dark domains now existing in the bright background ((e) and (f), about 20 minutes after spreading)). The enlarged picture of the dark pockets in the bright background showed that the dark pockets had bright LE regions in them ((f)). The bright LE regions in (e) and (f) were not equally bright since the lateral diffusion of NBD C_{12}-HPC may not be fast enough to generate a uniform dye monolayer within the time frame. Additional time might be needed to allow the dye to spread out more. However, due to the evaporation of the thin water layer (large surface area to volume ratio, about 1.5mm

in height, and 4 cm^2 area size) underneath the surface monolayer, no more than 30 minutes is allowed and the uneven brightness of the dye monolayer in the surface persists. Similar G/LE phase transition for $C_{14}E_6$ has been observed by Subramanyam *et al.* in a open channel Teflon flow cell experiment, in which, the dye in a dilute gaseous state was spread onto the air/water interface and surfactant solution was flowed under the interface, the transition from complete gaseous state to LE state was showed by visually monitoring surface fluorescence[7] of a guest NBD dye.

The effect on the spatial distribution of the photoluminescence of the G/LE NBD C_{12}-HPC only monolayer as surfactant adsorbs onto the surface is obtained by injecting .3 ml of a 15 CMC surfactant solution underneath the monolayer. The fluorescence emission spectrum of the dye monolayer was taken approximately 30 minutes after the injection in which time the adsorption of surfactant onto the surface equilibrated with the bulk, and the bulk concentration at equilibrium was 3 CMC. The fluorescence image of the surface monolayer with both dye and surfactant (Figure 5.16) shows that the surface appears completely bright. In this case the NBD amphiphile is the minor component in the monolayer of $C_{14}E_6$ which itself is in a liquid expanded state. The NBD amphiphile is spread throughout the $C_{14}E_6$ monolayer with its chromophore residing in the hydrophobic region of the monolayer composed of the surfactant chains. This results in a uniform luminescence which (see below) is greater than when the NBD is present by itself on the interface since some of the chromophores are in contact with water.

CLSM fluorescence emission spectrum of the NBD amphiphile in the surfactant monolayer is plotted together with the ones of NBD C_{12}-HPC monolayer on the water interface and pure water in Figure 5.17. The collecting window was set from 468 to

750nm with a slit width of 5 nm. The peaks at 470 and 500nm in the spectra are due to the incomplete blocking of the 470 and 500nm wavelength light which accompanies the 458nm exciting laser line. At the air/water interface, where the refractive index change is the maximum (from 1.33 of water to 1.0003 of air), the exciting laser was reflected back to the emission detector, leading to a nonzero signal to noise value in the spectrum of pure air/water interface. After the injection of surfactant solution, the dye monolayer on the surface is moved further away from the objective underneath the chambered coverglass in the inverted CLSM, and this tends to reduce the fluorescent signal recorded from the surface. However, since the adsorption of surfactant forced the NBD amphiphile to reside exclusively in an LE state with its chromophore exclusively in contact with the hydrophobic chains of the monolayer, an increase of the fluorescence signal was observed after introduction of surfactant solution. This was confirmed by monitoring fluorescence emission spectra of the dye monolayer layer on water interface, and the dye in the surfactant monolayer at the same height (Figure 5.18).

5.3.2.3 FRET Study of Micelle Direct Adsorption

In the first experiment, the transport of Nile Red to a clean air/water interface, with the donor NBD amphiphile on the surface, from submicellar solutions is studied. Surface fluorescence spectra were monitored after injection of 0.5 ml 0.5CMC $C_{14}E_6$ solution with 0.2μg/ml of Nile Red underneath a 1 ml volume water layer with an NBD amphiphile monolayer spread on its surface. In this case, most of the dissolved Nile Red was in water and only small amount of Nile Red may be partition into preaggregates if there is any in the surfactant solution. The excited donor NBD on the surface which emits with a maximum wavelength of 540 nm, can transfer nonradiatively energy to the

acceptor Nile Red (FRET) once the Nile red adsorbs onto the surface, with the emission wavelength of the acceptor having a maximum at 640 nm. The surface fluorescence spectrum was plotted in Figure 5.19 with excitation at the donor maximum of 458 nm and the collecting window was 468 to 750nm with a slit width of 5 nm. The donor fluorescence at 540 nm is evident from the beginning after the introduction of the surfactant (also evident in the emission spectrum in the absence of the surfactant taken prior to the introduction of the surfactant), but the Nile Red FRET fluorescence signal was not observed until 135 seconds after the introduction of the solution. After this time, both the NBD and Nile Red emission peaks increase in intensity, finally decreasing until an equilibrium is achieved (Figure 5.20). The interpretation of this spectrum is complicated by the following facts:

1. The donor NBD before the introduction of surfactant is situated in two phases, the more dense LE phase and the much less dense G phase. As surfactant adsorbs, these phases are broken up, and the donor ultimately becomes located as a guest in the surfactant monolayer. Donor previously in the gaseous state (of which most of the molecules are) has to re-orientate its chromophore into the LE state before it can fluoresce or provide excited states for FRET with acceptors. If it remains in contact with the water, its excitation is quenched by the water and fluorescence and FRET are not possible.
2. The donor distribution is initially non-uniform with regions of higher concentration where the LE phase of the donor once resided, and surface diffusion eventually makes the donor distribution more uniform. The Nile Red delivered to the surface (by whatever route) is delivered in a spatially uniform manner. The

energy transfer between the two, even if the concentration of Nile Red on the surface were constant, will become more pronounced the longer the time since the donor has to not only reorientate but also diffuse through the monolayer to become completely accessible to the acceptor.

3. The donor has some solubility in the bulk (even without micelles), and the donor does equilibrate with the bulk. When the donor is first placed on the surface, it is allowed to equilibrate with the subvolume, but with a second volume introduced with the surfactant, additional equilibration is necessary. In these experiments, the subvolume introduced contains surfactant at .5 CMC which dilutes to .17CMC with a change in volume of 1 to 1.5 ml. Thus we can expect some loss of the donor on the surface, and note that the presence of pre-aggregates can also draw donor into the sublayer.

With the above reviewed, we note from Figure 5.19 that the delay in the emergence of the acceptor fluorescence to 135 sec. reflects the fact that Nile Red acceptor, adsorbing from a sub-micellar solution at .17 CMC, adsorbs very slowly since the $C_{14}E_6$ surfactant monolayer has to built up first, passing through its own G/LE induction period. During the first 135 sec, the NBD donor emission also does not increase, as the monolayer has to build to situate the donor as a guest in the surfactant monolayer and provide the proper hydrophobic environment for fluorescence. There is NBD fluorescence from the LE islands of the NBD and NBD in the growing islands of the LE state of the surfactant monolayer. This fluorescence leads to no appreciable FRET since the amount of Nile Red adsorbed on the surface is negligible.

After 135 sec., until 210 sec., the emission of the donor increases, because, as the monolayer develops, the LE state of the surfactant now occupies the entire surface. A molecular re-arrangement of the NBD donor begins as the chromophore redistributes into the LE state of the surfactant monolayer, causing an increase in fluorescence of the donor. This increase in fluorescence alongside the adsorption of the Nile Red and the redistribution of the donor through the monolayer, leads to an increase in the FRET and the increase in the emission maximum of the acceptor. With time, desorption of the donor to the bulk reduces the fluorescence of the donor (which was confirmed by FRET measurement in the bulk, Cf. Figure 5.21), the FRET and the fluorescence of the acceptor until equilibrium is achieved.

The above transport of Nile Red from a sub-micellar solution to a clean interface with the NBD donor amphiphile is now compared with the transport to the surface from a micellar solution, with the Nile Red dissolved at the same concentration in the bulk. The fluorescence spectrum of the surface monolayer is carefully monitored after the injection of 0.5 ml 15CMC $C_{14}E_6$ solution with 0.2 μg/ml Nile Red underneath a 1 ml water layer with a NBD C_{12}-HPC monolayer, identical conditions as the submicellar experiment except for the concentration of surfactant in the .5 ml aliquot. The wavelength of the excitation is 458nm (the adsorption maximum of the NBD). The FRET between the NBD fluorophore on the surface and the Nile Red is observed in the first xyλ scanning which was conducted 30 seconds after the introduction of the micelle solution (Figure 5.22). This is consistent with the delivery of Nile red quickly to the surface by micelles rather than the adsorption of free Nile red – released by micelle disassociation in the bulk - to the surface.

In the time period between 30 sec. and 232 sec., the emission peaks of both the NBD and the Nile red increase. The increase in the NBD signal is due to the reorientation of the chromophores on the surface from their prior orientation in the gaseous state of lying down on the surface. The increase in the FRET signal is due partially to this re-orientation, as well as the redistribution of NBD on the surface from prior more highly concentrated LE state to make it more readily accessible to the acceptor for FRET. In this time period, the Nile Red delivered rapidly in the initial adsorption of micelles could be desorbing, but the increase in the FRET excitation over compensates for this desorption. The desorption, as was evident in the dynamic surface tension experiments, is driven by the recapture of the Nile red into the micelles.

Between 232 sec. and 300. sec the donor fluorescence decreases before once again increasing until 680 sec. This decrease is accompanied by a emission from the acceptor which does not change in the time period 232 to 300 sec. In this time period, the re-orientation of the NBD and the redistribution continue, providing highly favorable conditions for donor transfer. This may be the reason for the decrease. The energy transferred from the donor to the Nile Red acceptor would normally result in an increase in the acceptor emission maximum, but this is offset by the continued desorption in the acceptor as was evident in the dynamic tension experiments.

After 300 sec., the donor peak fluorescence intensity increases as the orientation of the chromophore becomes more complete and begins dominating as part of its shoulder the emission of the acceptor at 640 nm. The acceptor fluorescence maximum begins to decrease as more Nile red desorbs, and this further increases the donor signal as less energy is lost to FRET.

The surface fluorescence was monitored after a long time, showing that the fluorescence intensity of both the NBD fluorophore and the Nile Red reduced (Figure 5.23). The reduction of the NBD fluorescence intensity on the surface was a result of NBD C_{12}-HPC desorbed from the surface and dissolved into the bulk. Though the phospholipid NBD C_{12}-HPC has poor solubility in pure water, with micelle present in the bulk, the solubility of the NBD C_{12}-HPC is improved such that the micelle in the bulk acted as a reservoir which could incorporate the dissolved phospholipids into themselves, leading to much higher solubility of NBD C_{12}-HPC in the bulk. We anticipate this transport to be slower than that of the smaller molecule Nile Red, which begins desorbing after its initial delivery to the surface. However, in the end, both desorb off the surface.

The dissolved NBD C_{12}-HPC may be captured into the same micelle which may happened to incorporate Nile Red molecule as well. This was evident from the fluorescence scanning of the bulk, which showed strong FRET signal between NBD fluorophore and Nile Red using 458nm laser (Figure 5.24). Since, the critical distance for a donor chromophore in its excited state to transfer energy by a nonradiative, long-range dipole-dipole coupling mechanism to an acceptor chromophore is typically <10nm, the donor NBD must be incorporated into the same micelle as the one already incorporated the acceptor Nile Red. Also plotted in Figure 5.23, is the bulk Nile Red fluorescence signal when the bulk was excited by a 543nm laser with a collecting window from 550 to 750 nm.

We believed that the detected Nile Red peak on the surface was mostly due to the FRET from the excited donor on the surface, though there may be a small effect from the readsorption of the emission wavelength by Nile Red. We didn't believe readsorption

was a big effect here since the emitted light from the donor was not strong and the emission of the radiatively excited the Nile Red on the surface had to go through the bulk. The emission light scattering in the bulk and adsorption of the energy by bulk molecule could reduce the emission intensity further. Hence, such an observed strong Nile Red signal detected by the emission detector didn't seem to be a result of the radiative interaction between excited donor and acceptor. The powerful laser source and extreme sensitive setting of the CLSM used in order to detect the donor emission made it highly possible that the strong Nile Red signal was due to the FRET transfer rather than radiative interaction between the donor and acceptor Nile Red. Our hypothesis was supported by the mathematical models proposed by Loura et al., describing the resonance energy transfer in the biological membrane, which is a bilayer of phospholipids[8]. The FRET was more favorable in our study since we only had a single layer of phospholipids, hence increasing the FRET by reducing the distance between the donor and acceptor.

To demonstrate that the Nile Red signal detected on the surface fluorescence spectrum study was mostly due to FRET or nonradiative mechanism than radiative or readsorbtion mechanism, a xyz stack slicing from air into the sample bulk was conducted when the sample was excited using 458nm or 543nm laser line, and with collecting window from 600 to 750nm. The fluorescence signal as a function of z position was plotted in Figure 5.25. In the used inverted CLSM, the laser source coming from the side underneath the air/water layer, the laser signal reduced as it went through the bulk because of the light scattering in the bulk and absorption of the energy by the bulk molecules. Similarly, the emission light also got weakened as it went through the bulk to the emission detector which was located at the same side of the laser source. This reduced

543 nm laser power together with the reduced emission generated a declining Nile Red signal along the z axis from the bulk to the interface. The signal curve at the bulk side had a slope K_1. The huge signal peak at interface was due to the reflection as discussed previously. When 458 nm was used, the excited NBD fluorophore on the surface transferred energy to the Nile Red on the surface in both nonradiactive way (FRET) and radiative way (readsorbance). Since now we put the exciting light source on the surface, both the excitation laser and emission light got weakened as it passed through the bulk and reached the detector. If radiative transfer was the dominant one between the NBD fluorophore and Nile Red, we should expect the curve in the bulk side had a negative slope, which reflecting the reduced excitation and the emission in the direction of interface to bulk. The observed small but positive slope for the excitation at 458 nm indicated that the non-radiative energy transfer was the dominant effect.

In the third surface fluorescence study, 0.3 ml 15 CMC solution was injected into a 1 ml water layer with NBD C_{12}-HPC monolayer and the system was allowed to reach equilibrium, after which, 0.5 ml 15 CMC micelle solution with the 0.2μg/ml Nile Red was injected underneath the surface monolayer (with maximum $C_{14}E_6$ surface concentration and NBD fluorophore in the LE phase), the emission spectra were the carefully monitored. Surface fluorescence spectra showed Nile Red signal due to FRET interaction from excited donor NBD fluorophore on the surface around 180 seconds after the introduction of the micelle solution with Nile Red (Figure 5.26). Since the surface was already equilibrated with micelle solution, the maximum surfactant concentration prevented the newly introduced micelle incorporated with Nile Red from adsorbing onto the surface directly. This shut down the micelle direct adsorption route or minimized

micelle direct adsorption if there was any. The delayed Nile Red signal compared to the first fluorescence experiment in which the micelle and Nile Red solution was injected under NBD fluorophore surface monolayer, implied that direct adsorption of free Nile Red onto the surface monolayer delivered Nile Red slower than direct micelle adsorption route does. The inconsistent increase in emission signal may also due to the nonuniform NBD C_{12}-HPC on the surface or surface convection as discussed earlier. The FRET between NBD flurophore and Nile Red in the bulk was also observed in this experiment (Figure 5.27), confirming again that the NBD C_{12}-HPC dissolved into micelle solution from the surface monolayer, and was incorporated into the micelles which has Nile Red molecule shielded in them already.

5.4 Conclusions

The accelerated dynamic surface tension relaxation achieved using micellar solution with increasing concentration could not be explained by the monomer adsorption route, in which micelle in the bulk disassemble into monomer and then released monomer from the micelle will adsorb onto the surface to reduce the surface tension. The direct micelle adsorption route, in which micelle directly adsorbs onto surface without breaking up into monomer in the bulk first, then the adsorbed micelle breaks up into monomer on the surface and the monomer released from the adsorbed micelle can expedite the surface tension reduction. We have carried out dynamic surface tension study using Pendant Bubble Tensiometer and Fluorescence Resonance Energy Transfer using Confocal Laser Scanning Microscope to track direct micelle adsorption route by incorporating a

hydrophobic dye in the micelle, from which experimental evidences of the direct micelle adsorption route were obtained.

In the dynamic surface tension study, the further reduced surface tension achieved using the dye in a micellar solution compared the one of the micellar solution without the dye implied that the dye was delivered onto the surface monolayer by micelle direct adsorption, followed by micelle breakup on the surface. The equilibrium surface tension of these two solutions were the same since the dye on the surface which was overshoot with the dye by micelle fast adsorption when the surface was relatively clean, would desorb back into the micellar solution underneath the surface and replaced by surfactant monomer. In the FRET study, the surface spectra of the FRET couple, NBD as the donor and Nile Red as the acceptor monitored using CLSM, showed the FRET from the donor to the acceptor, which was delivered to the surface via micelle direct adsorption route too. The direct micelle adsorption route delivered Nile Red much faster that free Nile Red adsorption from the bulk.

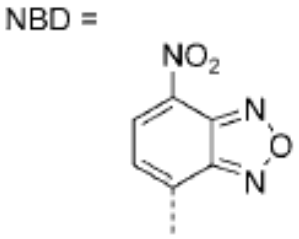

Nitrobenzoxadiazole (NBD) fluorophore

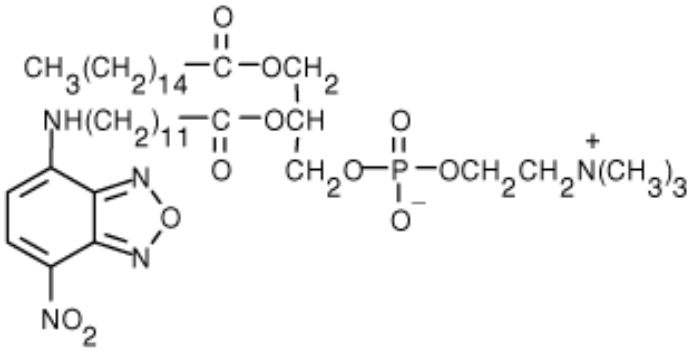

NBD C_{12}-HPC

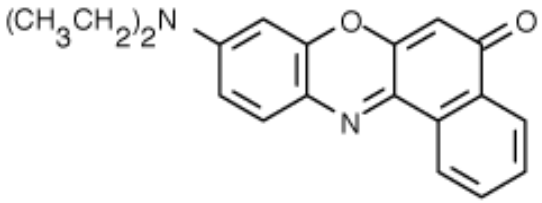

Nile Red

Figure 5.1: Structures of nitrobenzoxadiazole (NBD) fluorophore, NBD C_{12}-HPC and Nile Red. The FRET donor fluorophore NBD is attached to on the acyl chain of the phospholipids.

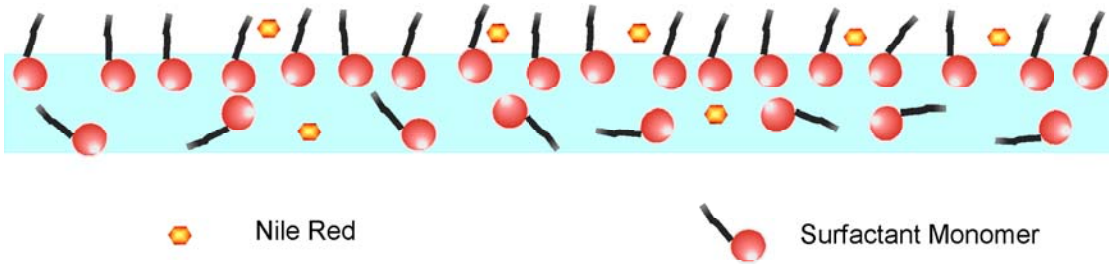

Figure 5.2: Schematic representation of the insertion of Nile Red into the hydrophobic part of the surfactant surface monolayer increases the surface pressure and reduces the surface tension of the monolayer.

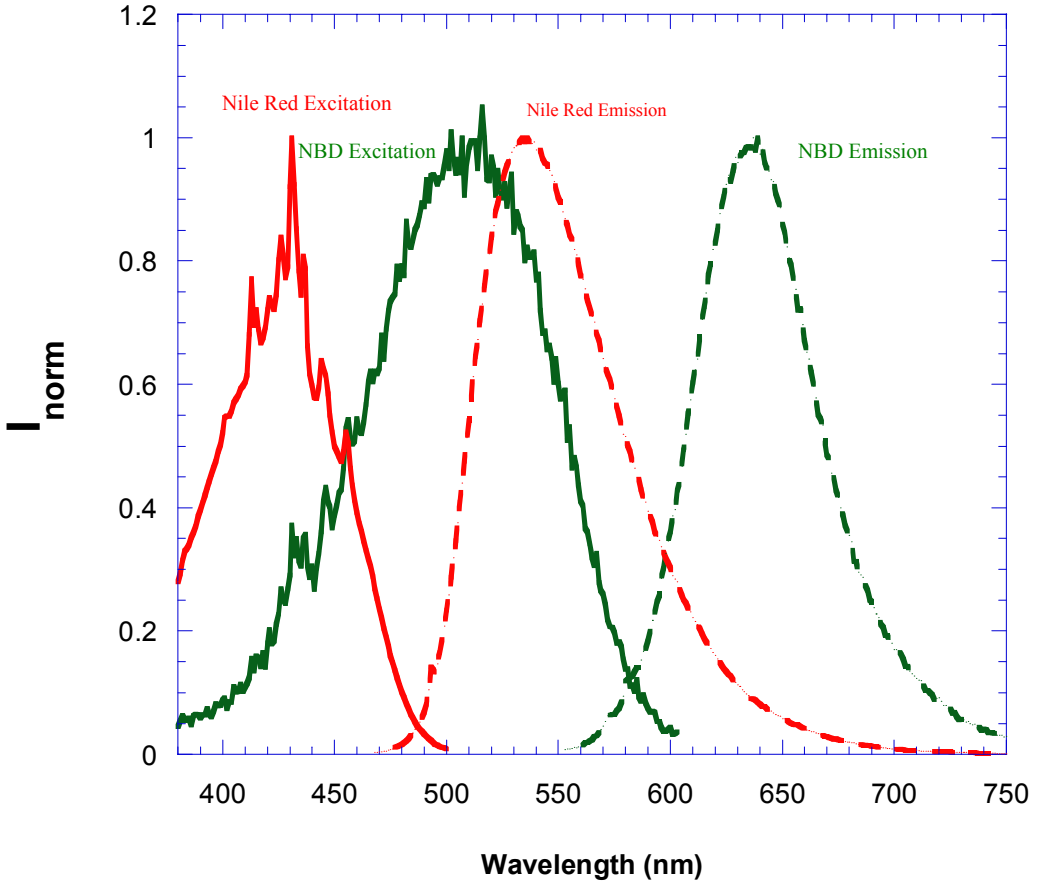

Figure 5.3: Excitation (———) and emission (--------) spectra of NBD C_{12}-HPC in chloroform (red) and Nile Red in 15 CMC $C_{14}E_6$ solution (green). Overlap of NBD fluorophore emission and Nile Red excitation was perfect to permit FRET. Emission spectra were recorded with excitation at 458 nm (NBD) and 543 nm (Nile Red). Excitation spectra were recorded with detection at 540 nm (NBD) and 640 nm (Nile Red).

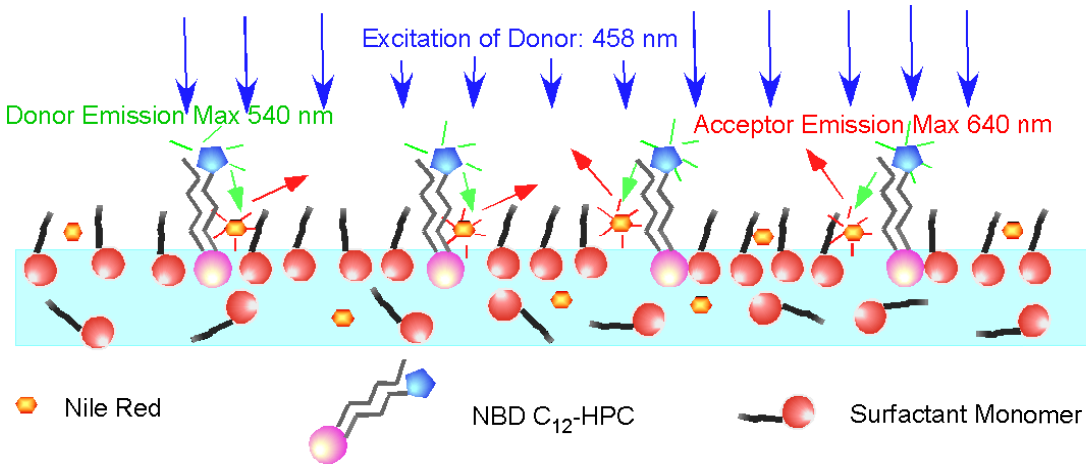

Figure 5.4: Schematic conceptualization of detecting dye on the surface utilizing fluorescence resonance energy transfer (FRET) technique.

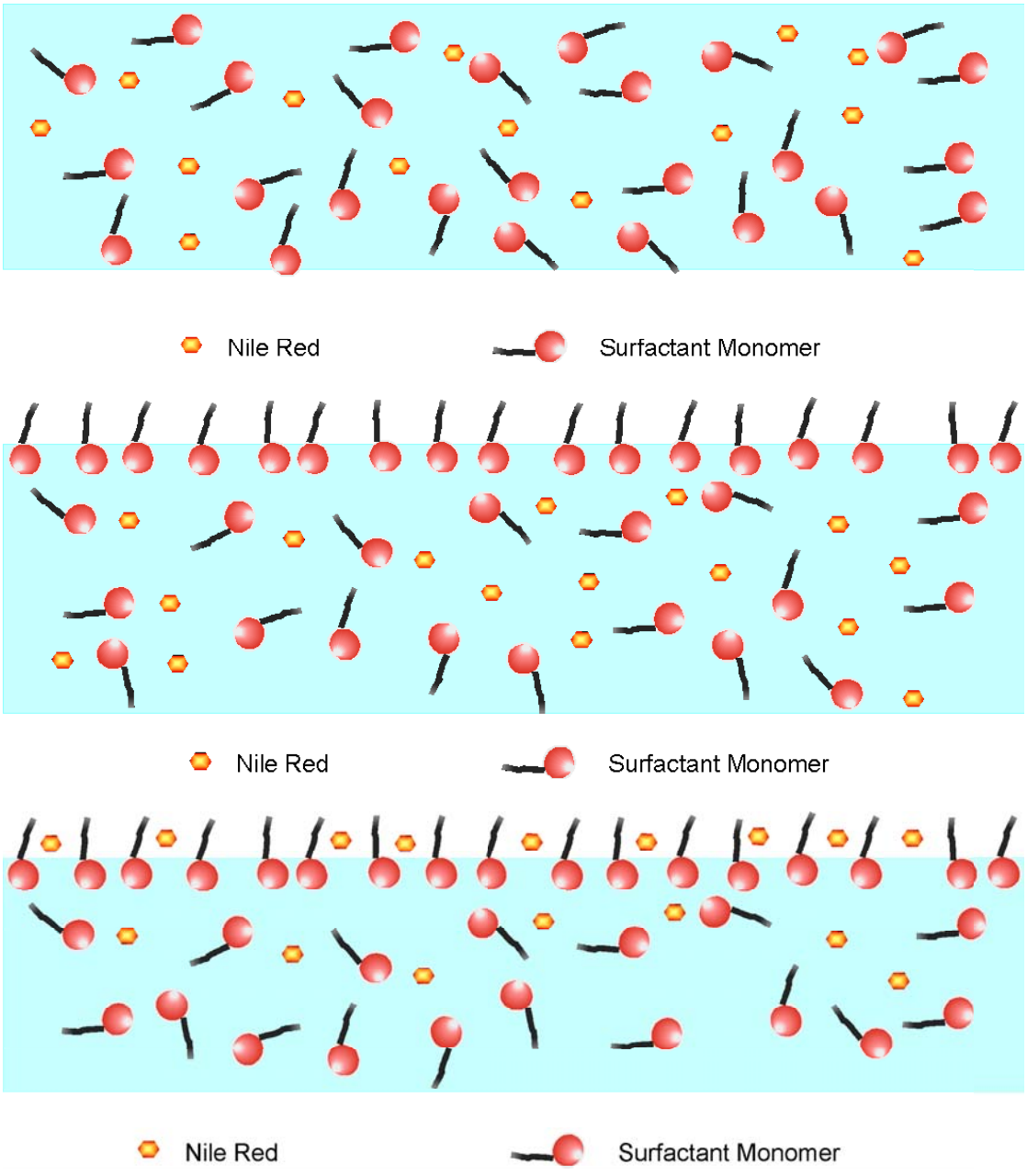

Figure 5.5: The adsorption of dye to the surface from surfactant solutions below CMC. The adsorption of the dye is delayed since the surfactant monolayer has to be formed first.

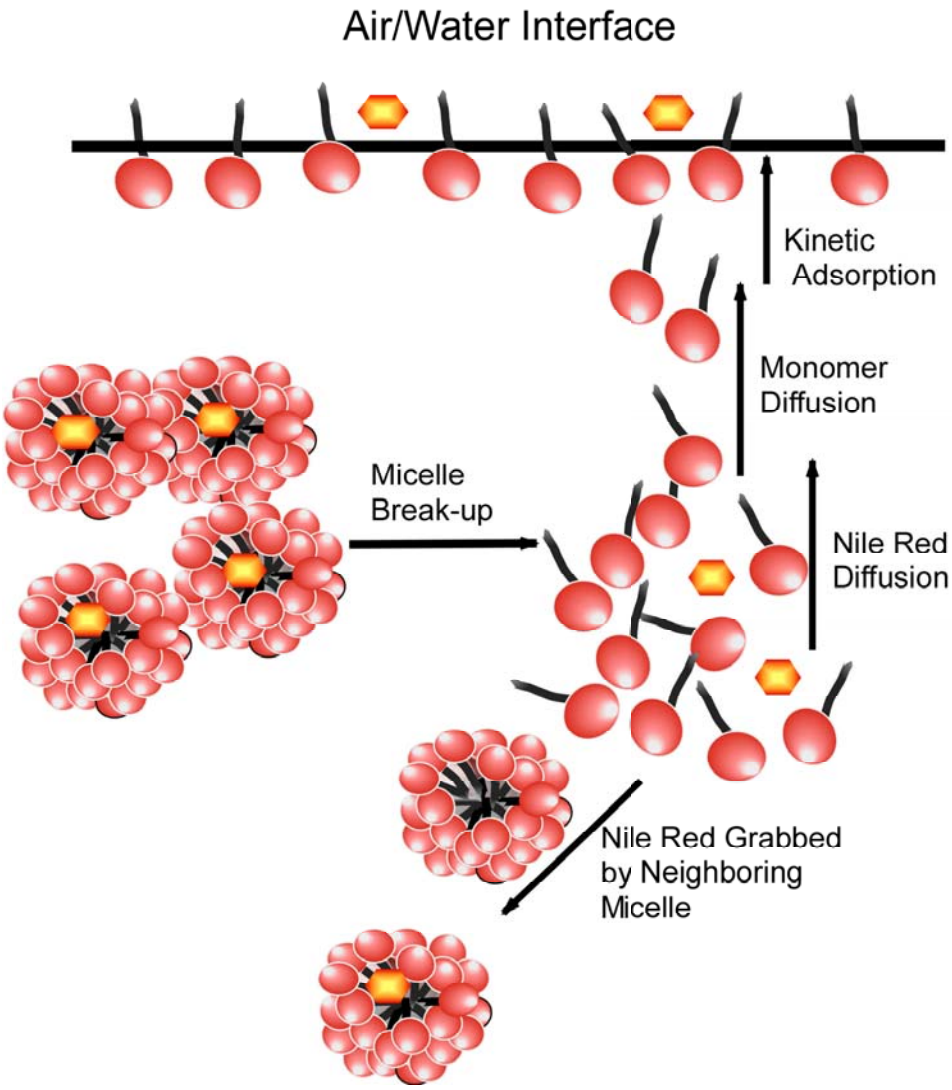

Figure 5.6: Schematic representation of surfactant transport by route in which micelle disassembly into monomer followed by monomer diffusion and adsorption onto the surface.

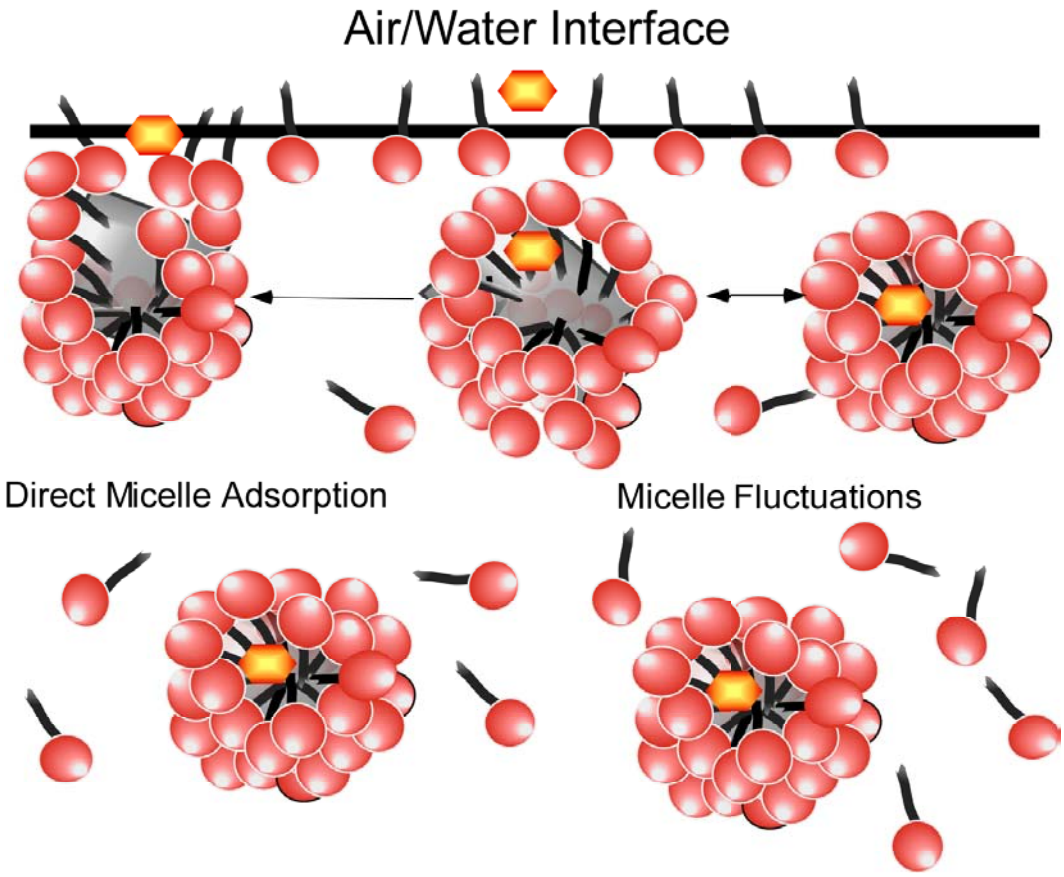

Figure 5.7: Schematic representation of surfactant transport by direct micelle adsorption route in which micelle directly adsorbs onto the surface, breaks up and releases monomers into the surface monolayer.

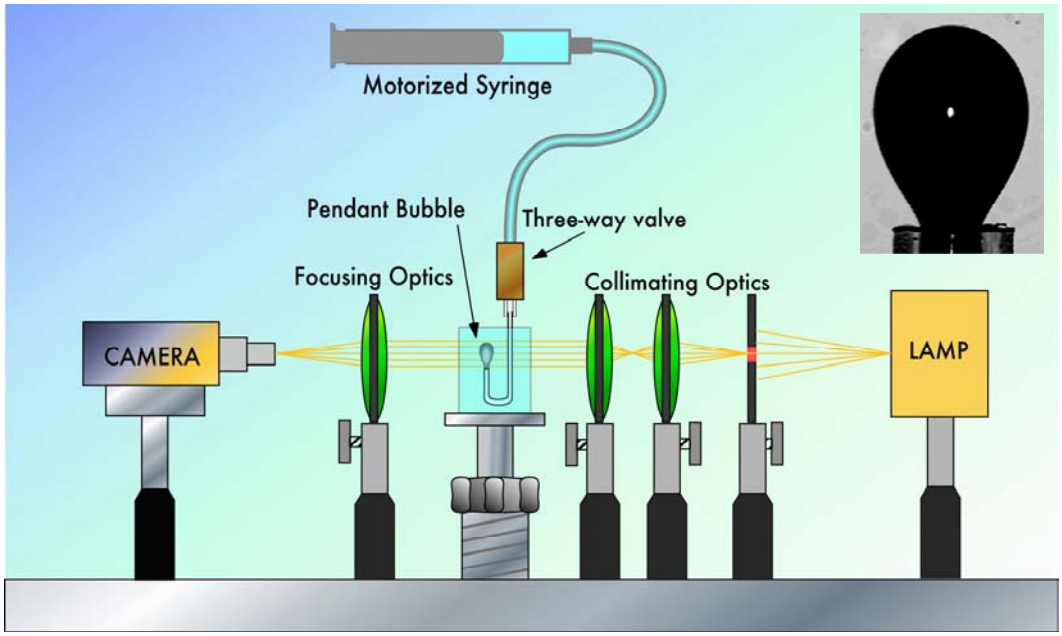

Figure 5.8: Schematic representation of the pendant bubble apparatus inserted with a typical digital image of the silhouette of the pendant bubble.

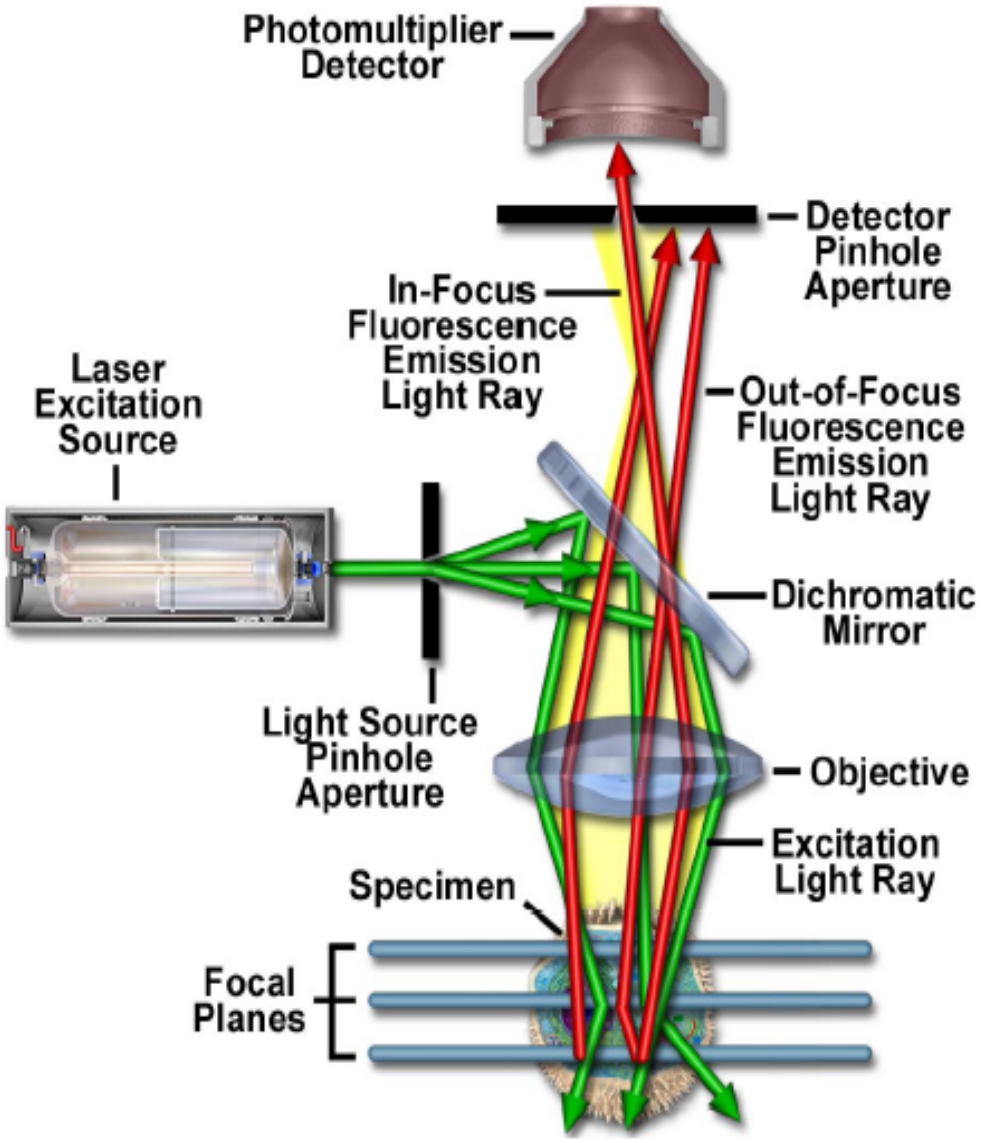

Figure 5.9: Schematic diagram of the optical pathway and principle components in a laser scanning confocal microscope.

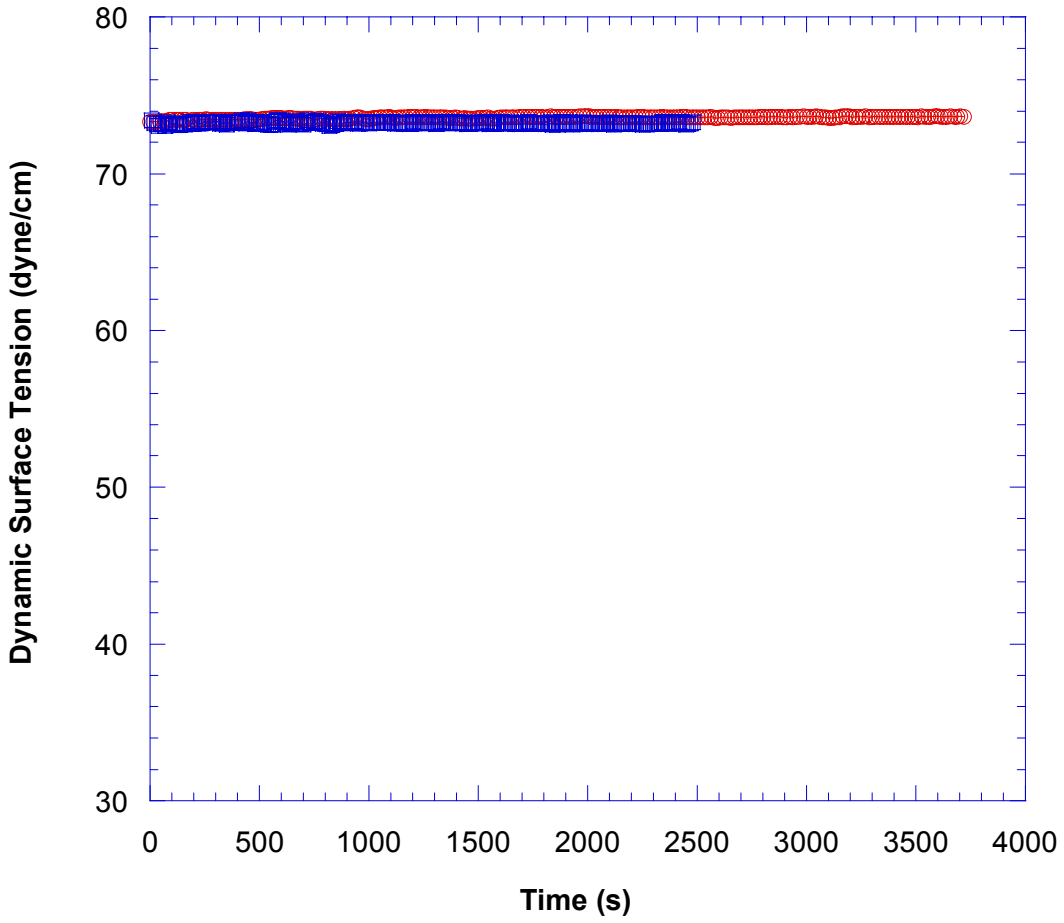

Figure 5.10: Dynamic surface tension relaxation measurements of 0.2 μg/ml Nile Red aqueous solution.

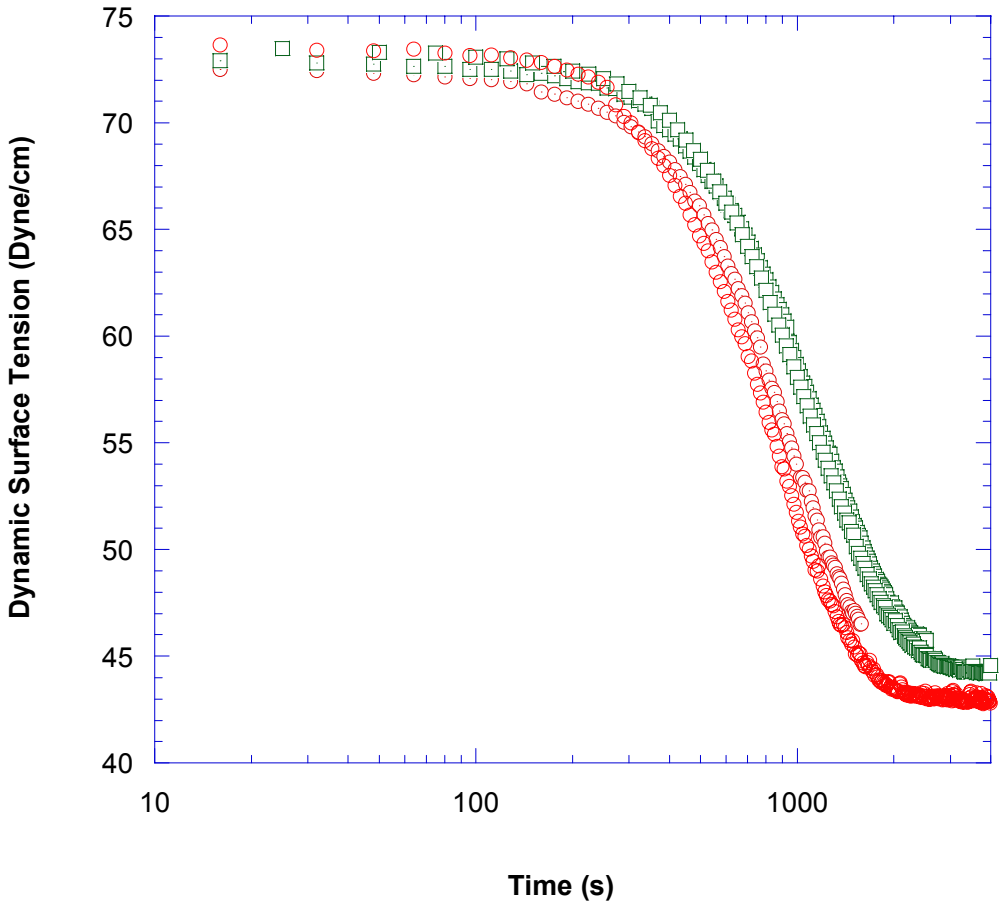

Figure 5.11: Dynamic surface tension relaxation measurements of 0.17 CMC $C_{14}E_6$ (□) and 0.17 CMC $C_{14}E_6$ with 0.2 µg/ml Nile Red (○).

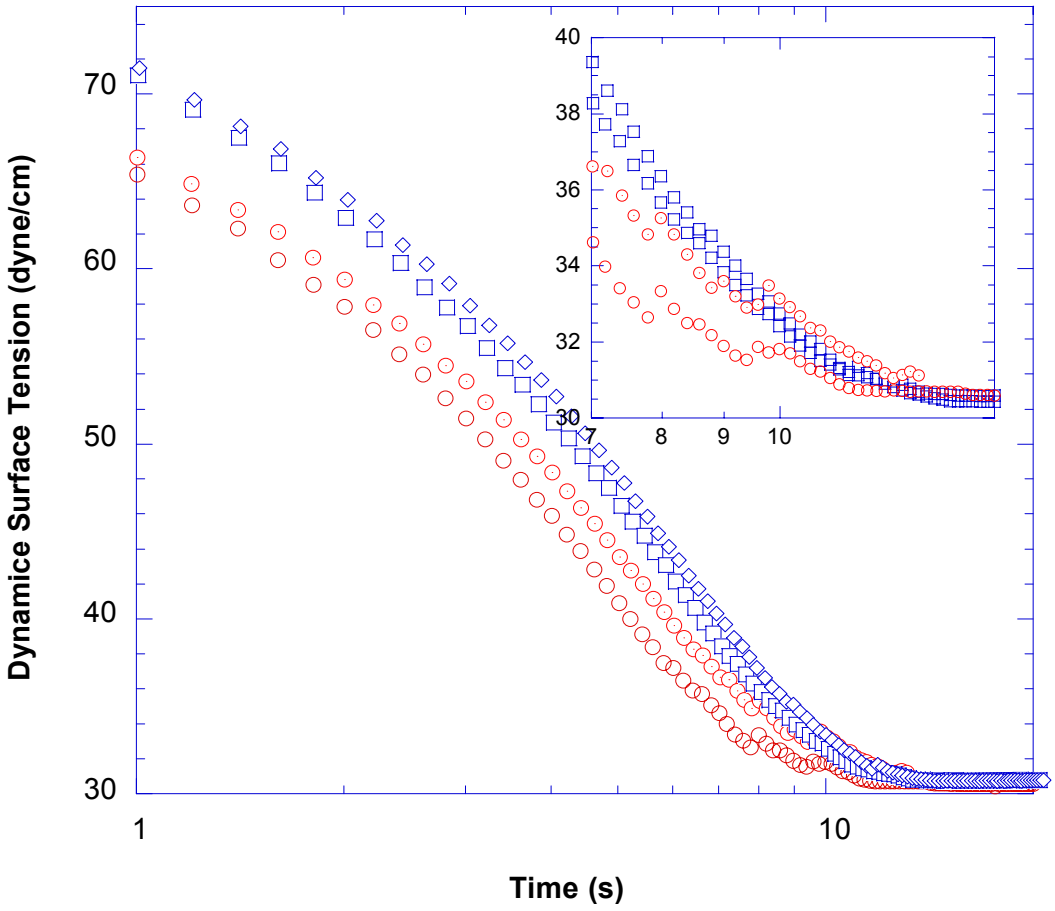

Figure 5.12: Dynamic surface tension relaxation measurements of 15 CMC $C_{14}E_6$ (□) and 15 CMC $C_{14}E_6$ with 0.2 µg/ml Nile Red (○).

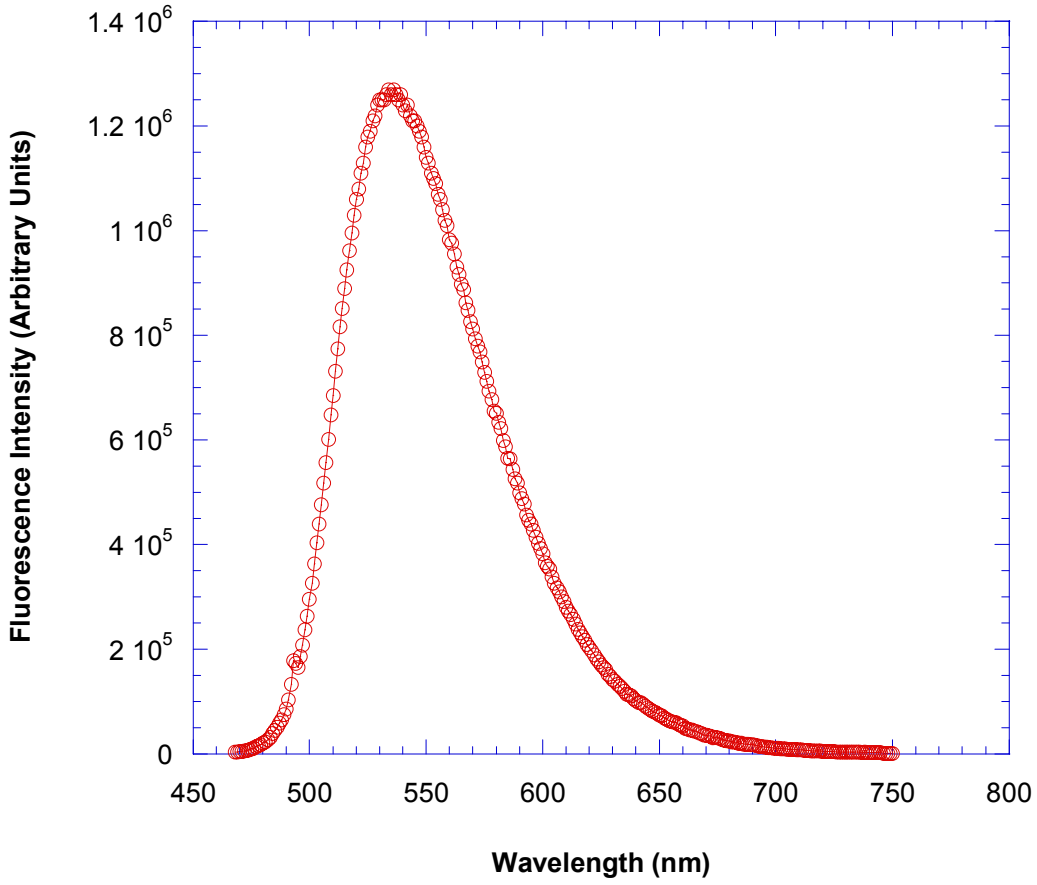

Figure 5.13: Spectrofluorimetry characterization of the NBD C_{12}-HPC dissolved in chloroform. Emission spectrum was recorded with excitation at 458 nm.

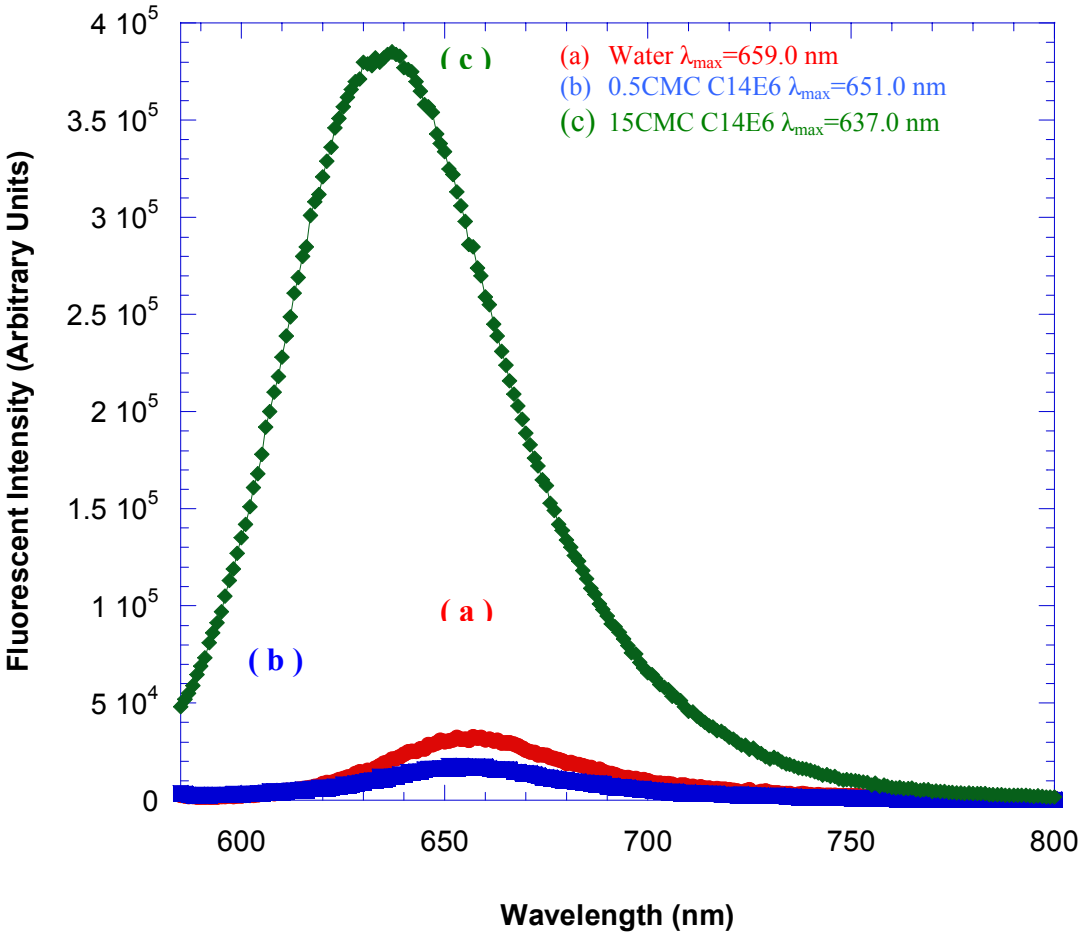

Figure 5.14: Spectrofluorimetry characterization of the 0.2 µg/ml Nile Red in water (a), 0.5CMC (b) and 15CMC (c) $C_{14}E_6$ solutions. Emission spectrum was recorded with excitation at 543 nm.

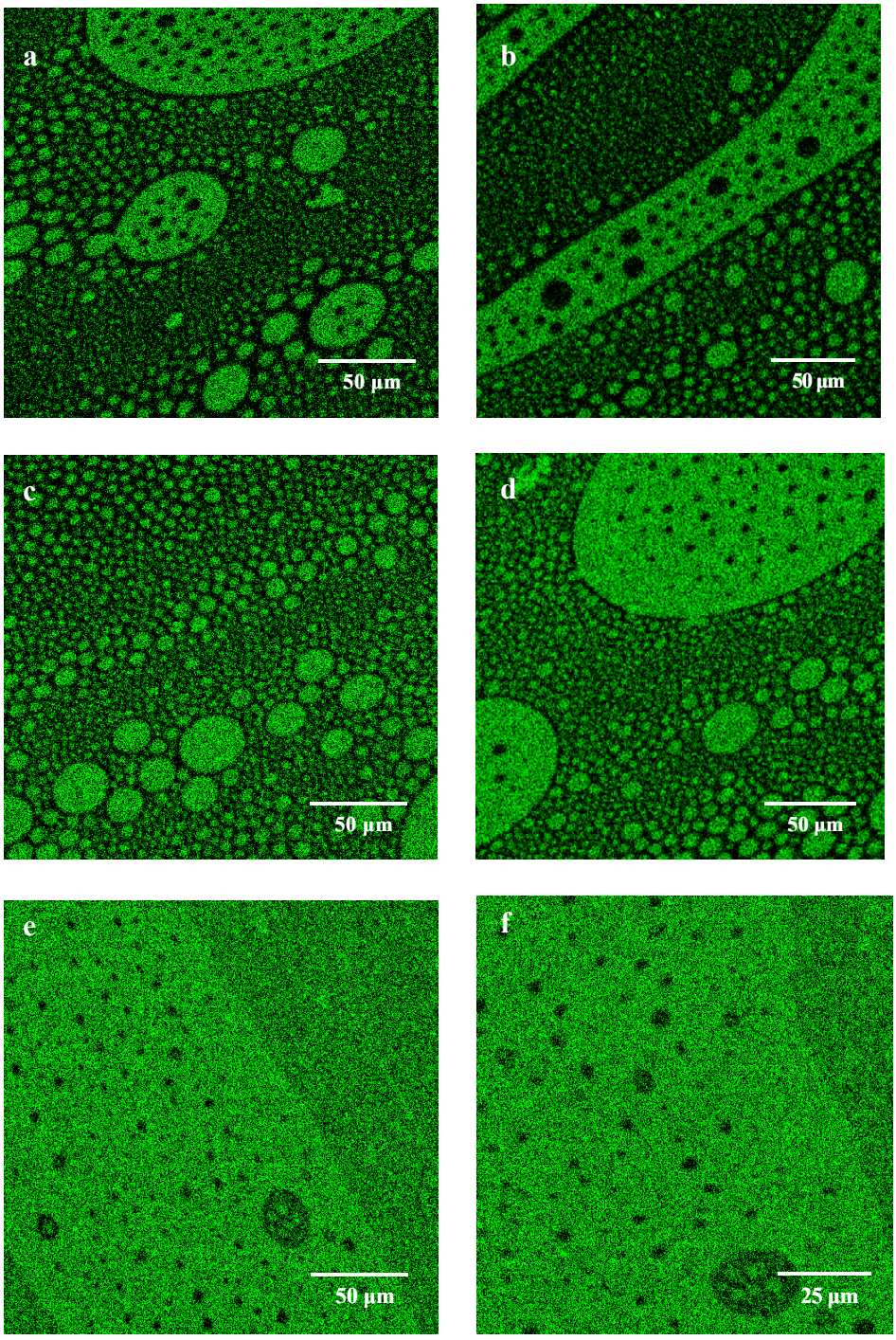

Figure 5.15: Phase behavior of NBD C_{12}-HPC monolayer on a clean air/water interface. Transition of dark Gaseous (G) and bright Liquid Expanded (LE) phases. (a), (b): 1 minute; (c), (d): 3 minutes; (e) ,(f): 20 minutes after initial spreading.

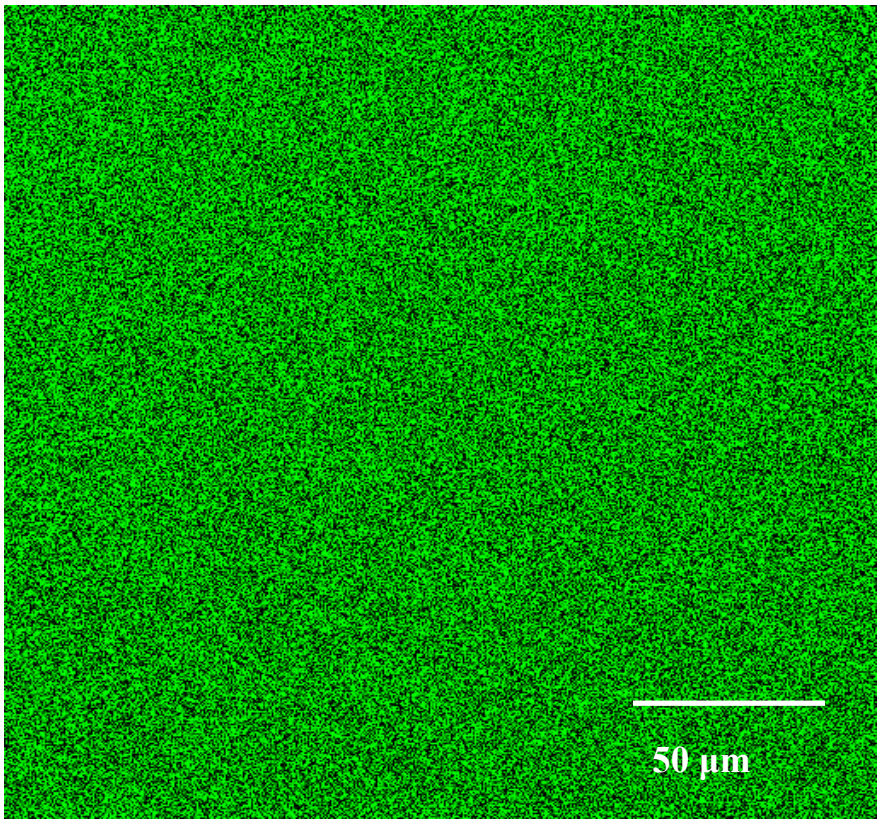

Figure 5.16: Uniformly bright fluoresce image of surface with dye in LE phase after adsorption of surfactant.

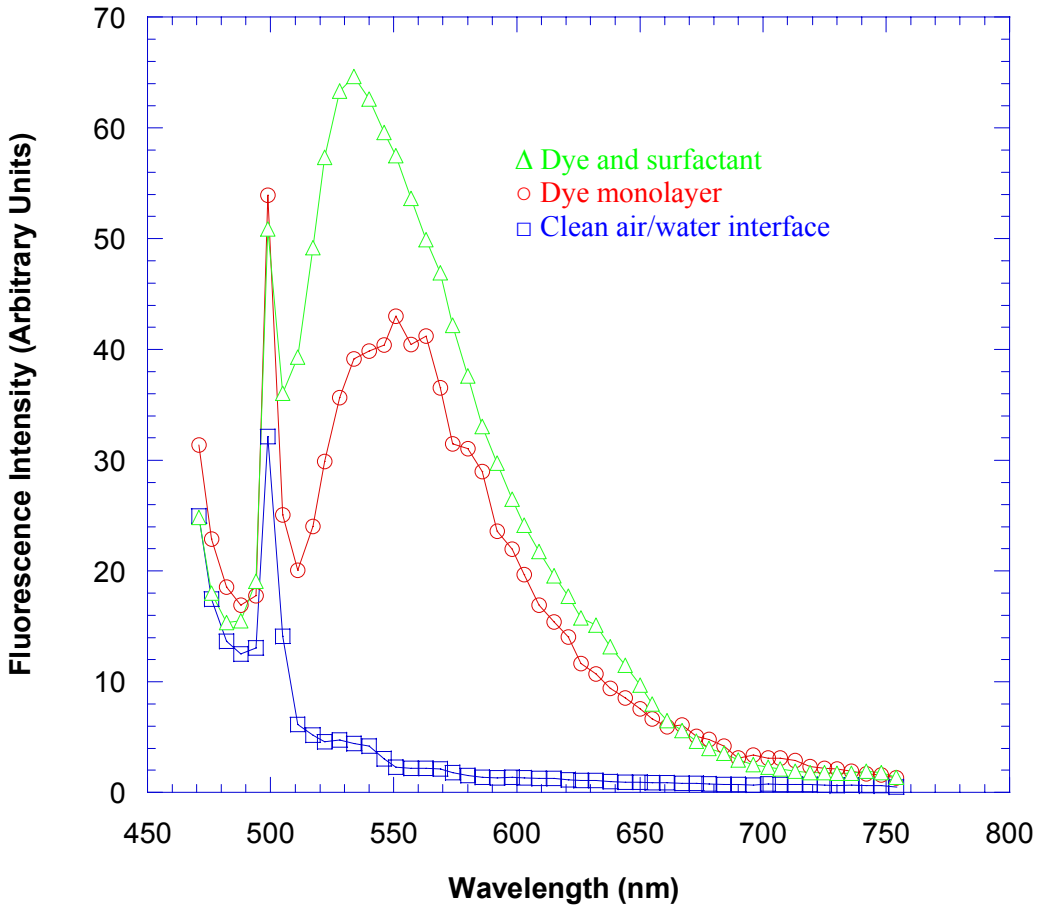

Figure 5.17: Fluorescence emission spectra of clean air/water interface (□), dye monolayer on water interface (○), dye in surfactant monolayer on water interface (Δ).

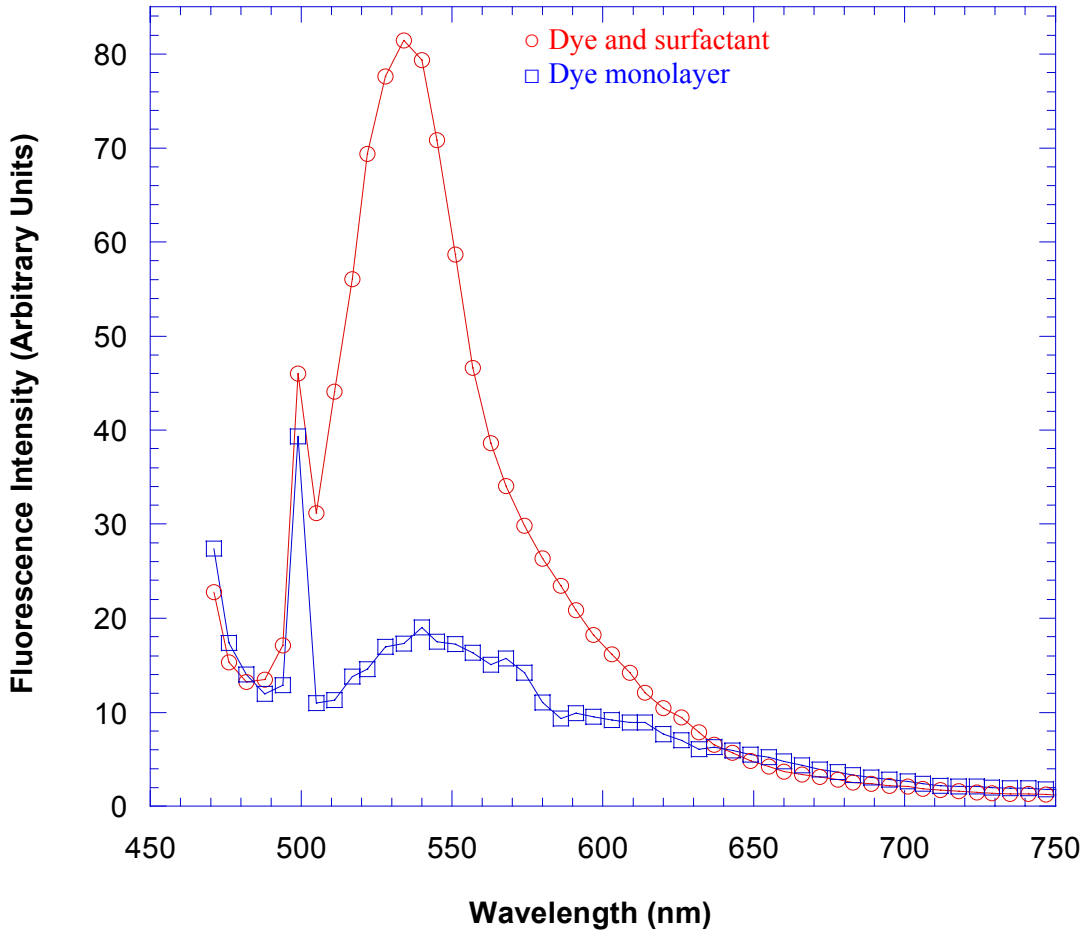

Figure 5.18: Fluorescence emission spectra of dye monolayer on water interface (○) and dye in surfactant monolayer on water interface (□) at the same height.

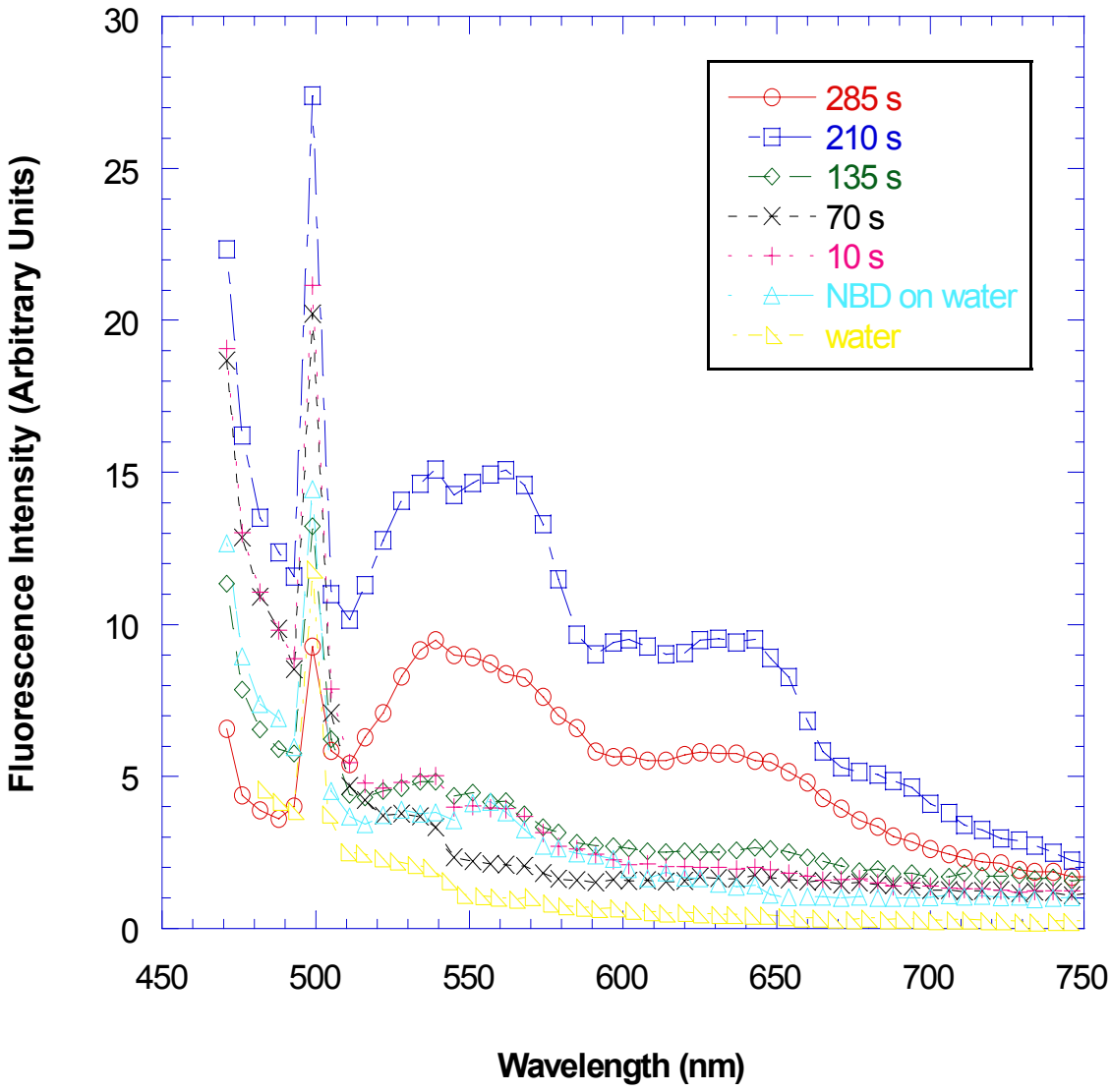

Figure 5.19: Surface fluorescence spectra showed FRET of Nile Red with NBD at 135 second after introduction of 0.5CMC $C_{14}E_6$ with 0.2 µg/ml Nile Red.

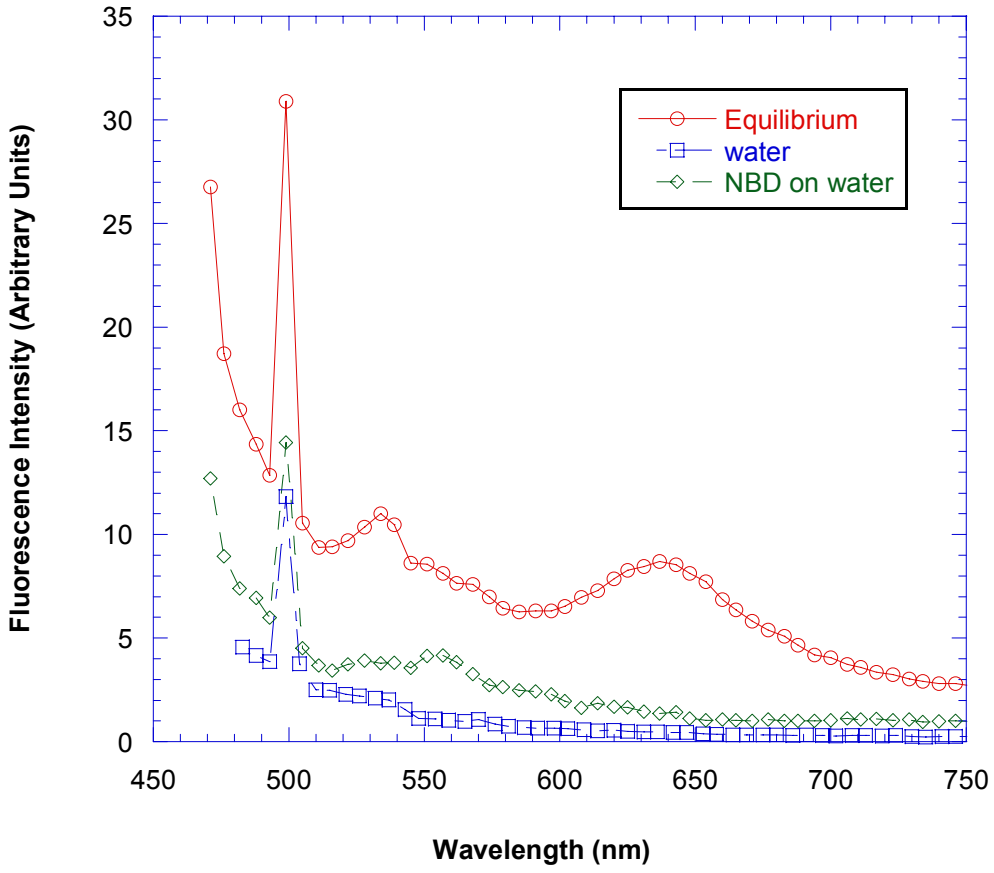

Figure 5.20: Equilibrium surface fluorescence spectra showed FRET of Nile Red with NBD after introduction of 0.5CMC $C_{14}E_6$ with 0.2 µg/ml Nile Red.

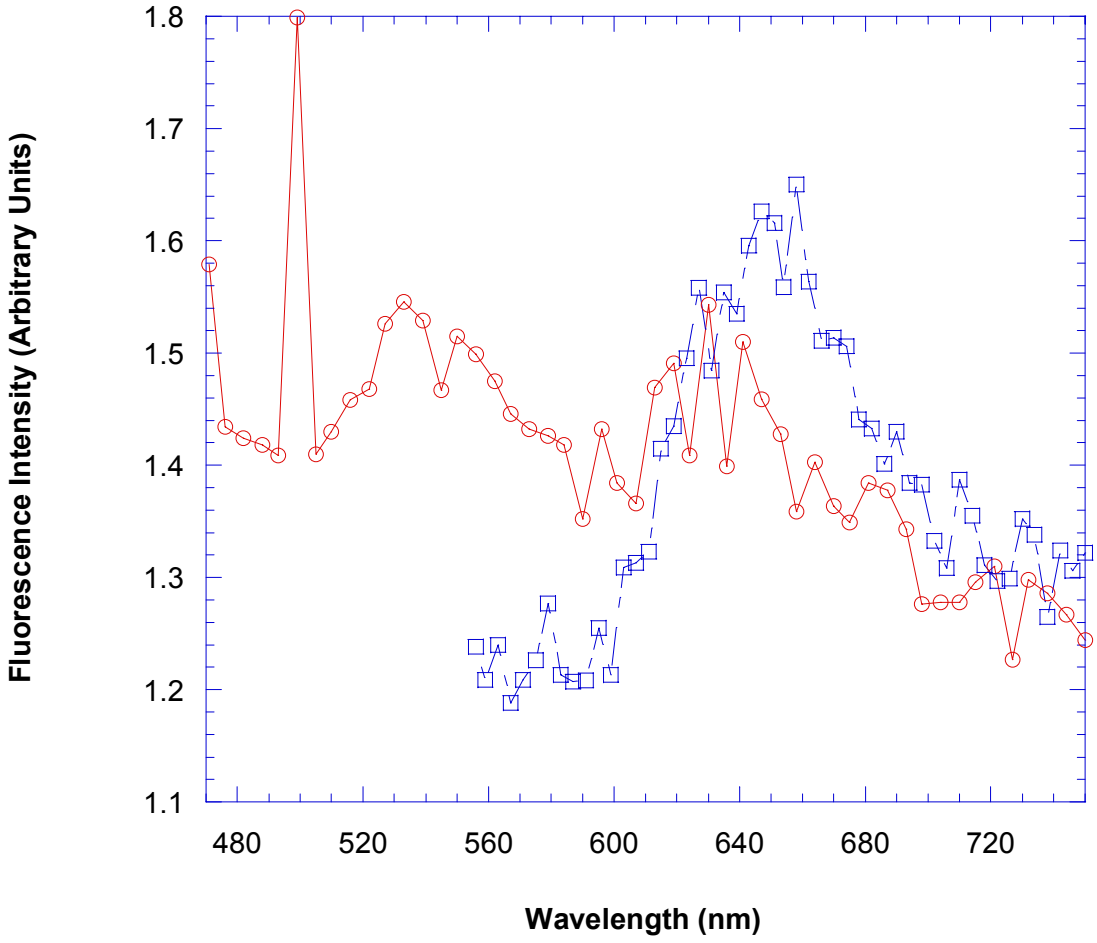

Figure 5.21: Fluorescence spectrum indicating FRET between NBD and Nile Red (○, excitation 458nm) in the bulk after introduction of micelle solution and Nile Red fluorescence spectrum (□, excitation 543nm) in the bulk of 0.5 CMC solution.

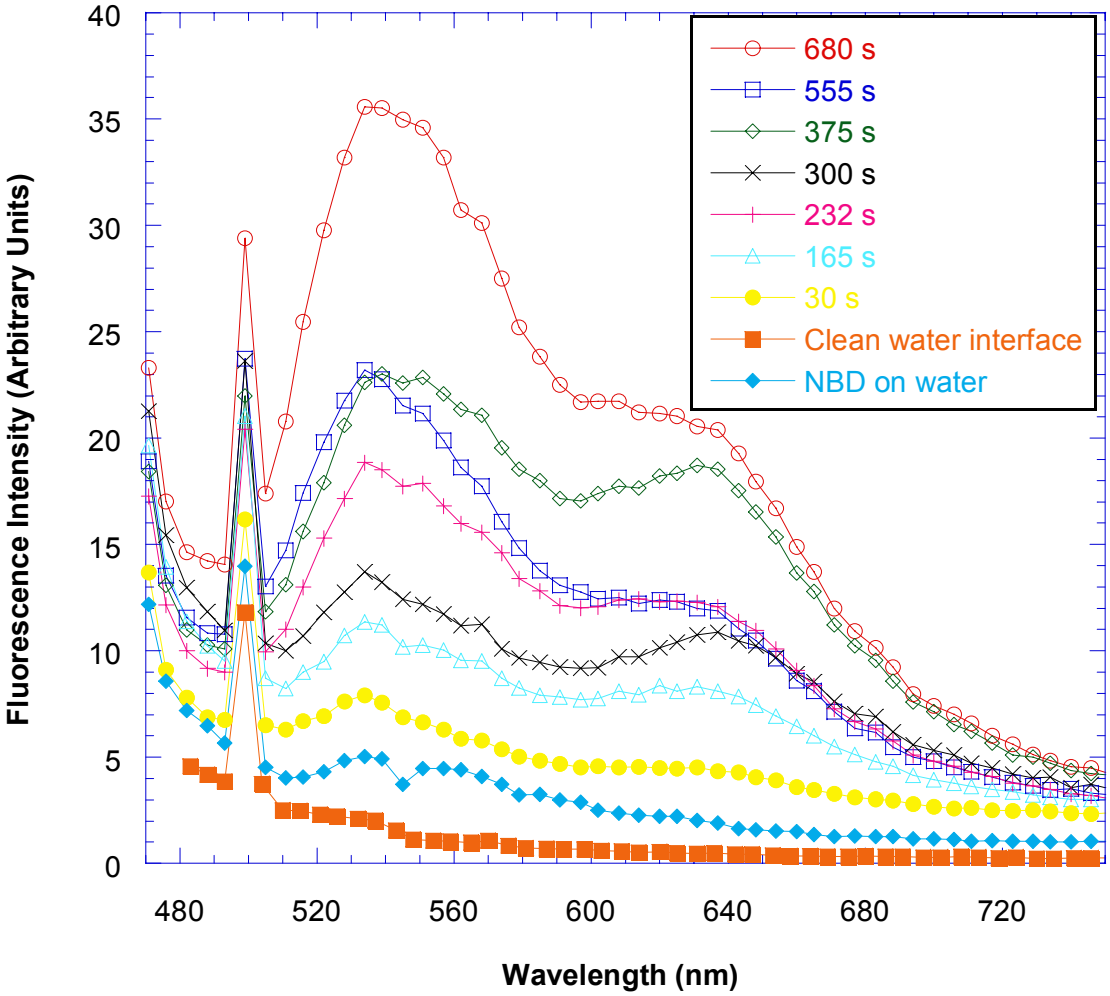

Figure 5.22: Surface fluorescence spectra showed FRET of Nile Red with NBD at 30 second after introduction of 15CMC $C_{14}E_6$ micelle solution which had with 0.2 µg/ml Nile Red incorporated in the micelle, indicating direct micelle adsorption onto the surface.

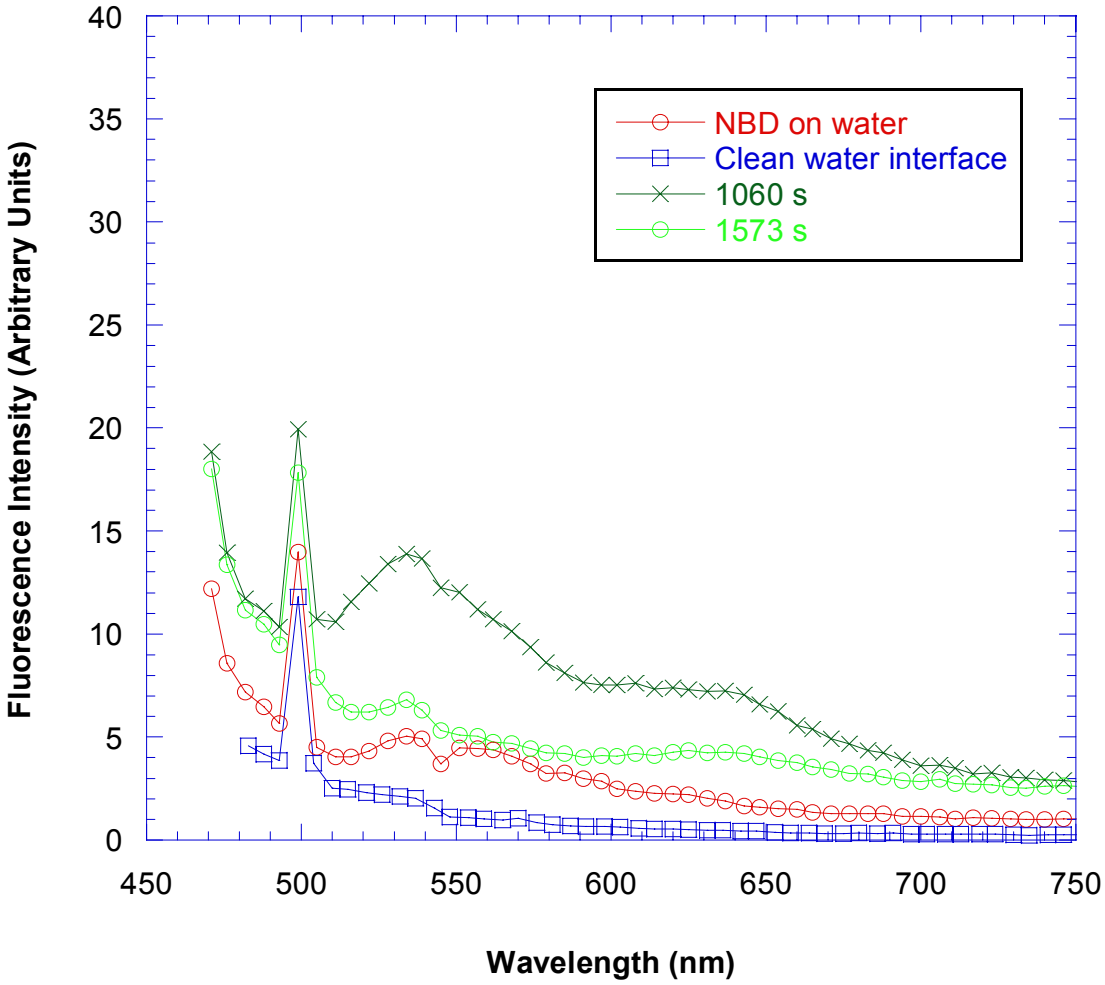

Figure 5.23: Reduction of fluorescence intensity of both donor NBD and acceptor Nile Red due to donor NBD C_{12}-HPC desorbed into the 15 CMC solution bulk and was incorporated into bulk micelle.

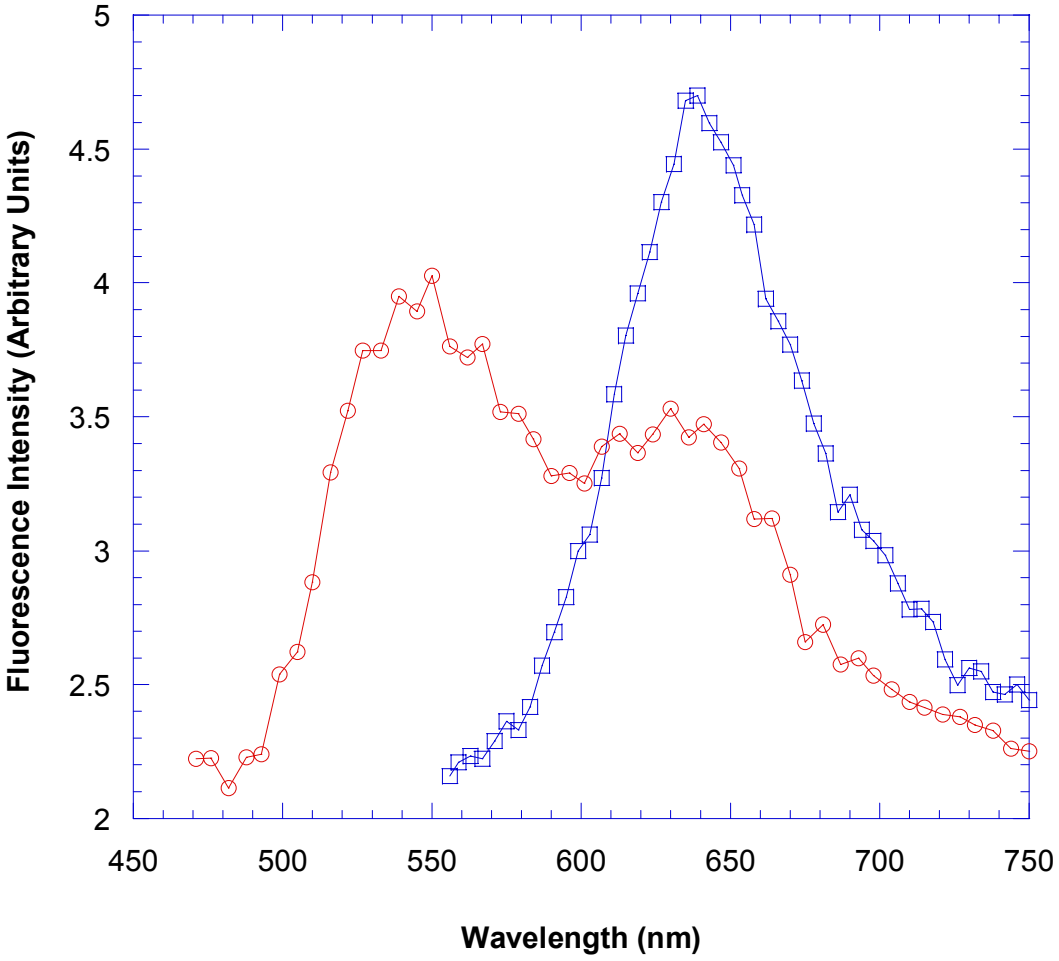

Figure 5.24: Fluorescence spectrum indicating FRET between NBD and Nile Red (○, excitation 458nm) in the bulk after introduction of micelle solution and Nile Red fluorescence spectrum (□, excitation 543nm) in the bulk.

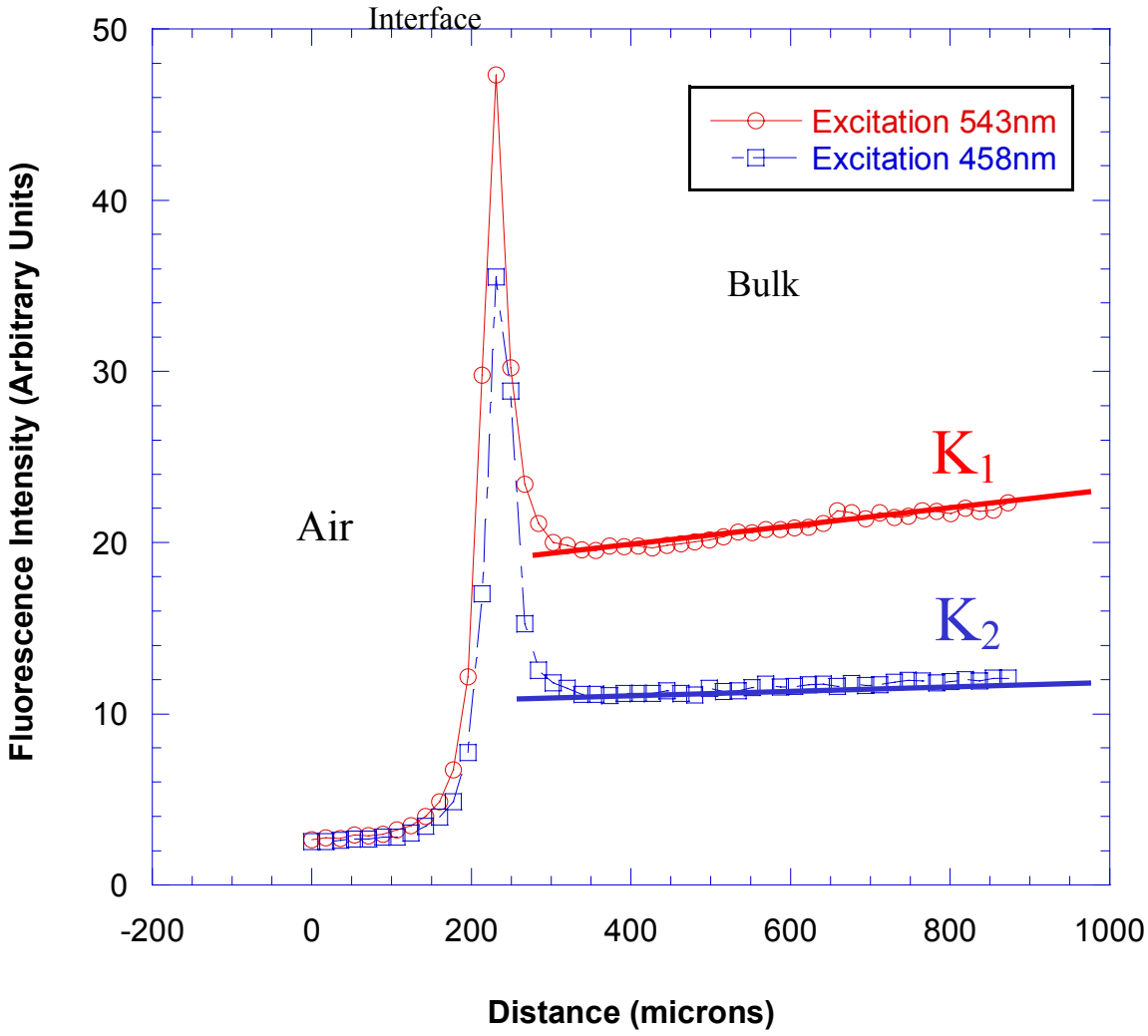

Figure 5.25: Bulk Nile Red fluorescence distribution when excited with 458nm (□) and 543nm (○) lasers.

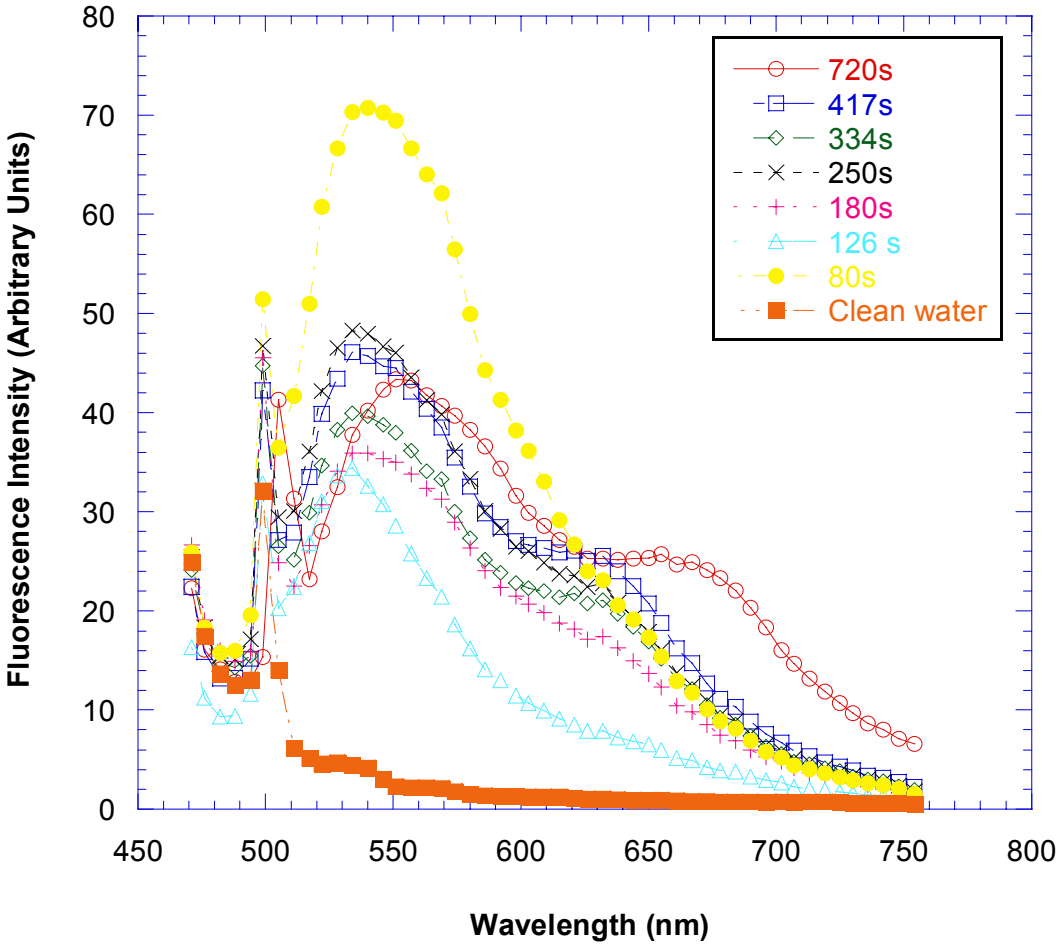

Figure 5.26: Surface fluorescence spectra showed FRET of Nile Red with NBD at 180 second after introduction of 15CMC $C_{14}E_6$ micelle solution which had with 0.2 µg/ml Nile Red incorporated in the micelle underneath a surface monolayer previously equilibrated with micelle solution.

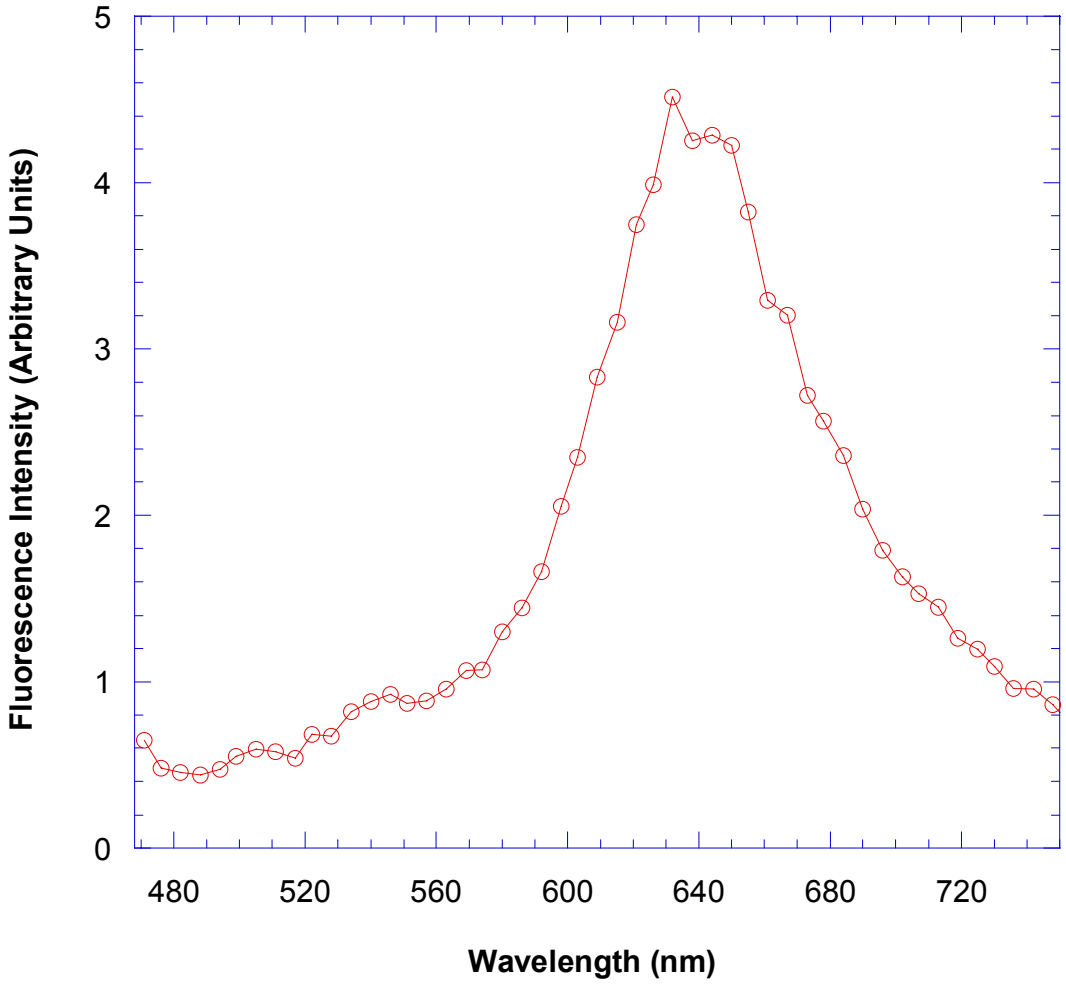

Figure 5.27: Bulk NBD fluorophore and Nile Red FRET after injection of micelle/Nile Red solution underneath surface monolayer previously equilibrated with micelle solutions.

Chapter 6

Future Work

6.1 Introduction

In chapter 4, we proposed a mathematical model for surfactant transport from a micellar solution onto a clean air/water interface for the model surfactant $C_{14}E_6$. The model was based on separation of time scales associated with the process, including the time scales of bulk micellization kinetics, bulk diffusion and the kinetic adsorption onto the surface. For the model surfactant $C_{14}E_6$, adsorption of infinite bulk micellization kinetics was used to facilitate the modeling of the surfactant transport. The model was demonstrated to predict the dynamic surface tension reduction at the air/water interface accompanying the surfactant transport process very well and the adsorption parameters and diffusivities of both monomer and micelle were evaluated by comparing the experimental surface tension data with the simulation results of the models. The model developed in chapter 4 can be extended to include the effect of micellization kinetics. This extension of theory is discussed in section 6.2.

A second area in which this study can be extended concerns using Quantum Dots as donors to detect the adsorption of Nile Red to the surface through Fluorescence Resonance Energy Transfer (FRET) and using Fluorescence Lifetime Imaging (FLI) technique to study more detail the FRET process. These extensions will be discussed in section 6.3 and 6.4.

6.2 Develop Theoretical Models for Other Nonionic Surfactants

We formulate in Table 6.1 below a summary of the critical micelle concentrations (C_{CMC}), the kinetic adsorption timescale (τ_K), the monomer diffusion timescale ($\tau_D^{monomer}$) and slow micellar kinetic relaxation time scale (τ_{SL}) for two series of the nonionic polyethylene oxide surfactants, C_iE_j ($CH_3(CH_2)_{i-1}(OCH_2CH_2)OH$). These surfactants are commonly used in industry. Entries with a "-" indicate that literature values are not available. Note particularly that the slow relaxation micelle break-up time scale has not been extensively measured. What is strikingly clear from this table is that (assuming the micellar break-up timescale for the rest of the polyethoxylates is of the order of a few seconds) the diffusion time scale of the monomer calculated at the C_{CMC} for the longer

Table 6.1: Time scales of $C_{14}E_6$ solution at the CMC

Surfactant	CAC mole/m^3	D ($x10^{10}$) m^2/sec	Γ_∞ ($x10^6$) mole/m^2	α/β ($x10^3$) mole/m^3	K	$\tau_D^{monomer}(C_{CAC}) = \frac{\Gamma_e^2(C_{CAC})}{DC_{CAC}^2}$ sec	$\tau_K = \left[\beta C_{CAC} + \alpha\right]^{-1}$ sec	τ_{SL} Slow Micelle Break-up Time sec
$C_{10}E_6$[a]	0.90	3.5	3.4	7.2	-	0.04	-	-
$C_{10}E_8$[b]	1.15	9.0	3.1	0.13	9.6	0.008	.12	-
$C_{12}E_6$[c]	0.089	6.0	3.5	0.034	6.6	2.5	2.8	10 , 5
$C_{12}E_8$[d]	0.10	11.0	2.7	0.025	5.2	.62	.82	4
$C_{14}E_6$[e]	0.009	4.0	3.3	0.0021	7.1	336	15.7	-
$C_{14}E_8$[f]	0.01	9.8	6,8	0.012	14	472	63	-
$C_{16}E_6$[g]	0.0005-.001	2.8	6.0	0.038	-	$4.5x10^5$	-	-

[a] D and Langmuir parameters from [1]; other Langmuir parameters are in [2]
[b] D and Frumkin parameters from [3-6]; Langmuir parameters in [1]
[c] D and Frumkin parameters from [7]; Frumkin parameters also in[5, 8]; Langmuir parameters in [2]; slow micelle break-up time measurements from [9] and [10]
[d] D and Frumkin values from [5, 6, 11, 12]; slow micelle break-up time measurements from [9]
[e] D and Frumkin parameters this work (see Chapter 4); Langmuir parameters also in [2, 14]
[f] D and Frumkin parameters from [6, 16] see also [5]

chain less soluble surfactants (14 and 16 chain lengths) is much larger than the micellar break-up time scale, while the shorter chain (10 carbon length) is much smaller and the middle chain length (12 carbon length) is of the same order as the break-up scale.

This separation of timescales suggests that we might consider different asymptotic regimes in the transport modeling. In this regard we distinguish three regimes:

Case 1: The surfactant monomer bulk diffusive transport timescales (i.e. $\tau_D^{monomer}$) is much longer than the slow timescale for the aggregate disassembly τ_{SL} as the case examined above for $C_{14}E_6$. For this case, the micelle disassembly kinetics is infinitely fast, and micelles and monomer are in instantaneous equilibrium. Thus the transport of surfactant to the surface is governed by the kinetic- adsorption and bulk diffusion.

Case 2: In this regime of the shortest methylene chain ethoxylates (8 or 10 carbons), monomer diffusion is much faster then the kinetic rate of micelle break-up, and therefore transport of the monomer to the surface is governed only by bulk diffusion and kinetic adsorption onto the surface. However, the micelle diffusion can be slower or faster than the micellar break-up rate depending on the bulk concentration of micelles. From the data given in Table 6.1, the value of micelle diffusivity is approximately 05-1.0$\times$ 10^{-10} m^2/(mole), it can be shown that by a micellar concentration approximately 10 times the C_{CMC}, bulk diffusion of micelles is also faster then the micelle break-up, and hence the micelle transport is governed only by bulk diffusion and possibly the kinetic step of direct adsorption onto the surface. This regime of high micellar concentration (which we note is the more industrially relevant) is what we will examine, particularly concentrating on the role of direct micelle adsorption.

Case 3: In this regime of the middle methylene chain ethoxylates (12 carbons), the rate of monomer diffusion is of the same scale as the kinetic break-up and micelle kinetics must be included in the monomer transport. However, once again at high enough bulk concentration of micelles (10 times the C_{CMC} and above), the bulk diffusion of the micelles can become much faster than the micelle kinetic break-up, and the transport of the aggregate species will be determined by bulk diffusion and the direct kinetic adsorption at the surface. The possibility exists (which we intend to explore by comparing simulations with measured dynamic tension reductions) that in the early times of adsorption onto an initially clean surface, the direct micellar adsorption may outscale the kinetic adsorption of monomer as the latter will be limited by diffusion and the finite time for break-up of micelles while for the former because of the high concentration and rapid bulk diffusion will have a large supply of micelles in the sublayer for direct adsorption.

As we can see from Table 6.1, the infinite micelle breakup assumption works for surfactants like $C_{14}E_8$ and $C_{16}E_6$, but is not valid for other nonionic surfactants like C_8E_5, $C_{10}E_6$, $C_{10}E_8$, or $C_{12}E_6$, $C_{12}E_8$. These surfactants can be treated by developing case 2 and case 3.

6.3 Use Fluorescent Semiconductor Nanocrystals (Quantum Dots) as the FRET Donor

The FRET donor used in this study was an NBD labeled phospholipid. Though its solubility in pure water is very low, its solubility in micellar solution can be enhanced by the presence of micelles in the bulk, which provides a hydrophobic shield for the phospholipids. So the phospholipids dissolved in the micellar bulk will partition into

micelle and this incorporation will keep driving the donor originally spread onto the surface to desorb from the surface monolayer and dissolve in the micellar solution. The reduced donor surface concentration resulted in the reduced acceptor FRET signal on the surface. (Besides the reduced donor surface concentration, the acceptor desorption from the surface and partition into micelle also reduced the acceptor FRET signal.)

To eliminate the desorption of the donor, fluorescent semiconductor nanocrystals also known as Quantum Dots (QDs) can be used as the donor instead. At the air/water surface, CdSe (core) and ZnS (shell) QDs with a hydrophobic trioctyl phosphine overcoat are dissolved in ethanol, and will be spread onto an air/water surface. This process is similar to the spreading of phospholipids onto an air/water surface. The diameter of the QDs is usually of the order of the diameter of one micelle (6-10 nm) and hence they will not be able to partition into a micelle due to the size restriction. Thus, if spread on the air/water interface, QDs will not desorb from the surface since there is no hydrophobic shield in the bulk large enough to incorporate them. Hence, once spread on the surface, the QDs will remain on the surface. QDs whose emission spectrum overlaps significantly with the excitation spectrum of the acceptor Nile Red will be used. The QDs has an added advantage of a narrower emission spectrum which allows an easier interpretation of energy transfer.

6.4 Study the FRET from Donor to Acceptor Using Fluorescence Lifetime Imaging Microscopy (FLIM)

The phenomenon of fluorescence resonance energy transfer is not mediated by photon emission, and furthermore, does not even require the acceptor chromophore to be fluorescent. In most applications, however, both donor and acceptor are fluorescent, and

the occurrence of energy transfer manifests itself through quenching of donor fluorescence and a reduction of the fluorescence lifetime, accompanied also by an increase in acceptor fluorescence emission. The fluorescence lifetime (τ) is defined as the average time that a molecule remains in an excited state prior to returning to the ground state. In practice, the fluorescence lifetime is defined as the time in which the fluorescence intensity decays to 1/e of the intensity immediately following excitation[13].

Fluorescence lifetime imaging microscopy (FLIM) is a technique in which the mean fluorescence lifetime of a chromophore is measured at each spatially resolvable element of a microscope image. The nanosecond excited-state lifetime is independent of probe concentration or light path length but dependent upon excited-state reactions such as fluorescence resonance energy transfer (FRET). FLIM is advantageous because it allows FRET to be measured directly by monitoring changes in fluorescence lifetimes rather than ratiometric analysis of fluorescence emission intensity[15].

By combining FRET and FLIM, the donor life time during the adsorption of the acceptor will be measured and will be will be compared against the life time of the donor in the absence of the acceptor to confirm FRET and provide another measurement of the adsorption of the acceptor.

Appendix: Simulation Result of Surfactant Transport from Surfactant Solution below CMC and Evaluation of Monomer Kinetic Parameters

For the $C_{14}E_6$ monomer, the Frumkin adsorption parameters K, Γ_∞, β and α, and the monomer diffusivity D_1 are obtained from fitting the transport equations and kinetics adsorption equations to equilibrium tension and dynamic tension measurements of the surfactant solution below CMC using pendant bubble tensiometer. Using the procedure outlined in the literature review (Cf. Section 2.1.3), first, equilibrium measurements of the tension as a function of the bulk concentration ($\gamma_e - \ln C_o$) are fit to the equilibrium adsorption isotherm ($\frac{\Gamma_e}{\Gamma_\infty} = \frac{[\beta C_o/\alpha]}{[\beta C_o/\alpha] + e^{K\Gamma_e/\Gamma_\infty}}$) and equation of state ($\gamma_e = \gamma_c + RT\Gamma_\infty \left\{ \ln\left[1 - \frac{\Gamma_e}{\Gamma_\infty}\right] - \frac{1}{2}K\left[\frac{\Gamma_e}{\Gamma_\infty}\right]^2 \right\}$) in order to determine the equilibrium parameters K, Γ_∞, and β/α. The equilibrium parameters obtained by Song et al. were adopted here since it gave satisfactory fittings (data not shown), which gave K=7.12, $\Gamma_\infty = 3.32\times10^{-6}$ mol/m^2 and $\alpha/\beta = 2.068\times10^{-6}$ mol/m^3.

The individual values of the kinetic constants β=4 m^3/(mol·s) and $\alpha = 8.272\times10^{-6}$ s^{-1}, and the monomer diffusion coefficient $D_1 = 6.0\times10^{-10}$ m^2/s, obtained by Song et al gave satisfactory fittings to dynamic surface tension curves. However, the diffusivity value of 6.0×10^{-10} m^2/s was too large for monomer based on a few diffusivity measurement of polyethoxylated surfactant monomers, a value of 3.9×10^{-10} m^2/s measured directly for $C_{12}E_5$ using pulsed field gradient NMR[1], and 3.8×10^{-10} m^2/s measured for $C_{12}E_8$ using a radiotracer method[2]. Thus the value of these kinetic constants are reevaluated in this study by measuring dynamic tensions reductions as surfactant adsorbs onto a clean

pendant bubble interface and comparing these relaxations to theoretical predictions from solution of the mass transfer equations (Cf. Section 2.1.4). In Figure A1, the dynamic surface tension relaxations are shown for adsorption onto the clean air/ water interface at five different bulk concentrations, with the lowest concentration equal to approximately .4CMC and the largest concentration equal to the CMC. For each concentration, several bubbles were formed and their relaxations were recorded, and these are shown as the different symbols at each concentration. The solution of the surfactant mass transfer is carried out in such a way that the pendant bubble is modeled as a sphere of radius *a*; at t=0, the bulk solution is uniform with concentration C_o and the interface is clean with zero surface concentration. Mass transfer of the non-aggregated surfactant to the interface takes place under quiescent conditions (as described by Fick's law) and maintains axisymmetry. The diffusive flux of monomer at the interface is equal to the rate of increase of the surface concentration, and we stimulate that the bulk concentration far from the interface remains at C_o. For this case, the Laplace transform procedure was used so that the surface concentration $\Gamma(t)$ can be written in terms of the sublayer concentration of monomer $C_s(t)$ (the Ward and Tordai equation[3, 4]):

$$\Gamma(t) = \frac{D}{a}\left[C_0 t - \int_0^t C_S(\tau) d\tau \right] + 2\sqrt{\frac{D}{\pi}}\left[C_0\sqrt{t} - \int_0^{\sqrt{t}} C_S(t-\tau) d\sqrt{\tau} \right] \qquad \text{(A1)}$$

This equation is solved numerically with the Frumkin kinetic equation as given in Equation (2.1) to provide the solutions for $\Gamma(t)$ and $C_S(t)$ as a function of D_1 and the adsorption parameters K, Γ_∞, β and α. For the diffusion coefficient of monomer, we use a value of 4×10^{-10} m^2/s at temperature of 22 ± 0.5 °C (temperature at which the pendant bubble technique is used to obtained experimental results). The diffusivity of

$C_{14}E_6$ is kept constantly at 4×10^{-10} m^2/s and this should be valid, given that the surfactant solutions of the analyzed concentration range are dilute enough. Simulations are run varying D_1 and β until the predicted relaxation fits the data of Figure A1 for all the bulk concentrations. Keeping D=4.0x10^{-10} m^2/s, the dynamic surface tension analysis of bulk solutions below the critical micelle concentration finds β=7.0 $m^3/(mol\cdot s)$ and $\alpha=1.448\times10^{-6}$ s^{-1}, with which the theoretical simulations which best fit the dynamic relaxations are indicated by the bold lines in Fig. A1.

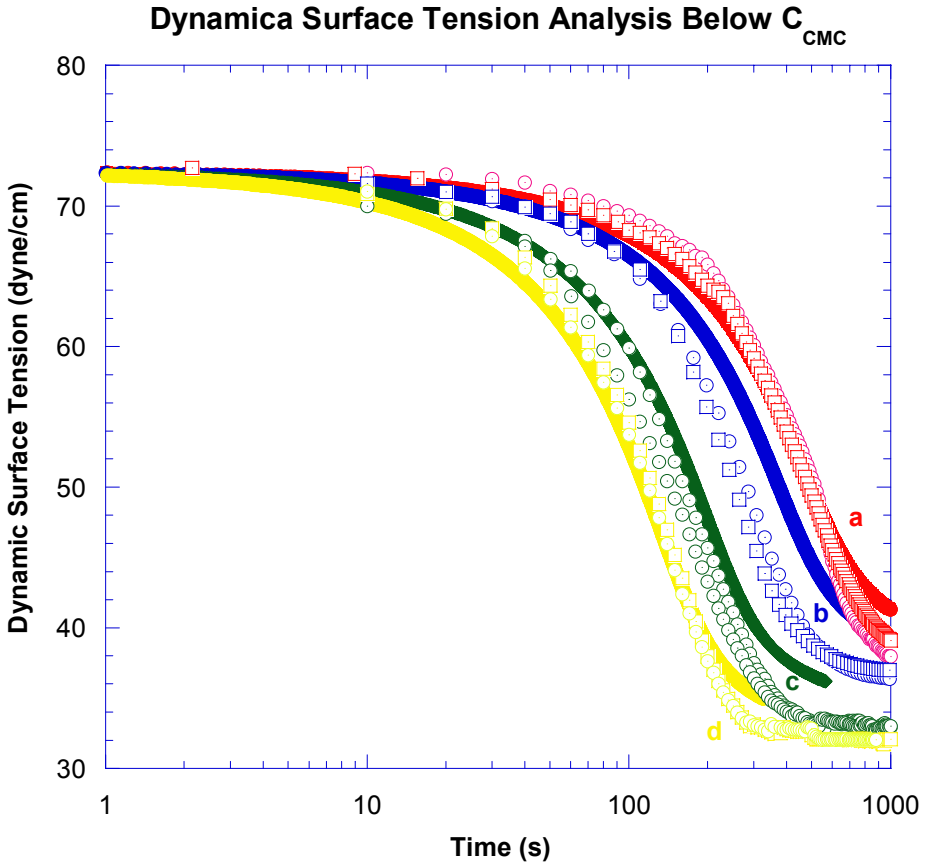

Figure A1: Dynamic surface tension predicted from Frumkin Rate Law with $D_1=4.0\times10^{-10}$ m^2/s, $\beta = 7$ $m^3/(mole\cdot s)$, $\alpha=1.448\times10^{-6}$ s^{-1} for $C_{14}E_6$: (a) $C_1^0=3.68\times10^{-3}$ mole/ m^3; (b) $C_1^0=4.39\times10^{-3}$ mole/ m^3; (c) $C_1^0=6.07\times10^{-3}$ mole/ m^3; (d) $C_1^0=9.18\times10^{-3}$ mole/ m^3. Dashed curves are the experimental data and continuous curves are the simulation results.

Bibliography

References for Chapter 1:

1. V. Schroder, O. Behrend, H. Schubert, *Effect of dynamic interfacial tension on the emulsification process using microporous, ceramic membranes.* Journal of Colloid and Interface Science, 1998. **202**: p. 334-340.

2. S. S. Dukhin, G.K., R. Miller, *Dynamics of Adsorption at Liquid Interfaces.* Elsevier, 1995.

3. Chang, C.-H., and E. I. Franses, *Adsorption Dynamics of Surfactants at the Air/Water Interface: A Critical Review of Mathematical Models, Data, and Mechanisms.* Colloids Surface, A, 1995. **100**(1).

4. G.Kretzschmar, R.M., *Dynamic Properties of Adsorption Layer of Amphiphilic Substances at Fluid Interfaces.* Advanced in Colloid and Interface Science, 1991. **36**: p. 65-124.

5. Miller, R., P. Joos, and V. Fainerman, *Dynamic Surface and Interfacial Tensions of Surfactant and Polymer Solutions.* Advances in Colloid and Interface Science, 1994. **49**: p. 249-302.

6. R. H. Notter, J.N.F., *Pulmonary surfactant: an interdisciplinary approach.* Journal of Applied Physiology, 1984. **57**(6): p. 1613-1624.

7. U. D. Rossi, O.B., B. Domanski, D*ynamic surface tension of UVcurable inkjet inks, in: IS&T's NIP20: International Conference on Digital Printing Technologies. S*ociety for Imaging Science and Technology, 2004. 20**:** p. 788-792.
8. U. Shavit, N.C., Th*e role of dynamic surface tension in air-assist atomization,. P*hysics of Fluids, 1995. **7**(1): p. 24-33.

9. J. E. Valentini, W.R.T., P. Sevenhuysen, T. S. Jiang, Y. Liu, H. O. Lee, S.-C. Yen, Ro*le of dynamic surface tension in slide coating. I*nd. Eng. Chem. Res., 1991. **30:** p. 453-461.

10. E. O. Machiste, G.B., Dy*namic surface tension studies of hydroxypropylmethylcellulose film-coating solutions. I*nternational Journal of Pharmaceutics, 1996. **145:** p. 197-201.

11. Bikeman, J., Fo*ams.* 1973, New York: Springer Verlag.

12. D. Beneventi, B.C., A. Gandini., Ro*le of surfactant structure on surface and foaming properties. C*olloids and Surfaces A: Physicochemical and Engineering Aspects, 2001. **189:** p. 65-73.

Reference of Chapter 2:

1. Chang, C.-H., and E. I. Franses, *Adsorption Dynamics of Surfactants at the Air/Water Interface: A Critical Review of Mathematical Models, Data, and Mechanisms.* Colloids Surface, A, 1995. **100**(1).

2. Ferri, J. and K. Stebe, *Which Surfactants Reduce SUrface Tension Faster? A Scaling Argument for Diffusion Controlled Adsorption.* Advances in Colloid and Interface Science, 2000. **85**: p. 61.

3. Lin, S.-Y., K. Mckeigue and C. Maldarelli, *Diffusion-Controlled Surfactant Adsorption Studied by Pendant Drop Digitization.* AICHE Journal, 1990. **36**(12).

4. Ward, A.H. and L. Tordai, *Time Dependence of boundary tension of solutions. I. The Role of Diffusion in Time Effects.* Journal of Chemical Physics, 1946. **14**: p. 453-461.

5. Chang, C.-H. and E. Franses, *Adsorption Dynamics of Surfactants at the Air/Water Interface: A Critical Review of Mathematical Models, Data and Mechanisms.* Colloids and Surfaces A: Physicochemical and Engineering Aspects, 1995. **100**: p. 1-45.

6. Borwankar, R.P. and D.T. Wasan, *The Kinetics of Adsorption of Surface Active Agents at Gas-Liquid Surfaces.* Chemical Engineering Science, 1983. **38**: p. 1637-1649.

7. Ward, A.F.H., and L. Tordai, *Time-Dependence of Boundary Tensions of Solutions.* Journal of Chemical Physics, 1946. **14**: p. 454.

8. Sutherland, K.L., Australia Journal of Scientific Research, 1952. **A5**(683).

9. Reinhard Miller, P.J.a.V.B.F., *Dynamic surface and interfacial tensions of surfactant and polymer solutions.* Advances in Colloid and Interface Science, 1994. **49**: p. 249-302.

10. G.Kretzschmar, R.M., *Dynamic Properties of Adsorption Layer of Amphiphilic Substances at Fluid Interfaces.* Advanced in Colloid and Interface Science, 1991. **36**: p. 65-124.

11. Kretzschmar, R.M.a.G., *Adsorption kinetics of surfactants at fluid interfaces.* Advances in Colloid and Interface Science, 1991. **37**: p. 97-121.

12. Ferri, J.K., and K. J. Stebe, *Which Surfactants Reduce Surface Tension Faster? A Scaling Argument for Diffusion-Controlled Adsorption.* Advanced in Colloid and Interface Science, 2000. **85**: p. 61.

13. Miller, R., P. Joos, and V. Fainerman, *Dynamic Surface and Interfacial Tensions of Surfactant and Polymer Solutions.* Advances in Colloid and Interface Science, 1994. **49**: p. 249-302.

14. Muramatsu, M., *Radiaactive Tracers in Surface and Colloid Science, in E. Matijevic(Ed).* Surface and Colloid Science, 1973. **6,** Wiley -Interscience.

15. Song, Q., *A Theoretical and Experimental Study of Surfactant Transport from A Micellar Solution to A Clean Air/Water Interface.* 2004, PhD dissertation theis.

16. Kwok, D.Y.V., D.; Miller, R.; Li, D.; Neuman, A.W., *Axisymmetric drop shape analysis as a film balance.* Colloids and Surfaces A: Physicochemical and Engineering Aspects, 1994. **88**: p. 51-58.

17. Junbai Li, R.M., Rainer Wüstneck, Mouml Hwald H and A. Wilhelm Neumann, U*se of pendent drop technique as a film balance at liquid/liquid interfaces.* Colloids and Surfaces A: Physicochemical and Engineering Aspects, 1995. **96:** p. 295-299.

18. Pan, R., J. Green, and C. Maldarelli, T*heory and Experiment on the Measurement of Kinetic Rate Constants for Surfactant Exchange at the Air-Water Interface.* Journal of Colloid and Interface Science, 1998. **205:** p. 213-230.

19. M. Douglas Levan, T.V., B*inary Langmuir and Freundlich Isotherms for Ideal Adsorbed Solutions.* Journal of Physical Chemistry, 1981. **85:** p. 3247.

20. Elias I. Franses, F.A.S., Dong June Ahn, T*hermodynamically Consistent Equilibrium Adsorption Isotherms for Mixture of Different-Size Molecules.* Langmuir, 1995. **11:** p. 3177-3183.

21. Schwuger, M.J., E*ffects of adsorption on detergency phenomena: II.* Journal of the American Oil Chemists' Society, 1982. **59:** p. 265.

22. Schwuger, M.J., E*ffects of adsorption on detergency phenomena: I.* Journal of the American Oil Chemists's Society, 1982. **59:** p. 258.

23. Lemlich, R., Ad*sorption Bubble Separation Techiniques. A*cademic Press, New York, 1972.

24. Bikerman, J.J., Fo*ams. N*ew York, 1973.

25. Ockrent, J.A.V.B.a.C., St*udies in Electrocapillarity. III. J*ournal of Physical Chemistry, 1930. **34:** p. 2841.

26. E.C.Marklam, A.F.B., TH*E ADSORPTION OF GAS MIXTURES BY SILICA. J*ournal of American Chemical Society, 1931. **53:** p. 497.

27. A. L. Myers, J.M.P., Th*ermodynamics of mixed-gas adsorption. A*merican Institute of Chemical Engineers Journal, 1965. **11:** p. 121.

28. LeVan, E.N.R.a.M.D., St*andard states for the adsorbed-solution theory. C*hemical Engineering Science, 1992. **47:** p. 1239.

29. Alan L. Myers, F.M., Sl*urry sorption separations: Equilibrium adsorption of gases by suspensions of solid adsorbents in liquids. Ch*emical Engineering Science, 1977. **32**.

30. Schlunder, W.F.a.E.U., Com*petitive adsorption of two dissolved organics onto activated carbon: Adsorption equilibria. Che*mical Engineering Science, 1981. **36**: p**.** 731.

31. Ch. Sheindorf, M.R., M. Sheintuch, A Fr*eundlich-type multicomponent isotherm. Jou*rnal of Colloid Interface Science, 1981. **79**: p. 136.

32. Israelachvili, J., Inte*rmolecular and Surface Forces. 2n*d ed. 1992, San Diego: Academic Press.

33. Israelachvili, J.N.M., D.J.; Ninham, B.W, Journal of chemical Society Faraday Transaction I, 1976. **72**: p**.** 1525.

34. Evans, D.F. and H. Wennerstrom, The *Colloidal Domain: Where Physics, Chemistry and Biology Meet. 199*9, New York: Wiley-VCH.

35. Mukerjee, P., *Size distribution of small and large micelles. Multiple equilibrium analysis*, Journal of Physical Chemistry, 1972. 76: p. 565.

36. Mukerjee, P., Journal of Pharmaceutical Science, 1974. **68**: p**.** 972.

37. P.Mukerjee, Advances in Colloid and Intrface Science, 1967. **1**: p**.** 241.

38. P.Mukerjee, Journal of Physical Chemistry, 1969. **73**(2054).

39. Kahlweit, M. and M. Teubner, On t*he Kinetics of Micellization in Aqueous Solution. Adv*ances in Colloid and Interface Science, 1980. **13**: p. 1-64.

40. Aniansson, E.A.G., et al., Theo*ry of the kinetics of micellar equilibrium and quantitative interpretation of chemical relaxation studies of micellar solutions of ionic surfactants. The* Journal of Physical Chemistry, 1976. **80(9)**: p. 905-922.

41. Aniansson, E.A.G. and S.N. Wall, On t*he kinetics of step-wise micelle association. The* Journal of Physical Chemistry, 1974. **78**: p. 1024-1030.

42. Aniansson, E.A.G. and S.N. Wall, A co*rrection and improvement of " On the kinetics of step-wise micelle association" by E.A.G. Aniansson and S.N.Wall. The* Journal of Physical Chemistry, 1975. **79**: p. 857.

43. Lucassen, J. and D. Giles, Dyna*mic Surface Properties of Nonionic Surfactant Solutions. Jou*rnal of the Chemical Society, Faraday Transactions I, 1975. **71**: p. 217-232.

44. Miller, R., On t*he Solution of Diffusion Controlled Adsorption Kinetics for any Adsorption Isotherm. Col*loid and Polymer Science, 1981. **259**: p. 375-381.

45. Joos, P. and J. Vanhunsel, Adso*rption kinetics of micellar Brij 58 solutions. Col*loids and Surfaces A: Physicochemical and Engineering Aspects, 1988. **33**: p. 99.

46. Joos, E.R.a.P., Rate *of demicellization from the dynamic surface tensions of micellar solutions. Jou*rnal of Physical Chemistry, 1982. **86(177):** p. 3471-3478.

47. Fainerman, V.B., Y.M. Rakita, and V. Zadara, Diff*usion Controlled Kinetics of the Adsorption from Solutions of Surface Active Substances Containing Micelles. Zh.* Fiz. Khim., 1984. **58**: p. 2006.

48. Dushkin, C.D., I.B. Ivanov, and P.A. Kralchevsky, The *Kinetics of the Surface Tension of Micellar Surfactant Solutions.* Colloids and Surfaces, 1991. **60**: p. 235-261.

49. Dushkin, C.D. and I.B. Ivanov, Effe*ct of the Polydispersity of Diffusing Micelles on the Surface Elasticity.* Colloids and Surfaces, 1991. **60**: p. 213-233.

50. Dushkin, C.D. and I.B. Ivanov, An A*symptotic Approach to the Kinetics of Formation of Polydisperse Micelles. Jou*rnal of Surface Science and Technology, 1990. **6**: p**.** 269.

51. Noskov, B.A., Kine*tics of Adsorption from Micellar Solutions. Adv*ances in Colloid and Interface Science, 2002. **95**: p**.** 237-293.

52. Dushkin, C.D., T.H. Iliev, and Y.S. Radkov, Dyna*mic Surface Tension of Micellar Solutions Studied by The Maximum Bubble Pressure Method 3. Theory of Solutions COntaining Micelles. Col*loid and Polymer Science, 1995. **273**: p. 370-379.

53. Illiev, T.H. and C.D. Dushkin, Dyna*mic Surface Tension of Micellar Solutions Studied by The Maximum Bubble Pressure Method 1. Experiment. Col*loid and Polymer Science, 1994. **272**: p. 1157-1165.

54. Mitrancheva, J.V., C.D. Dushkin, and P. Joos, Kine*tics of the Surface Tension of Micellar Solutions: Comparison of Different Experimental Techniques. Col*loid and Polymer Science, 1996. **274**: p. 356-367.

55. Danov, K.B., P.M. Vlahosvska, and P.A. Kralchevsky, Adso*rption Relaxation for Nonionic SUrfactants Under Mixed Barrier-Diffusion and Micellization-Diffusion Control. Jou*rnal of Colloid and Intrface Science, 2002. **251**: p. 18-25.

56. Liao, Y., O. Basaran, and E. Franses, Effe*cts of Micellar Dissolution and Micellar Diffusion Rates of Aqueous Surfactants on Dynamic Adsorption and Surface Tension. AIC*hE Journal, 2004. **340**: p. 22.

References of Chapter 3:

1. Faisal A. Siddiqui, E.I.F., *Equilibrium Adsorption and Tension of Binary Surfactant Mixture at the Air/Water Interface.* Langmuir, 1996. **12**: p. 354.

2. R. Nagarajan, E.R., *Self-Assembled Systems.* Chapter 15 of IUPAC in Equations of State for Fluids and Fluid Mixtures, 2000.

3. J. Talbot, X.J., N.-H L. Wang, *New Equations for Multicomponent Adsorption Kinetics.* langmuir, 1994. **10**: p. 1663-1666.

4. Elias I. Franses, F.A.S., Dong June Ahn, *Thermodynamically Consistent Equilibrium Adsorption Isotherms for Mixture of Different-Size Molecules.* langmuir, 1995. **11**: p. 3177-3183.

5. Widom, B., *Some Topics in the Theory of Fluids.* The Journal of Chemical Physics, 1963. **39**: p. 2808.

6. Paul D. T. Huibers, V.S.L., Alan R. Katritzky, Dinesh O. Shah, Mati Karelson, *Prediction of Critical Micelle Concentration Using a Quantitative Structure - Property Relationship Approach. 1 Nonionic Surfactants.* langmuir, 1996. **12**: p. 1462-1470.

7. Wyn Brown, R.J., Peter Stllbs, *Size and Shape of Nonionic Amphiphile (C12E6) Micelles in Dilute Aqueous Solutions as Derived from Quasielastic and Intensity Light Scattering, Sedimentation, and Pulsed-Field-Gradient Nuclear Magnetic Resonance Self-Diffusion Data.* Journal of Physical Chemistry, 1983. **87**: p. 4548-4553.

8. Walter H. Richtering, W.B., E. Jahns, H. Finkelmann, *Light Scattering from Aquesous Solutions of a Nonionic Surfactant (C14E8) in a Wide Concentration Range.* Journal of Physical Chemistry, 1988. **92**: p. 6032-6040.

9. W. Brown, Z.P., R. Rymden, *Size and shape of nonionic micelles: NMR self-diffusion and static and quasi-elastic light scattering.* Journal of Physical Chemistry, 1988. **92**: p. 6086-6094.

10. W. Binana-Limbele, R.Z., *Effect of Temperature on the Aggregation Behavior of the Nonionic Surfactant C12E8 in H2O and D2O Solutions.* Journal of Colloid and Interface Science, 1988. **121**.

11. D. Danino, Y.T., R. Zana, *Aggregation and Microstructure in Aqueous Solutions of the Nonionic Surfactant C12E8.* Journal of Colloid and Interface Science, 1996. **186**: p. 170-179.

References of Chapter 4:

1. J. Talbot, X.J., N.-H L. Wang, *New Equations for Multicomponent Adsorption Kinetics.* langmuir, 1994. **10**: p. 1663-1666.

2. Elias I. Franses, F.A.S., Dong June Ahn, *Thermodynamically Consistent Equilibrium Adsorption Isotherms for Mixture of Different-Size Molecules.* langmuir, 1995. **11**: p. 3177-3183.

3. A. Patist, S.G.O., R. Leung, D.O. Shah, *Kinetics of Micellization: Its Significance to Technological Process.* Colloids and Surfaces A: Physicochem. Eng. Aspects, 2001. **176**: p. 3-16.

4. Tadashi Kato, D.N., *Structure and Dynamics of Concentrated Micellar Phase in Nonionic Surfactant-Water Systems.* Journal of Molecular Liquids, 2001. **90**: p. 167-174.

5. Tadashi Kato, T.T., Michiko Tsukada, Tsutomu Seimiya, *Self-Diffusion Process in Semidilute Solutions of Nonionic Surfactant (C16E7) Studied by Light Scattering and Pulsed-Gradient Spin Echo Methods.* Journal of Physical Chemistry, 1993. **97**: p. 3910-3917.

6. W. Brown, R.R., *Static and dynamic properties of a nonionic surfactant (C12E6) in aqueous solution,.* Journal of Physical Chemistry, 1987. **91**: p. 3565-3571.

7. Daniel M. Colegate, C.D.B., *Adsorption Kinetics in Micellar Solutions of Nonionic Surfactants.* Physical Review Letters, 2005. **95**: p. 198302.

References of Chapter 5:

1. Pan, R.G., J., Maldarelli, C., *Theory and Experiment on the Measurement of Kinetic Rate Constants for Surfactant Exchange at the Air-Water Interface.* Journal of Colloid and Interface Science, 1998. **205**: p. 213-230.

2. Lin, S.-Y., K. McKeigue, and C. Maldarelli, *Diffusion Controlled Surfactant Adsorption Studied by Pendant Drop Digitization.* American Institute of Chemical Engineers Journal, 1990. **36**: p. 1785-1795.

3. K. Braeckmans, L.P., N.N.Sanders, S.C. De Smedt and J. Demeester,, *Three-dimensional fluorescence recovery after photobleaching with confocal scanning laser microscope.* Biophysical Journal, 2003. **85**(4): p. 2240-2252.

4. Deye JF, B.T., Anderson AG., *Nile Red as a solvatochromic dye for measuring solvent strength in normal liquids and mixtures of normal liquids with supercritical and near critical fluids.* Analytical Chemistry, 1990. **62**(6): p. 615-622.

5. Marc C. A. Stuart, J.C.v.d.P.a.J.B.F.N.E., *The use of Nile Red to monitor the aggregation behavior in ternary surfactant-water-organic solvent systems.* Journal of Physical Organic Chemistry, 2005. **18**: p. 929-934.

6. J. Shobha, V.S., and D. Balasubramanian, *Differential modes of incorporation of probe molecules in micelles and in bilayer vesicles.* Journal of Physical Chemistry, 1989. **93**: p. 17-20.

7. Rejeev Subramanyam , C.M., *Fluorescence Evidence that a Phase Transition Causes the Induction Time in the Reduction in Dynamic Tension during Surfacant Adsorption to a Clean Air/Water Interface and a Kinetic-Diffusion Transport Model for the Phase-Induced Induction.* Journal of Colloid and Interface Science, 2000. **253**: p. 377-392.

8. Luis M. S. Loura, R.F.M.d.A., Manuel Prieto, *Methodologies and formalisms of resoance energy transfer in biophysics. Application to membrane model systems.* International Journal of Photoenergy, 2003. **5**: p. 223-231.

References of Chapter 6:

1. Daniel, R. and J. Berg, *A Simplified Method For Predicting the Dynamic Surface Tension of Concentrated Surfactant Solutions.* Journal of Colloid and Interface Science, 2003. **260**: p. 244-249.

2. Zhmud, B., F. Tiberg, and J. Kizling, *Dynamic Surface Tensiion in Concentrated Solutions of CnCm Surfactants: A Comparison of Theory and Experiment.* Langmuir, 2000. **16**: p. 2557.

3. Hsu, C.-T., C.-H. Chang, and S.-Y. Lin, *Comments on the Adsorption Isotherm and Determination of Adsorption Kinetics.* Langmuir, 1997. **13**(23): p. 6204-6210.

4. Chang, H.-C., C.-T. Hsu, and S.-Y. Lin, *Adsorption Kinetics of C10E8 at the Air-Water Interface.* Langmuir, 1998. **14**(9): p. 2476-2484.

5. Lin, S.-Y., et al., *Surface Equation of State of Nonionic CmEn Surfactants.* Langmuir, 2003. **19**: p. 3164-3171.

6. Lee, Y.-C., et al., *Adsorption and Desorption Kinetics of CmE8 on Impulsively Expanded or Compressed Air-Water Interfaces.* Colloids and Surfaces A: Physicochemical Engr. Aspects, 2003. **220**: p. 139-150.

7. Pan, R., J. Green, and C. Maldarelli, *Theory and Experiment on the Measurement of Kinetic Rate Constants for Surfactant Exchange at the Air-Water Interface.* Journal of Colloid and Interface Science, 1998. **205**: p. 213-230.

8. Lin, S.-Y., Y.-C. Lee, and M.-J. Shao, *Adsorption Kinetics of C12E6 at the Air-Water Interface.* Journal of the Chinese Institute of Chemical Engineers, 2002. **33**(6): p. 631-643.

9. Patist, A., et al., *Kinetics of Micellization: Its Significance to Technological Processes.* Colloids and Surfaces A: Physicochemical and Engineering Aspects, 2001. **176**: p. 3-16.

10. Eastoe, J., et al., *Dynamic Surface Tensions of Nonionic Surfactant Solutions.* Journal of Colloid and INterface Science, 1997. **188**: p. 423-430.

11. Lin, S.-Y., et al., *Adsorption Kinetics of C12E8 at the Air-Water Interface: Adsorption onto a Clean Interface.* Langmuir, 1996. **12**: p. 6530-6536.

12. Tsay, R.-Y., et al., *Adsorption kinetics of C12E8 at the Air/Water Interface: Desorption from a Compressed Interface.* Langmuir, 1997. **13**: p. 3191-3197.

13. Lakowicz, J.R., *Principles of Fluorescence Spectroscopy, 2nd edn.* Plenum Press, New York., 1999.

14. Liao, Y., O. Basaran, and E. Franses, *Micellar Dissolution and Diffusion Effects on Adsorption Dynamics of Surfactants.* AIChE Journal, 2003. **49**: p. 3229-3240.

15. Ailsa G. Harpur1, F.S.W., Philippe I.H. Bastiaens, *Imaging FRET between spectrally similar GFP molecules in single cells.* Nature Biotechnology, 2001. **19**: p. 167-169.

16. Lin, S.-Y., et al., *A study on surfactant adsorption kinetics: The role of the data of equation of state .gamma.(.GAMMA.) for C14E8.* Journal of Colloid and Interface Science, 2001. **244**(2): p. 372-376.

References of Appendix:

1. M. Schonhoff, O.S., *PFG-NMR diffusion as a method to investigate the equilibrium adsorption dynamics of surfacants at the solid/liquid interface.* Journal of PHysical Chemistry B, 1997. **101**: p. 8237?242.

2. K.L.Mittal, B.L.E., S*urfactants in Solution,.* Plenum, New YOrk, 1984: p. 359.

3. Miller, R., A*dsorption kinetics of surfactants from micellar solutions.* Colloid & Polymer Science, 1981. **259:** p. 1124-1128.

4. Z. Adamczyk, J.P., A*dsorption and Desorption Kinetics of Molecules and Colloidal Particles.* Journal of Colloid and Interface Science, 1987. **118:** p. 20-49.